Recrystallization of deformed copper - kinetics and microstructural evolution

Lin, Fengxiang; Juul Jensen, Dorte; Pantleon, Wolfgang

Publication date:
2013

Document Version
Publisher's PDF, also known as Version of record

Recrystallization of deformed copper – kinetics and microstructural evolution

DTU Wind energy
PhD Report 2013

Fengxiang Lin
DTU Wind Energy PhD-0011 (EN)
March 2013

DTU Wind Energy
Department of Wind Energy

Author: Fengxiang Lin
Title: Recrystallization of deformed copper – kinetics and microstructural evolution
Division: Materials Science and Advanced Characterization Section, Department of Wind Energy

This thesis is submitted in partial fulfilment of the requirements for the Ph.D. degree at the Technical University of Denmark.

DTU Wind Energy PhD-0011 (EN)
March 2013

ISSN 0106-2840
ISBN 978-87-92896-24-7

Abstract:

The objective of this study is to investigate the recrystallization kinetics and microstructural evolution in copper deformed to high strains, including copper deformed by cold-rolling and copper deformed by dynamic plastic deformation (DPD). Various characterization techniques were used, including electron backscatter diffraction (EBSD), Vickers hardness test, 3D X-ray diffraction (3DXRD) and differential scanning calorimetry (DSC).

For the cold-rolled samples, a series of initial parameters was investigated for their effects on the recrystallization kinetics and textures, including initial grain size, sample widening, strain, annealing temperature, impurity content, storage time, etc. The recrystallization in the cold-rolled samples with coarse and fine initial grain sizes is the focus of the present study. It is found that a strong cube recrystallization texture is only developed in the initially fine grained sample. The strong cube texture is related to a few extremely large cube grains, named supercube grains in this study. The development of supercube grains is compared with that of the other cube grains and noncube grains.

Recrystallization in the DPD sample with and without additional rolling was investigated. The spatial distribution of the recrystallizing grains is very different: severely clustered in the DPD sample versus a more random distribution in the one with additional rolling. This difference is inherited from the deformation structures. The effects of annealing on the mechanical properties are also discussed.

The recrystallization kinetics in all the samples investigated in this study shows relatively low Avrami exponents. The average growth rates of the recrystallizing grains are found to decrease with time. The growth curves of individual recrystallizing grains also show decreasing growth rates. The effects of the variation within the deformation structures on various length scales on the recrystallization kinetics are discussed.

Sponsorship:

Danish National Research Foundation

Danmarks Tekniske Universitet
DTU Vindenergi
Nils Koppels Allé
Bygning 403
2800 Kgs. Lyngby

www.vindenergi.dtu.dk

Recrystallization of deformed copper – kinetics and microstructural evolution

Fengxiang Lin

Supervised by Dorte Juul Jensen and Wolfgang Pantleon

Materials Science and Advanced Characterization Section

Department of Wind Energy

Technical University of Denmark

March 2013

Contents

Preface

This thesis is submitted in partial fulfillment of the requirements for the PhD degree at the Technical University of Denmark. The project was carried out within the Danish-Chinese Center for Nanometals. The study was conducted during the period from December 2009 to November 2012.

My deepest gratitude goes first and foremost to my supervisors Drs. Dorte Juul Jensen and Wolfgang Pantleon, who have been always instructing, encouraging and supporting me with their wide knowledge and extraordinary patience. I am thankful to Dr. Yubin Zhang for helps in many aspects and in many years. A number of people deserve a word of thanks for inspiring discussion: Drs. Neils Hansen, Leffers Torben, Andrew Godfrey, Roy Vandermeer, Grethe Winther, Nairong Tao, Guilin Wu, Chuanshi Hong, Tianbo Yu, and Hongwang Zhang. Lars Lorentzen, Preben Olesen, Steen Bang, Gitte Christiansen and Xiao Si are acknowledged for their skillful work in sample preparations. I would also like to thank Jacob Kidmose, Helle Hemmingsen, Lene Danielsen, Guoming Le, Zhaoping Luo and all the other colleagues at DTU and at IMR. I am grateful to Professor Brian Ralph for his comments during the preparation of the thesis.

The X-ray diffraction experiments were carried out at the Deutsches Elektronen-Synchrotron (DESY). I am very grateful to Norbert Schell and all the other staff and scientists at the beamline P07. Special thanks go to Dr. Stefan Poulsen for his help in the experiments and data analysis.

Finally, I would express my gratitude to my family and friends, for supporting me through the years.

Chapter 1

Introduction

Recrystallization (sometimes also termed primary recrystallization) is a thermally activated microstructural evolution process, whereby new strain-free grains emerge from a deformed metal, and the new grains increase in size by interfacial migration thereby consuming the deformed volume. Recrystallization typically occurs, when deformed metals are annealed, and leads to significant changes in both the metals' microstructures and mechanical properties. Detailed characterization of the microstructural evolution during recrystallization is necessary for a better understanding of changes in properties and for optimizing the properties for applications.

Although recrystallization has been used practically and studied for many years, the knowledge of the recrystallization kinetics is essentially only based on statistical, average data which also generally limits the recrystallization models to average overall kinetic models. With experimental techniques developed recently, it has become possible to characterize and analyze the recrystallization kinetics of groups of grains of specific crystallographic orientations as well as of individual grains. Particular interest is to study recrystallization kinetics in metals deformed to high strains, which may have a nanostructure. The investigation of recrystallization kinetics is helpful for understanding the thermal stability of these metals.

The aim of this project is to study the recrystallization kinetics and microstructural evolution in cold-rolled copper samples and in nanostructured copper samples by in-situ and statistical methods. The thesis is structured as

follows: Chapter 2 gives a short review of the background; Chapter 3 introduces the characterization techniques used in this study; Chapter 4 reports the recrystallization kinetics and microstructural evolution in samples produced by cold-rolling to medium and high strains (90% and 95% thickness reduction); Chapter 5 reports the recrystallization kinetics and microstructural evolution in nanostructured samples produced by dynamic plastic deformation with and without additional rolling; Chapter 6 concludes and proposes an outlook.

Chapter 2
Background

This chapter provides theoretical and experimental background information for the present study. The first part is a brief introduction of typical deformation microstructures after plane strain compression (PSC), e.g. cold-rolling and channel-die compression. The driving force for recrystallization is the stored energy, which is accumulated through the deformation process. The deformation microstructures determine to a large part the subsequent recrystallization behavior. The second part is a general description of theoretical and experimental investigations of the recrystallization kinetics, as well as the microstructural evolution during recrystallization.

2.1 Deformation microstructure

During deformation, a small amount of the work remains in the material as stored energy. Most of the stored energy is in the form of dislocations, which often interact with each other, and form dislocation boundaries. The original grains of the material are subdivided by the dislocation boundaries, which enables grain refinement through high strain plastic deformation. The deformation microstructure is introduced in the following with an emphasis on face centered cubic (FCC) metals with medium-to-high stacking fault energies (SFEs), e.g. aluminum (166 mJ/m^2), nickel (128 mJ/m^2) and copper (78 mJ/m^2). At room temperature, these metals generally deform by dislocation slip. At low strains ($\varepsilon < 0.8$), as shown in Fig. 2.1a, the

microstructure is composed of cell blocks or bands, which are bounded by dense dislocation walls (DDWs) and microbands (MBs). These dislocation boundaries are aligned approximately at angles within the range of 25-40° to the rolling direction (RD) on the longitudinal plane, and may be close to one of the (111) slip plane depending on the orientation of the grain (Huang and Hansen 1997, Huang and Winther 2007). At high strains ($\varepsilon > 0.8$), as shown in Fig. 2.1b, the microstructure is characterized by extended lamellae, separated by lamellar boundaries (LBs), which are almost parallel to the RD. The transition between low strain cell block structures and high strain lamellar structures is aided by coarse slip in S-bands (Hughes and Hansen 1993). At some intermediate stages, MBs and LBs coexist.

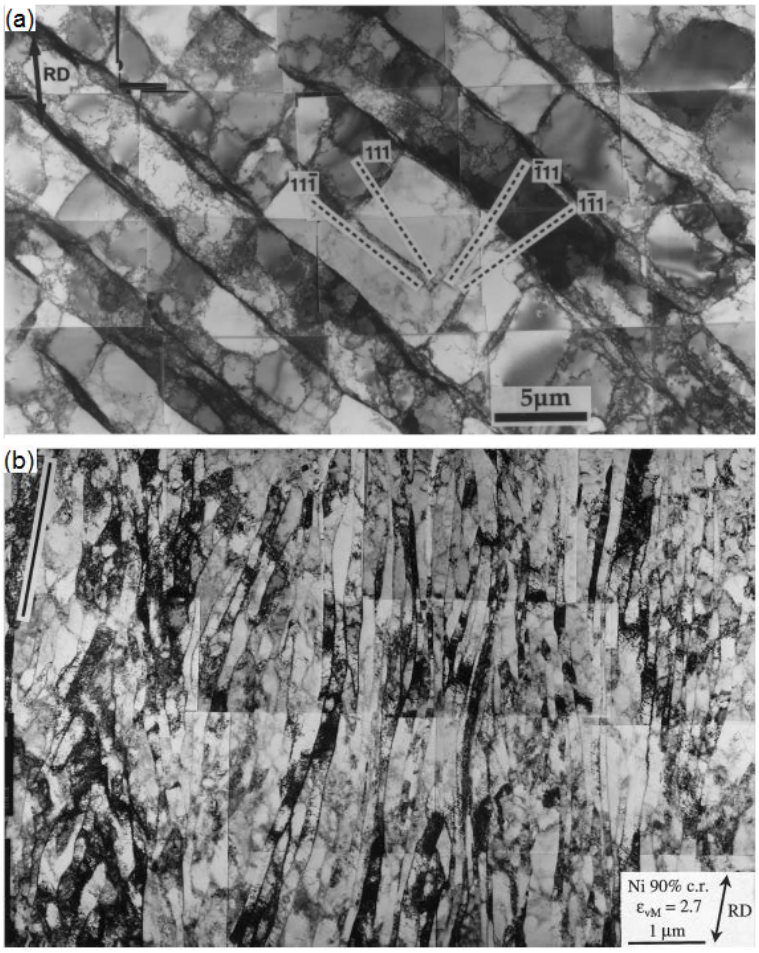

Fig. 2.1: a) A cell block structure in aluminum cold-rolled to 10% thickness reduction, reproduced from Liu et al. (1998). b) A lamellar structure in nickel cold-rolled to 90% thickness reduction, reproduced from Hughes and Hansen (2000). Both images are in the longitudinal plane view.

Accompanying the grain subdivision, grains rotate towards some stable orientations, which forms the deformation texture. For the FCC metals mentioned above, the major deformation texture components after cold-rolling are the copper, S, and brass orientations listed in Tab. 2.1. The copper and brass orientations have two symmetric variants each, while the S orientation has four symmetric variants. A very weak cube texture can also be found in deformed samples.

Tab. 2.1: Important texture components in rolled FCC metals. {hkl} and <uvw> represent the crystallographic direction of the rolling plane and the rolling direction respectively. (φ1, ϕ, φ2) represents the Euler angle of a specific orientation.

Component symbol	{hkl}	<uvw>	φ1	ϕ	φ2
copper	112	111	90	35	45
			270	35	45
S	123	634	59	37	63
			239	37	63
			301	143	243
			121	143	243
brass	011	211	35	45	90
			325	135	270
cube	001	100	0	0	0

2.1.1 Parameters affecting deformation microstructures

The morphology, as well as the crystallographic alignment of the dislocation boundaries, depends strongly on the crystallographic orientation of the grain (Huang and Winther 2007, Lin et al. 2009). The orientation dependence of the dislocation structures originates from the interaction between available dislocations, which are generated by crystallographic slip on a number of systems (Winther and Huang 2007).

Fig. 2.2 shows the microstructures typically observed in copper, S and brass oriented aluminum single crystals. All these three orientations are stable orientations after PSC. The microstructure has more local variations in

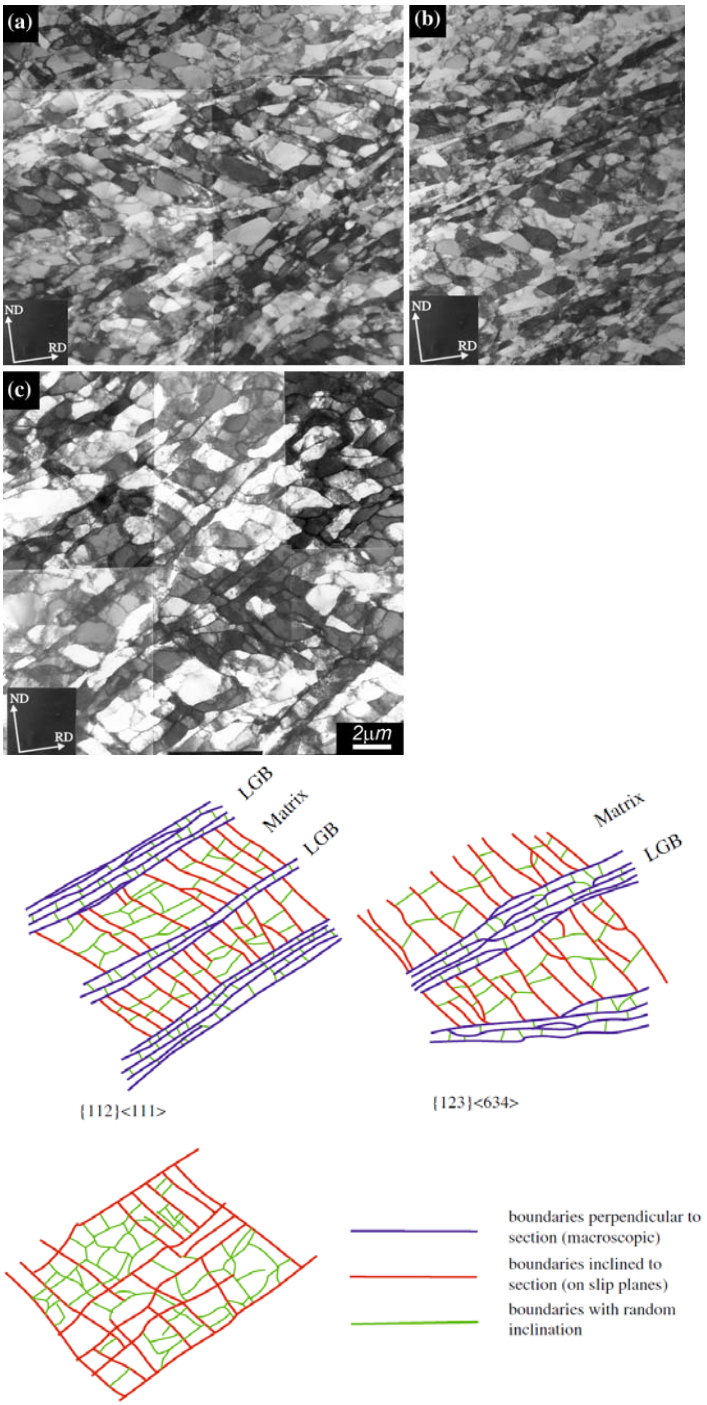

Fig. 2.2: The microstructures observed after channel-die compression at room temperature to a strain of 1.5 in three aluminum single-crystal samples of a) copper and b) S and c) brass orientations, respectively. The microstructures are illustrated by sketches in d). Reproduced from Godfrey et al. (2007).

the copper and S oriented crystals, with the appearance of a set of coarsely spaced bands, named localized glide bands (LGBs) by Godfrey et al. (2007). The microstructure in the brass oriented crystal is characterized by two sets of

MBs equally spaced. The stored energies are different in these microstructures, which is highest inside the LGBs of the copper oriented grains, and lowest in the brass oriented grains (Godfrey et al. 2007).

The initial grain size typically has strong effects on the boundary spacing after deformation. An initially small grained sample may have finer boundary spacing than an initially large grained sample. The effects of the initial grain size can be observed even in samples deformed to very high strains (Jazaeri and Humphreys 2004). Another aspect of the initial grain size is related to the appearance of some heterogeneous features on a larger scale, among which shear bands are one important feature. Shear bands usually form when a strain instability occurs. In rolled samples, they align at approximately 35° to RD and parallel to the transverse direction (TD), and usually cut through several grains, or even the whole sample. It was reported previously that shear bands occurred much more readily in coarse grained metals (Korbel et al. 1986).

Metals with medium-to-high SFEs, such as copper, are in general deformed by dislocation slip, but when deformed at low temperatures or high strain rates, twinning may become an active deformation mechanism. The onset of twinning was suggested to be determined by the ratio of the resolved shear stresses for twinning and slip (Köhlhoff et al. 1988), i.e. it is also orientation related. Apart from twinning, low temperatures and high strain rates have also been recognized to facilitate the formation of shear bands (Duckham et al. 2001).

2.2 Recrystallization

The deformed microstructure is thermally unstable due to the high stored energy. Upon annealing, the deformed microstructure is replaced by almost dislocation-free grains, by which the stored energy is lowered. The recrystallization process is normally described in terms of nucleation and growth stages. The nucleation stage is the initial stage, during which dislocation-free grains form. The growth stage is the following stage, during

which grain boundaries migrate through the deformation structure. The recrystallization process is complete when the entire deformed volume has disappeared. In the recrystallization literature, a recrystallizing crystal is called a nucleus during the nucleation stage and a grain during the growth stage. However, the borderline between the two stages is not very clear. In this thesis, the term recrystallizing grains is used for both stages.

2.2.1 Recrystallization kinetics and the JMAK model

Several mathematical models have been established to describe the recrystallization process. The classic model is the Johnson-Mehl-Avrami-Kolmogorov (JMAK) model (Kolmogorov 1937, Johnson and Mehl 1939, Avrami 1939, Avrami 1940, Avrami 1941), and it can be written as a simple mathematical equation (the JMAK equation):

$$V_V = 1 - exp(-Bt^n) \tag{2.1}$$

where V_V is the recrystallized volume fraction, and t is the annealing time. The coefficient B depends on the nucleation rate /the nucleation density, and the growth rate, while the exponent n is related to the time dependence of the nucleation rate and the growth rate, as well as the growth dimensionality (Christian 2002). The JMAK model is based on the assumption that recrystallizing grains are spatially randomly distributed. The idealized JMAK model assumes that all recrystallizing grains grow at one constant growth rate. Two limiting cases of nucleation are site saturation (i.e. recrystallizing grains appear at the beginning of recrystallization) and a constant nucleation rate. The idealized JMAK model predicts the exponent n as listed in Tab. 2.2.

Tab. 2.2: Ideal JMAK exponents under different nucleation and growth conditions.

Growth dimensionality	Site saturation	Constant nucleation rate
3-D	3	4
2-D	2	3
1-D	1	2

Experimental measurements of recrystallization kinetics are usually fitted to the JMAK equation by plotting $-ln(1-V_V)$ against t on a log-log scale (also termed an Avrami plot). Fig. 2.3 is a typical Avrami plot of the recrystallization kinetics (Vandermeer and Rath 1989). The JMAK model is not adequate to describe the recrystallization kinetics in two aspects. First, the exponent n has been frequently observed to have low values, despite the recrystallizing grains growing approximately in 3D. For example, in Fig. 2.3, the exponents n are around 1.9. There are numerous other examples of recrystallization kinetics, where even lower exponents, typically n=1, have been reported (reviewed by Doherty et al. 1986). Second, data points do not fall on a straight line and prominent negative deviations are detected for longer annealing time periods. In Fig. 2.3, data of the low temperature annealed sample show such obvious deviations. The failure of the JMAK model in describing recrystallization kinetics can be attributed to the too simplified assumptions. These assumptions are fulfilled only rarely, e.g. in lightly deformed fine grained samples, in which the grain size after recrystallization is much larger than that before deformation (Doherty et al. 1986).

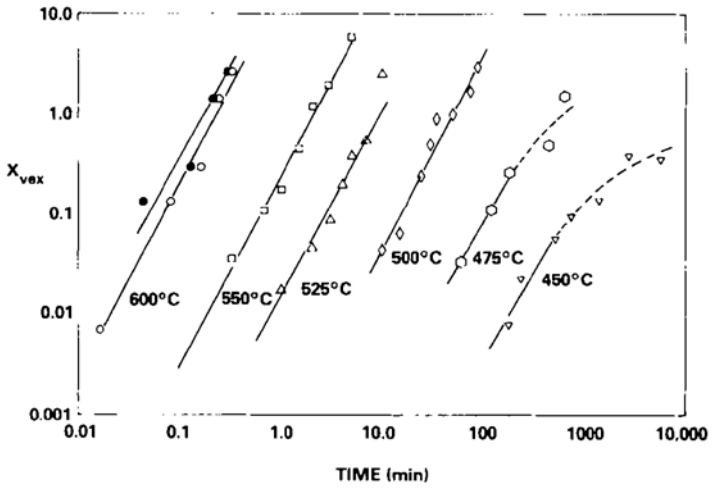

Fig. 2.3: Avrami plots of recrystallization kinetics in pure iron cold-rolled to 70% thickness reduction, reproduced from Vandermeer and Rath (1989).

2.2.2 Nucleation sites

It has been widely recognized that nucleation sites for recrystallization are not randomly distributed. Preferred nucleation sites in pure metals include original grain boundaries (especially triple junctions), transition bands and shear bands. This preference causes a clustering of recrystallizing grains. For example in cold-rolled metals, grains become laths after deformation, i.e. there are more boundaries parallel to the rolling plane, and recrystallizing grains are observed to cluster also in planes parallel to the rolling plane (Sükösd et al. 2007). The clustering of recrystallizing grains changes the recrystallization kinetics due to early impingement. The effects of clustered nucleation on recrystallization kinetics have been investigated and simulated (Storm and Juul Jensen 2009, Vandermeer 2005), showing obvious deviations from the JMAK model.

2.2.3 Growth of recrystallizing grains

The assumption of constant growth rates for all grains through the entire recrystallization process is not satisfied either. Fig. 2.4a is an example of measured growth rates of recrystallizing grains (Juul Jensen 1995a). First, grains with different orientations grow with different growth rates. The effects of orientation on the growth during recrystallization have been reviewed by Juul Jensen (1995b). Second, the growth rates usually decrease dramatically with time (e.g. Vandermeer and Juul Jensen 1994), although there are a few reports of constant growth rates (e.g. Li et al. 2007). In Fig. 2.4a, the growth rates decrease with time as $G = G_0 t^{-r}$, where r is around 1. The decrease of growth rates may be related to recovery for some samples, as suggested by Vandermeer and Rath (1989). The non-uniform distribution of stored energy is also considered as an important factor, as regions of high stored energy recrystallize first. This idea has been confirmed by measurements of the release of stored energy as a function of the recrystallized volume fraction (e.g. Hutchinson et al. 1989). The effects of the

variation within the deformation structures on the overall kinetics have been modeled by many researchers (e.g. Doherty et al. 1986, Vandermeer and Juul Jensen 2001, Rollett et al. 1989).

Recently the growth curves of individual grains have been measured by the 3D X-ray diffraction (3DXRD) technique (Lauridsen et al. 2000). Fig. 2.4b shows some typical growth curves in aluminum cold-rolled to 90% thickness reduction (Lauridsen et al. 2003). It was found that every grain had its own growth curve, and the growth rates of individual grains varied substantially as a function of annealing time. Based on these observations, Godiksen et al. (2007) simulated the effects of the distributions of growth rates on recrystallization kinetics, and observed obvious deviations from the JMAK model.

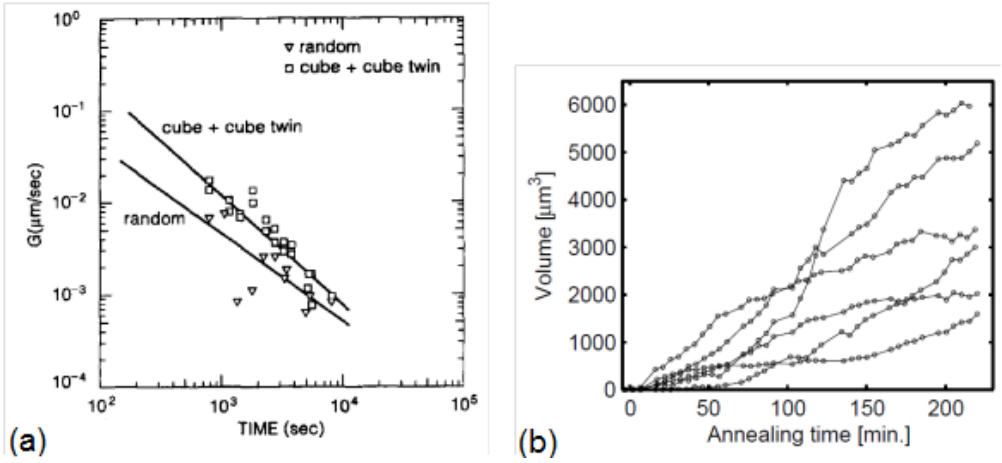

Fig. 2.4: a) Cahn-Hagel growth rates measured in copper cold-rolled to 92% thickness reduction and annealed at 121 °C, reproduced from Juul Jensen (1995a). Details of Cahn-Hagel growth rate determination are introduced in Chapter 4. b) A selection of growth curves of individual recrystallizing grains in aluminum cold-rolled to 90% thickness reduction, reproduced from Lauridsen et al. (2003).

2.2.4 Texture evolution during recrystallization

The replacement of a deformed volume by recrystallizing grains typically also involves texture changes, since the orientations of recrystallizing grains in most cases are different from the average texture of the deformation

structure. The texture after recrystallization has been a hot topic for many years, especially the origin of a strong cube recrystallization texture developed in many FCC metals with medium-to-high SFEs rolled to a high strain. There are basically two points of view: oriented growth (OG) and oriented nucleation (ON).

The OG theory attributes the strong cube recrystallization texture to cube grains growing faster than other grains. This has been related to the idea that special grain boundaries may have high mobility, and thus move faster. For example, boundaries with a 40°<111> misorientation or the so-called Σ7 boundaries have been observed to have a higher mobility (Beck et al. 1950). The cube orientation has a close to 40°<111> relationship with all 4 variants of the S orientation, which is the strongest texture component in FCC metals rolled to a high strain. The special boundary relation allows cube grains to grow faster, and thus form a strong cube texture after recrystallization. Another mechanism which contributes to the OG theory is the orientation pinning (Doherty et al. 1995, Juul Jensen 1995b). It comes from the idea that cube grains have less chance to form low misorientation angle boundaries (LABs) with the deformed matrix. The LABs have been proved to have low mobility (e.g. Viswanathan and Bauer 1973). Cube grains thus have less chance to be inhibited by these low mobility boundaries, and can therefore grow faster into the deformed matrix compared with other oriented grains.

The ON theory attributes the strong recrystallization texture to the preferential nucleation of recrystallizing grains of certain orientations. Ridha and Hutchinson (1982) suggested that cube grains developed from transition bands, where a cube oriented deformation structure is favorable for nucleation due to rapid recovery. Zaefferer et al. (2001) suggested that a continuous orientation gradient inside cube bands/subgrains is also favorable for nucleation of cube grains. Another mechanism among the ON theory is called micro-growth selection (Duggan et al. 1993). It suggested that the cube grains developed from cube bands/subgrains, which had 30-40° <111> relations with their immediate neighbors. The basic idea of this micro-growth selection mechanism is similar to that of the OG theory, i.e. the high mobility of

boundaries between a cube grain/subgrain and its neighbors with rolling textures.

2.3 Overview of the thesis

In this study, the recrystallization behavior of two types of deformed copper samples is investigated. The first sample is cold-rolled copper, which has been widely investigated. In particular, the formation mechanisms of a strong cube recrystallization texture have been discussed intensively. However, the formation of a strong cube texture is sensitive to many parameters, and the effects of individual parameters are not entirely clear. In this study, a large range of parameters is included concerning their effects on the recrystallization. Moreover, recrystallization kinetics of cube and noncube grains in samples forming or not forming a strong cube texture is investigated, in order to understand why the cube texture only becomes strong in one of the samples. The second sample is nanostructured copper processed by dynamic plastic deformation (DPD). DPD is a high strain rate deformation mode, which is effective in producing nanostructured materials. The deformation structure of a DPD sample is relatively complicated (Li et al. 2008a), and no systematic recrystallization kinetic study has been carried out for this sample. A sample processed by DPD and additional cold-rolling (DPD+CR) is also studied.

Chapter 3 introduces the characterization techniques applied in this study, including electron backscatter diffraction (EBSD), Vickers hardness tests, 3DXRD and a differential scanning calorimetry (DSC).

Chapter 4 reports the recrystallization of cold-rolled samples. A series of parameters is analyzed, concerning their effects on the recrystallization kinetics and on the textures after recrystallization. The initial grain size is found to be an important parameter. Recrystallization kinetics in samples with two different initial grain sizes, both cold-rolled to 90% thickness reduction, is compared. The formation of a strong cube recrystallization texture in the

initially fine grained sample is discussed. The recrystallization in a sample with significant widening during rolling and in a sample cold-rolled to 95% thickness reduction is also reported.

Chapter 5 reports the recrystallization in nanostructured copper samples processed by DPD. Particular attention is on the different recrystallization behaviors in different regions, connected with heterogeneities of the DPD sample. The recrystallization in the DPD+CR sample is studied, and compared with the DPD sample and the cold-rolled samples reported in Chapter 4. Mechanical properties of the DPD and the DPD+CR samples annealed to partial recrystallization are compared and discussed.

Chapter 6 summarizes the findings of the work and an outlook is also given in this chapter.

Chapter 3

Characterization techniques

This chapter introduces the characterization techniques used in this work. Experimentally, recrystallization kinetics is investigated by measuring the volume fraction of recrystallized material, V_V in a series of partly recrystallized samples annealed for different time periods at a given temperature. In this work, the electron backscatter diffraction (EBSD) technique was used. With this technique, microstructural and grain orientation information can be correlated, which provides information on the orientation dependence of the recrystallization kinetics. EBSD was also used to characterize deformation structures. 3DXRD technique was applied for the in-situ measurement of recrystallization kinetics of individual grains. In some samples, Vickers hardness tests were also used for analysis of the recrystallization kinetics. A DSC was used to measure the stored energy in the samples.

3.1 Electron backscatter diffraction

EBSD is a scanning electron microscope (SEM) based technique. The principles of this technique are illustrated in Fig. 3.1. When a focused electron beam hits the surface of a tilted crystalline sample, a backscatter pattern is generated, from which crystallographic orientation can be determined. Orientation maps can be obtained by an automatically controlled system, involving controlled movement of the stage or the beam, acquisition of diffraction patterns and indexing of the patterns.

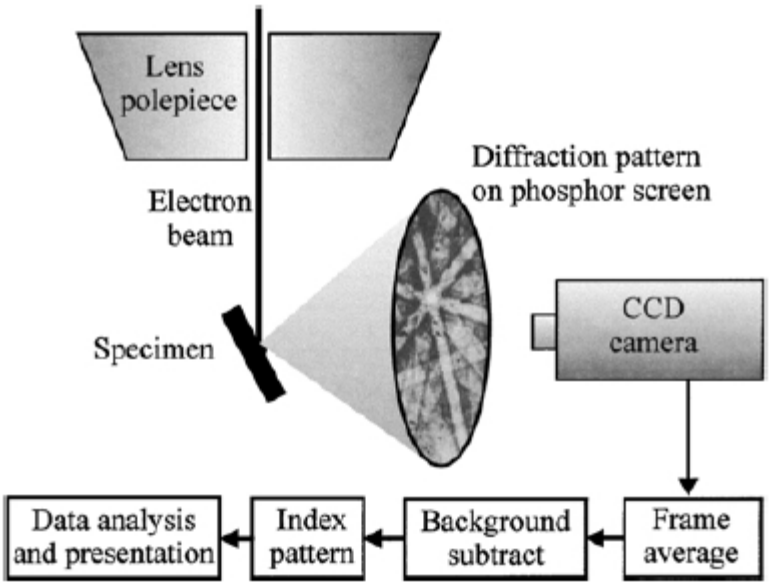

Fig. 3.1: Schematic diagram of a typical EBSD installation, reproduced from Humphreys (2001)

In the present work, a Zeiss Supra-35 FEG scanning electron microscope, equipped with an HKL Channel-5 EBSD system, was used. Samples for EBSD characterization were mechanically polished followed by electropolishing in a D2 electrolyte (30.5%wt phosphoric acid, 23.7%wt ethylene glycol and 45.8%wt water) at room temperature for 70 seconds with a potential difference of 5 V. The microscope was operated at an acceleration voltage of 20 kV. For rolled samples, longitudinal sections (containing the rolling and normal directions) were characterized and for compressed samples, cross sections (perpendicular to the compression plane) were characterized. For analysis of the recrystallized kinetics (i.e. characterization of partly recrystallized samples), a step size of 1 µm was used for the cold-rolled samples, and 0.5 µm for the nanostructured samples. Finer step sizes (30nm, 50nm) were used for characterization of the deformation structures.

The microstructures were reconstructed from the EBSD data. Unless otherwise stated, in this thesis, all orientation maps are colored according to the crystallographic direction of the normal direction (ND) of the rolled samples or the compression axis of the DPD samples. Low angle boundaries (LABs) are defined as boundaries with a misorientation between 2° and 15°,

which are shown by gray lines in the orientation maps. High angle boundaries (HABs) are defined as boundaries with a misorientation larger than 15°, which are shown by black lines in the orientation maps. Twin boundaries are shown by red lines. The cube, copper, brass and S texture components are considered in this study, and the texture components are defined using a maximum 15° deviation from the ideal orientations (see Tab. 2.1). In cases where an orientation is within 15° of more than one ideal orientation, the nearest ideal orientation is used. All orientations beyond the 15° deviation to these texture components are grouped as "other" texture.

Recrystallizing grains were identified automatically from the EBSD data by the DRG program developed previously for the same purpose (Wu and Juul Jensen 2008). The recrystallizing grains must fulfill the following criteria:

1) The pixel to pixel misorientation inside a recrystallizing grain should be smaller than 1°.
2) The grain size defined as the equivalent circular diameter (ECD) should be larger than a specific value. The minimum ECD which can be determined depends on the scanning step size. In this study, 3 μm and 1.5 μm were used for the cold-rolled and the nanostructured samples, respectively.
3) At least, part of the boundaries surrounding the recrystallizing grain should be HABs.

The recrystallized volume fraction V_V was calculated for each annealing time as the fraction of pixels assigned to recrystallizing grains. Since the samples were copper, typically a large density of twin boundaries develops inside recrystallizing grains. These twin boundaries were treated in two ways for defining recrystallizing grains: 1) as normal high angle boundaries 2) ignored (i.e. one grain and its twin parts are considered as one grain). The first method is termed the "consider twin boundaries" (CTB) method in the following. It can be used to determine the recrystallization kinetics of different textured grains. The second method is termed the "ignore twin boundaries" (ITB) method. It is more suitable for the overall recrystallization

kinetics investigation, since some small twin parts may not fulfill the size requirement, and are therefore considered unrecrystallized in the CTB method. In this work, both methods were applied.

3.2 3D X-ray Diffraction

The 3DXRD technique relies on the diffraction of monochromatic X-ray by crystalline samples. When the X-ray beam impinges under an angle θ_{hkl} to crystal planes of type *{hkl}*, and the wavelength λ fulfills the Bragg condition:

$$n\lambda = 2d_{hkl}sin\theta_{hkl} \tag{3.1}$$

the incoming X-ray beam will be diffracted by the crystal planes of spacing d_{hkl} with a diffraction angle $2\theta_{hkl}$. The sample is rotated around the vertical axis during the experiments to cover diffraction peaks from all/most grains. For metals with highly symmetric crystal lattices, such as FCC metals, the rotation range can be reduced without loss of information.

The 3DXRD concept includes a set of methods optimized for spatial, angular, or time resolution (Poulsen et al. 2004). In this study, a 3DXRD experimental set-up focusing on high time resolution was used, as illustrated in Fig. 3.2. True bulk characterization is ensured by use of high-energy X-rays from a synchrotron source (typically in the order of 40-100 keV). The penetration depth is several millimetres in copper. Another advantage of the high-energy X-rays is the small diffraction angles 2θ, which means that diffraction peaks from different crystal planes can be monitored simultaneously by a 2D detector. An X-ray transparent furnace was used to heat the sample during the measurements.

Fig. 3.3 shows a diffraction image after some annealing. This image shows 8 diffracted Debye-Scherrer rings which is largely formed by diffraction from the deformation structure. The variation of the intensities along the rings is related to the texture of the deformation structure. These Debye-Scherrer rings are referred to as the texture background in the following. Some sharp

diffraction peaks appear on top of this texture background. These peaks are from the diffraction of the recrystallizing grains. The intensities of the peaks are proportional to the volumes of the corresponding grains. The 3DXRD method monitors the growth of individual grains by measuring the intensity increase of these diffraction peaks.

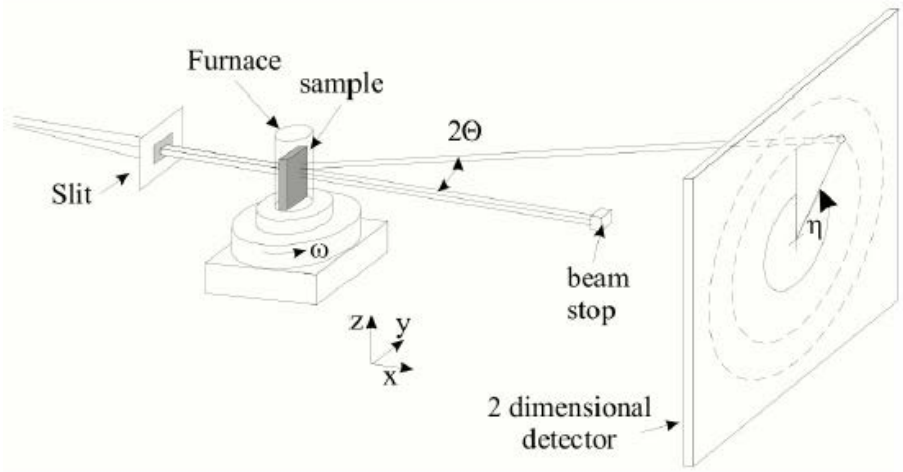

Fig. 3.2: Experimental set-up of the 3DXRD microscope for measuring growth curves, reproduced from Lauridsen et al. (2003).

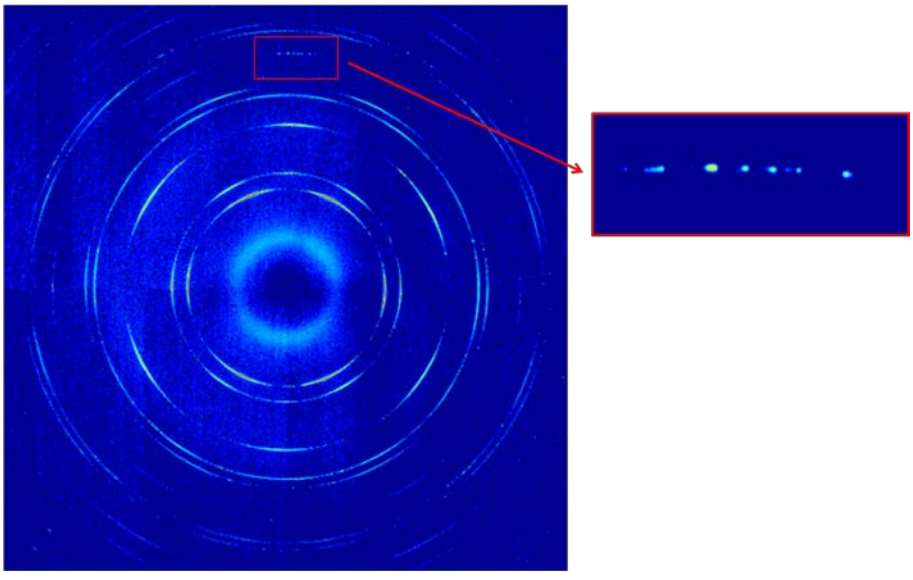

Fig. 3.3: Example of a diffraction image, showing the Debye-Scherrer rings arising from the deformation structure and a few sharp diffraction peaks from the recrystallizing grains.

The present 3DXRD experiments were conducted at beamline P07 PETRAIII at Deutsches Elektronen-Synchrotron (DESY). Samples were cut into dimensions of about 500 × 750 × 2000 μm^3, and were carefully electropolished to avoid nucleation from surface damage. The experimental details are listed in Tab. 3.1.

Tab. 3.1: Experimental details of the 3DXRD experiments.

Beam size	0.5 mm × 0.5 mm
X-ray energy	50 keV monochromatic
2D detector	2048 × 2048 pixels Pixel size 200 × 200 μm^2
Distance between sample and detector	~ 600 mm
Rotation range of the sample stage (ω)	0° to 30°
Rotation interval	0.5°
Exposure time	0.5 s
Time resolution	5.7 minutes

During the measurements, the X-ray transparent furnace heated the sample at one preset temperature. The sample was rotated from 0° to 30° at intervals of 0.5°, and at the same time diffraction images were taken during the rotation. The stage was rotated back to the 0° position after all 61 images comprising a full rotation had been acquired, and the rotation repeated automatically until the measurement was stopped manually. For each sample, the measurement included 18~42 full sweeps over 30°. The rotation range of 30° is a conventional choice used in several previous experiments (e.g. Poulsen et al. 2011), which covers diffractions from most of the grains. In this work, it is not required to determine the precise orientations of the diffraction peaks, but a good time resolution (time between images with the same ω position) is needed. A relatively large rotation interval is therefore suitable. However, recrystallization textures are strong in some of the samples, so on the other hand the rotation interval may not be too large. Otherwise diffraction peaks may overlap. In this study, a 0.5° rotation interval was used and the time resolution for the 30° sweep (61 intervals) was thus about 6

minutes. A 50 keV monochromic X-ray beam was employed. The beam size was defined by the opening of the slits (500 × 500 μm^2). The illuminated sample volume (V_{gauge}) at ω=0° position was around 500 × 500 × 750 μm^3, which changed with the ω position of the stage. The slits were opened to 600 × 600 μm^2 every 6 sweeps (around every 30 minutes), acquiring diffraction images for one sweep over 30°, and were moved back to the normal size again. If a recrystallizing grain had grown out of the illuminated gauge volume, the intensity of the diffraction peak would show an abrupt increase when the slits were open, and would drop back when the slits were moved back to the normal dimensions. Grains growing out of the illuminated gauge volume could thus be excluded during the data analysis. The distance between the sample and the detector was about 600 mm, and diffraction peaks from 8 crystal planes ({111}, {200}, {220}, {311}, {222}, {400}, {331} and {420}) were recorded. With this set-up, no information on shapes or positions of the grains is obtained. It is therefore not possible to know if a grain has impinged on other grains. Because of this, it was decided to anneal the samples only slightly (20%-30% recrystallized), so that the impingement was not severe during the measurements.

The processing of the 3DXRD data consists of three major parts:

1) Detect diffraction peaks and determine their intensities
2) Transform peak intensities to grain sizes
3) Determine the orientations of the recrystallizing grains corresponding to the diffraction peaks

The Debye-Scherrer rings were first transformed to lines by polar transformation of the raw diffraction images using the FIT2D program (Hammersley 2012). The polar transformed Debye-Scherrer rings were then summed over their width in 2θ (i.e. along the radial direction in the diffraction images) to give one-dimensional profiles. The positions and widths of the diffraction peaks were determined from the profiles of the last 30° sweep, i.e. from the measurement of the most recrystallized state, which were then traced back to the one-dimensional profiles at the same sample rotation angle ω at earlier annealing times to find the corresponding peaks

from the same grains. The intensity of a peak was integrated over the peak width. The local texture background was calculated as the average intensity of four neighboring points of the peak (two points in each side) in the one-dimensional profile, and it was subtracted from the profile of the peak.

The intensity of a diffraction peak I_{grain} is given by (Warren 1990):

$$I_{grain} = I_0 \left(\frac{d\varpi}{dt} \right)^{-1} \frac{\lambda^3 r_0^2}{v_{Cu}^2} \frac{\left|F_{hkl}\right|^2 P_{hkl}}{\sin 2\theta_{hkl} \left|\sin \eta\right|} V_{grain} \tag{3.2}$$

where I_0 is the incoming intensity, $d\omega/dt$ is the angular velocity of the sample rotation during each interval, λ is the X-ray wavelength, r_0 is the Thomson scattering length, v_{Cu} is the unit cell volume of copper, F_{hkl} is the structure factor, P_{hkl} is the polarization factor, η is the azimuthal angle of the diffraction peak (see Fig. 3.2) and V_{grain} is the volume of the diffracting recrystallizing grain. All material parameters can be found in the literature, but the incoming intensity I_0 is unknown. The general way for determination of I_0 is by measuring the diffraction intensities of a powder sample and using the following relationship:

$$I_{powder} = I_0 t \frac{\lambda^3 r_0^2}{v_{Cu}^2} \frac{m_{hkl} \left|F_{hkl}\right|^2 P_{hkl}}{4 \sin \theta_{hkl}} V_{gauge} \tag{3.3}$$

where t is the exposure time and m_{hkl} is the multiplicity of the $\{hkl\}$ reflection. In this study, a powder sample was not available. Instead, the deformed samples were used. The deformed samples were scanned over 360° rotations before annealing. The average integrated intensity of a Debye-Scherrer ring of the deformed sample $(I_{def})_{average}$ is approximately equal to the intensity of a non-textured powder sample, i.e. I_{powder}. It should be noted that during rotation, the gauge volume changes as a function of ω position. I_{powder}/V_{gauge} was then estimated by $(I_{def}/V_{gauge})_{average}$. The grain volume was therefore calculated as:

$$V_{grain} = \frac{d\varpi}{dt} \frac{t}{2} m_{hkl} \cos \theta_{hkl} \left|\sin \eta\right| \frac{I_{grain}}{(I_{def} / V_{gauge})_{average}} \tag{3.4}$$

The volumes were converted to equivalent sphere diameters (ESDs) as

$$d = \sqrt[3]{6V_{grain}/\pi} \tag{3.5}$$

The growth curves of the individual grains were plotted as the changes of ESDs as a function of annealing time in the following chapters. The nucleation time was determined from the growth curves as the time corresponding to the first nonzero ESD. The growth curves were fitted by spline functions, and growth rates were calculated as the slopes of the fitted spline functions.

The position of the diffraction peak has a one to one correlation with the diffraction plane of the recrystallizing grain, and a diffraction peak can be plotted in the corresponding pole figure by a stereographic projection of the scattering vector. Identification of the full crystallographic orientation of each recrystallizing grain requires correlating more than one diffraction peak (Lauridsen et al. 2001). In this study, strong recrystallization textures were developed in some samples, i.e. many recrystallizing grains have similar orientations, which make it very difficult to correctly identify diffraction peaks for a single grain. Therefore, a simple approach was used based on the partial orientation information from just one diffraction peak. Recrystallizing grains were classified into different texture groups according to the projections of their diffraction peaks in the pole figure. For simplicity only the {200} and {400} diffraction peaks were considered. The diffraction peaks were divided into two groups: cube and noncube. The diffraction peaks were classified as from cube recrystallizing grains if the projections of the peaks fell within 10° from that of the ideal cube orientation in the pole figure. The {200} and {400} diffractions are very suitable for cube texture analysis, since such peaks from cube grains appear always in the diffraction images with η around 0°, 90°, 180° and 270°. Furthermore, a large number of twins form during recrystallization for the copper samples, and individual {111}, {220} and {222} diffraction peaks may include contributions from one grain and some of its twins, while {200} and {400} diffraction peaks do not have this problem.

It has to be noted that the detection limit in this experiment is not as good as in EBSD, which is related to the background of the acquired diffraction images and the data processing. As mentioned previously, the recrystallizing grains were identified from the diffraction images collected during the last 30° sweep. Only diffraction peaks with a certain integral intensity in the last sweep (i.e. above a minimum size) were included in the present data processing. Otherwise, a large number of noisy growth curves would be collected, which required too much manual work to select valid curves. According to Eq. 3.2, intensities of cube peaks for η near 0° and 180° are enhanced. Therefore, the detection limit for cube grains may be smaller than that for other grains. In general, a grain needs to reach a size limit of about 5-10 µm to be included in the analyses. It should however be noted that since the peaks were traced back to an earlier time, the initial stage of individual recrystallizing grains (i.e. grains with sizes below the 5-10 µm) can still be recorded as long as the local background noise is not too strong.

3.3 Vickers Hardness test

The Vickers hardness test indents the material with a diamond indenter of pyramidal shape, with a square base and an angle of 136° between opposite faces (Fig. 3.4). By measuring the diameters of the indentation (d1 and d2 in Fig. 3.4), the hardness (kgf/mm^2) is calculated as:

$$HV = 2F \sin\frac{136°}{2} / \left(\frac{d_1 + d_2}{2}\right)^2 \tag{3.6}$$

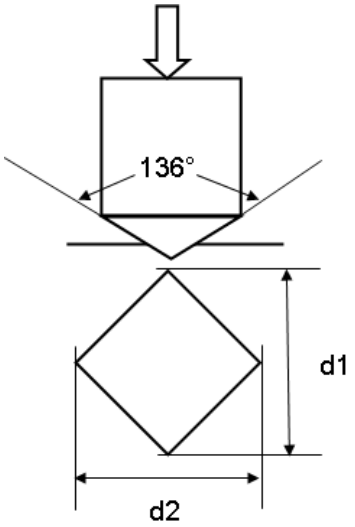

Fig. 3.4: A sketch of the Vickers hardness test and the indentation formed.

In this study, a Struers DuraScan fully automatic hardness tester was used. A load of 200 g was applied for 10 s during the tests. The recrystallized volume fraction V_V is estimated from the hardness as follows:

$$V_V = \frac{HV_{def} - HV}{HV_{def} - HV_{rex}} \tag{3.7}$$

where the HV_{def} and HV_{rex} are hardness values of the sample in the deformed and fully recrystallized state. Although a hardness test is an indirect measurement of V_V, it gives relatively good estimation of V_V for copper (Richards et al. 1956, Woldt and Juul Jensen 1995).

3.4 Differential scanning calorimetry (DSC)

DSC measures the temperatures and heat flows associated with transitions in materials as a function of time and temperature in a controlled atmosphere. In this study, a Perkin-Elmer DSC-7 system was used. Samples were heated at a constant heating rate of 20 K/minute in an argon atmosphere. The sample was heated twice at the same heating rate, and the characteristic DSC curve was obtained by subtracting the second curve from the first. An accurate DSC measurement can be used for a recrystallization kinetics

investigation (e.g. Woldt 1992). In this study DSC measurements were only used for determination of the overall stored energy.

Chapter 4
Recrystallization in cold-rolled samples

This chapter reports the recrystallization kinetics in samples rolled to 90% and 95% thickness reductions. It begins with a summary of various materials and rolling parameters, and their effects on the recrystallization kinetics and the recrystallization textures. The recrystallization kinetics was investigated in detail in two samples with coarse and fine initial grain sizes both cold-rolled to 90% thickness reduction. The formation of the cube recrystallization texture is discussed. Recrystallization behaviors in a sample with significant widening during rolling and in a sample rolled to 95% thickness reduction are also reported.

4.1 Materials and the rolling process

Three batches of oxygen free high conductivity (OFHC) copper (Batch A, B and C) were used for the present study. The chemical compositions were slightly different, as measured by optical emission spectroscopy (Tab. 4.1). The three batches of copper were pretreated thermo-mechanically to obtain weak initial textures and various initial grain sizes (Tab. 4.2). In order to facilitate reading, the different starting materials will be named as follows: the first letter (A, B and C) represents the chemical composition, and the second letter (I and II) is used to differentiate the states before rolling, connecting with the pretreatment. It has to be noted that the as-received

material of Batch C had already been cold-rolled to 50% and 95% reductions, and had been stored at room temperature for 27 years. The samples were reported to have a random texture and a grain size of 35 μm before rolling (Juul Jensen 1983). The Batch C sample cold-rolled to 95% reduction was used directly for the recrystallization investigation. The one cold-rolled to 50% reduction was annealed to obtain another initial material (CII) with a grain size of 20 μm. The volume fractions of the cube component in the initial materials are listed in Tab. 4.2. The volume fractions of the cube component are very low, except that the sample AI has a weak cube texture before rolling.

Tab. 4.1: Chemical compositions (wt - %) of OFHC copper used in this study.

	Cu (%)	Fe (%)	Ni (%)	Mg (%)	Al (%)	Ag (%)	Zn (%)
A	99.9	0.003	0.002	0.002	0.003		<0.001
B	99.9	<0.001	0.002	0.002	0.002		<0.001
C	99.9	<0.0006	0.003			0.005	0.002

Tab. 4.2: List of initial materials: pretreatments, initial grain sizes and initial volume fractions of the cube component.

Materials	Pretreatment	Initial grain size (μm)	volume fraction of the cube component
AI	As received	78	15.6%
BI	Annealed at 650 °C for 2 h	77	3.5%
BII	BI cold-rolled to 50% reduction, and annealed at 450 °C for 1 h	22	2.0%
CI	N/A	35	N/A
CII	CI cold-rolled to 50% reduction, and annealed at 450 °C for 2 h	20	2.4%

Two rolling mills with different roll diameters (340 mm and 75 mm) were utilized. They are referred to as the big and the small rolling mills in the following. The rolling speed was between 80 to 90 mm/s for both. The rolling processes were controlled to ensure a homogeneous rolling condition, i.e. the ratio of contact length over average thickness L/h was between 0.5 and 5. The

definitions of L and h are shown in Fig. 4.1. This condition is to avoid too severe through thickness texture gradients (Truszkowski et al. 1980). Oil lubrication was applied for all the samples (except the CI sample, where the rolling condition is unavailable) to reduce surface friction.

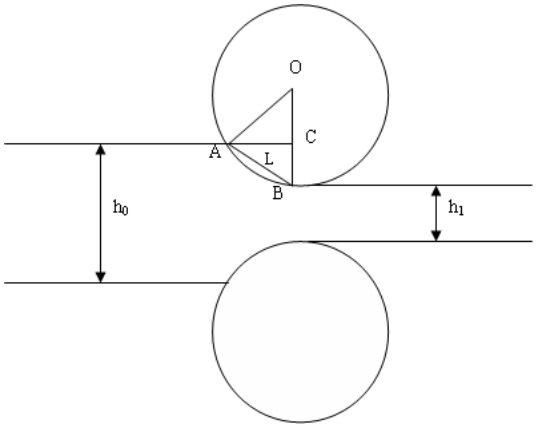

$$\frac{L}{h} = \frac{\sqrt{r(h_0 - h_1)}}{(h_0 + h_1)/2} \tag{4.1}$$

Fig. 4.1: Rolling geometry and the definition of ratio of contact length over thickness (L/h).

It is normally assumed that rolling is equivalent to plane strain compression, i.e. that there is no change in the sample dimension along the transverse direction (TD). However, when the initial TD dimension of the sample is small, significant widening during rolling may be observed. The relative widening (W) is defined as

$$W=(w-w_0)/w_0 \tag{4.2}$$

where w_0 and w are the sample widths before and after rolling, respectively. The relative widening is related to the sample widths, the roll dimensions and rolling strains, as shown in Fig. 4.2. The amount of relative widening increases roughly linearly with the thickness reduction. Samples BII3 and BII4 have similar specimen dimensions, but were rolled in different rolling mills. The big rolling mill produces a much larger widening compared with the small one. To avoid significant relative widening when rolled in the big rolling mill, a sample needs a larger initial width, such as for BII5. It has to be noted that the absolute widening w-w_0 is around 4 mm in both the BII4 and BII5 samples after 90% reduction, which were both rolled in the big rolling

mill, but with different initial sample widths. This observation is consistent with the statement of Bunge (1970) that the absolute widening varies only a little with the width of the rolled sheet when the other parameters are identical.

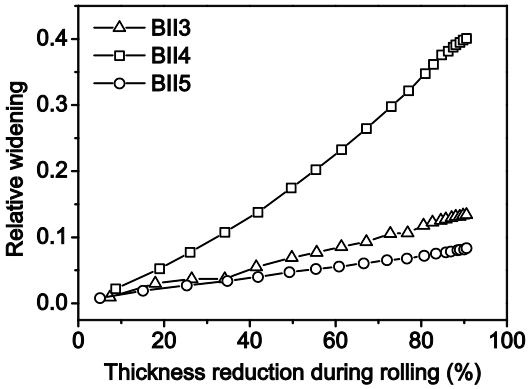

Fig. 4.2: Relative widening as a function of thickness reductions in samples BII3, BII4 and BII5. Initial dimensions of the samples are listed in Tab. 4.3. The thicknesses of the three samples are identical. BII3 and BII4 have similar widths, while BII5 is much wider. Sample BII3 was rolled in the small rolling mill (75 mm rolls), while BII4 and BII5 were rolled in the big rolling mill (340 mm rolls).

4.2 Effects of initial parameters

It has long been recognized that the strength of the cube texture in cold-rolled copper after subsequent recrystallization is sensitive to various initial parameters (Wassermann and Grewen 1962). The effects of individual parameter are, however, still not absolutely clear. In this work, the development of the cube texture in a series of samples with different initial parameters was investigated quantitatively. Tab. 4.3 summarizes details of the samples investigated. The volume fractions of the cube recrystallization texture vary from 3% to 81% over the samples in the table. The recrystallization kinetics is also very different. Most of the samples in the table were cold-rolled to 90% thickness reduction. For simplicity, the strains of the samples will only be indicated for samples rolled to other than 90% reductions. For example, the BI1 sample cold-rolled to 90% reduction is

Tab. 4.3: List of samples with different initial parameters. The recrystallized volume fractions V_V and the volume fractions of the cube texture component after recrystallization under different annealing conditions are summarized. In samples that are still not fully recrystallized with the longest annealing time, the volume fraction of the cube recrystallization texture is calculated as $V^0_{V,cube} = V_{V,cube} / V_V$. The CTB method was used.

sample	specimen dimensions before rolling thickness (mm) × width (mm)	rolling				room temperature storage (years)	annealing										
							150 °C			167 °C			230 °C			450 °C	
		strain	widening	D_roll (mm)	remark		time (h)	V_V	$V^0_{V,cube}$	time (h)	V_V	$V^0_{V,cube}$	time (h)	V_V	$V^0_{V,cube}$	time (h)	$V^0_{V,cube}$
AI1	20 × 49	90%	11%	340	1*					337	0.918	3.3%	4	0.915	3.9%		
		90%	17%	340	1*		192	0.749	3.6%				1	0.953	6.0%		
																2	32.8%
BI1	20 × 42	95%	18%	340	1*					6	0.825	14.1%	1	0.992	10.3%	2 (a)	27.7%
BI2	N/A	95%	N/A	340	N/A	2							1	0.992	13.6%	2	34.0%
BI5	5.4 × 10.7	90%	13%	75	1*								1	0.957	4.8%		
BII1	9.3 × 13.4	90%	39%	340	1*		24	0.827	13.1%				1	0.970	13.5%		
		73%	11%	75	1*								1	0.916	2.9%		
BII3	5.2 × 10.5	90%	13%	75	1*								1	0.977	52.2%		
BII4	5.2 × 11.2	90%	40%	340	1*								1	0.959	18.0%		
BII5	5.2 × 44.1	90%	8%	340	1*		4	0.847	48.5%				1	0.982	51.2%		
BII_IMR1	5.2 × 10	90%	13%	75	1*								1	0.994	52.5%		
BII_IMR2	5.2 × 10	90%	14%	75	2*								1	0.993	58.4%		
BII_IMR3	5.2 × 10	90%	10%	75	3*								1	0.985	56.9%		
CI1	N/A	95%	N/A	N/A	N/A	27							1	0.972	75.6%	2	81.0%
													1	0.890	4.0%		
CII1	6.9 × 12.6	90%	37%	340	1*								1 (b)	0.877	3.8%		

1*. unidirectional, turn over every pass

2*. unidirectional, keep one surface up

3*. reverse, keep one surface up

samples BII_IMR series were rolled with a different mill at IMR, Shenyang, China

a: pre-annealing at 230 °C for 1 h

b: pre-annealing at 100 °C for 24 h

noted as BI1, while the same sample rolled to 95% reduction is noted as BI1_95cr.

Impurity content. AI1 and BI1 have similar initial grain sizes but slightly different impurity contents. In these samples cold-rolled to 90% reductions, the cube recrystallization textures are both very weak. There have been reports that a minor difference of some impurity contents can change the recrystallization texture completely (e.g. Hansen et al. 1981, Ridha and Hutchinson 1982). However, in the present work the different impurity contents in AI1 and BI1 do not have strong effects on the cube texture development during recrystallization. Furthermore, AI1 has a slightly stronger initial cube texture compared with BI1. Doherty et al. (1995) suggested that some cube texture in the initial material might be maintained during rolling, which was favorable for the development of the cube texture after recrystallization. However, the different initial texture does not significantly affect the development of the cube recrystallization texture in these two samples. The recrystallization process is slower in AI1, which can be expected from the larger impurity content.

Initial grain size. The BI1 and BII5 samples have different initial grain sizes. A strong cube texture is developed in BII5, which has a finer initial grain size. A dependence of the cube texture on the initial grain sizes has been reported earlier (Wassermann and Grewen 1962, Ryde et al. 1990, Sindel et al. 1990). Ryde et al. (1990) found that the initial grain size for the transition of the recrystallization texture from a cube texture to a noncube texture was at about 35 μm, which agrees well with the present observation. However, there are also several reports on the development of a strong cube recrystallization texture in samples with initial grain sizes of 50 μm to 100 μm after about 90% cold-rolling (Necker et al. 1991, Ridha and Hutchinson 1982). The different dependence of the cube texture on the initial grain size may be related to the different sample impurity contents. The recrystallization kinetics is also much faster in BII5, which develops a strong cube recrystallization texture. This is consistent with observations of Hutchinson et al. (1989).

Widening. Sample BII4 and BII5 were rolled under identical conditions, except that the initial sample width of BII4 was smaller. The relative widening in BII4 and BII5 are 40% and 8%, respectively. A strong cube recrystallization texture is developed in BII5, while the cube development in BII4 is much weaker. Similarly, the cube texture is less developed in sample BII1 and CII1, both of which have relative widening of more than 35%. In all the other samples of the BII series, the relative widening is between 10%-20%, and the cube recrystallization texture is strong. In aluminum, it was reported that a significant widening was unfavorable for the development of the cube texture during recrystallization (Mao 1990). On the other hand, the complete elimination of widening as in a channel-die compression has also been found to reduce the strength of the cube recrystallization texture (Hammelrath et al. 1991). In general, samples in Tab. 4.3 can be divided into two groups: widening samples (BII1, BII4 and CII1, with relative widening of more than 35%) and no widening (or better normal widening) samples (for all the other samples, the relative widening was less than 20%). When comparing BII1 and BII5, the recrystallization kinetics is observed to be retarded in the widening sample.

Strain. Sample BI1 was rolled to 90% and 95% reductions. Although the cube recrystallization texture is weak in both samples, the volume fraction of the cube component increases slightly with increasing strains. Additionally, a strong cube recrystallization texture is developed in BII3, but the cube recrystallization texture is still rather weak in BII3_73cr. The volume fraction of the cube component does not increase linearly with strain in the present samples. Instead, it shows a large increase when the strain reaches a certain threshold. This observation is consistent with that of Necker et al. (1991) and Gerber et al. (2003).

Annealing temperature. The BI1, BII1 and BII5 samples were annealed at 150 °C and 230 °C. After annealing, the samples are all fully or almost fully recrystallized, without obvious grain growth. The different annealing temperatures do not significantly affect the volume fractions of the cube component. The average grain sizes obtained after recrystallization at

different temperatures are similar, also. A long time low temperature annealing (100 °C 24 h) was applied to sample CII1 before the annealing at 230 °C. This low temperature pre-annealing does not change the volume fraction of the cube component either. It is therefore concluded that the cube recrystallization texture in the present series of samples is not very sensitive to the annealing temperatures.

Sample BI1_95cr was annealed at 450 °C for 2 h, during which grain growth occurred. The fraction of the cube component is about 30%, while that in the same sample after 230 °C annealing is only 10%. In order to figure out whether this increase is related to the very high temperature or the subsequent grain growth, the same sample was annealed at 230 °C for 1 h (almost fully recrystallized) before the 450 °C annealing. A similar fraction of the cube component was obtained with and without pre-annealing. This demonstrates that, it is the grain growth following the recrystallization, instead of the high temperature, that causes the strengthening of the cube texture.

Other rolling conditions. Rolls of two different dimensions were used. It is observed that as long as no significant widening appears, the roll dimension does not have important effects. The BII_IMR series samples were processed under unidirectional and reverse rolling, but they develop similar cube texture after recrystallization.

Shear texture. The CI1_95cr sample develops the strongest cube texture after recrystallization, but this strong cube texture is only in the central region, which is about 250 μm thick. In the surface layers (150 μm thick each side), the cube recrystallization texture is very weak (Fig. 4.3c). The different recrystallization textures originate from the different deformation textures in the surfaces and in the center. {111} pole figures in Fig. 4.3 show that the deformation texture of the center is the typical rolling textures for pure copper, while that of the surface is characterized by a {001}<110> shear texture. Details of the rolling process are not available for this sample. The shear texture in the surface is usually related to the friction between the rolls

and the material and/or the rolling geometry. It has been suggested that the influence of the friction is usually limited to a thin surface layer (<50 μm) (Asbeck and Meching 1978), and it is therefore more likely that the appearance of the surface shear texture is due to the ratio of contact length over thickness L/h out of the homogeneous range (Truszkowski et al. 1980). All the other samples in Tab. 4.3 were rolled following the homogeneous rolling requirement, and no through thickness variations were observed in either the deformation textures or recrystallization textures.

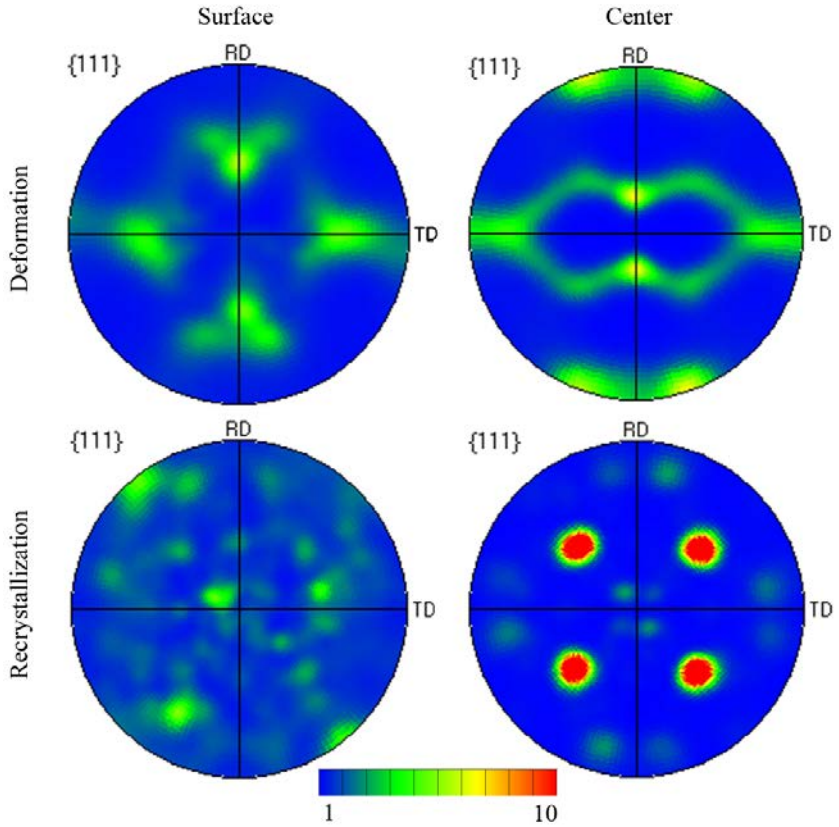

Fig. 4.3: {111} pole figures showing the deformation textures of the CI1_95cr sample in the surfaces and the central layer and the recrystallization textures in the surfaces and the central layer.

Storage. BI2_95cr and CI1_95cr samples had been kept at room temperature for extended periods of time before furnace annealing. The textures after recrystallization are very similar in BI2_95cr and BI1_95cr. The 2 years room temperature storage has very limited effects on the recrystallization textures. The CI1_95cr sample was kept for very long time. It was observed that recrystallization had begun during the long term room

temperature storage. In particular, some large cube grains together with their twins were observed in the central layer. Recrystallization was not obvious in the surfaces. It was however not clear whether the microstructure had recovered, since the fresh rolled microstructure was not available.

As a summary, among all the parameters discussed above, the initial grain size, the widening and the strain have strong effects on the recrystallization textures and the recrystallization kinetics.

4.3 Recrystallization kinetics and microstructural evolution in samples with different initial grain sizes

In the following, the recrystallization of BI1 and BII5 is investigated and compared. These two samples were both cold-rolled to 90% thickness reduction without significant widening. The initially fine grained sample (BII5) develops a strong cube texture after recrystallization, while the coarse one (BI1) does not. The formation of the cube texture during recrystallization will be discussed in particular.

4.3.1 Deformation textures and microstructures

After being cold-rolled to 90% reduction, both BI1 and BII5 samples developed typical rolling textures. The volume fractions of important texture components are listed at Tab. 4.4. The deformation textures of the two samples are similar, and the fractions of the rolling texture components (copper, S and brass components) are 76% and 77% respectively for BI1 and BII5. Sindel et al. (1990) found that the deformation texture in an initially large grained sample was less sharp, which is not observed in this work. This may be related to the significantly different grain sizes in their samples (500 µm vs. 50 µm), while the grain size is not so different in BI1 and BII5 (77 µm vs. 22 µm). In both samples, a small amount of cube texture existed in the deformation structures. The existence of a cube texture in the deformation

structure has been observed in many cold-rolled FCC metals (e.g. Duggan et al. 1993, Zaefferer et al. 2001, Alvi et al. 2008). The cube texture may arise from transition bands (Dillamore and Katoh 1974) or grains with cube or near cube orientations in the initial material (Doherty et al. 1995).

Tab. 4.4: Deformation and recrystallization textures in BI1 (coarse) and BII5 (fine). The recrystallization textures were measured in the 150 °C annealed samples. It has to be noted that both samples are not fully recrystallized after the longest annealing time (192 h for BI1 and 4 h for BII5), and the volume fraction of each texture component is calculated as $V_{V,i}^{0} = V_{V,i} / V_V$

Sample	State	cube	copper	brass	S	other
BI1	Deformation	1%	14%	22%	40%	22%
	Recrystallization	4%	5%	5%	19%	67%
BII5	Deformation	2%	16%	19%	42%	21%
	Recrystallization	48%	1%	3%	15%	33%

The deformation structures of BI1 and BII5 are shown in Fig. 4.4 and 4.5. On an overall scale the microstructures are composed of bands with different orientations, while on a smaller scale each band is composed of cell blocks bounded by microbands (MBs) or lamellae bounded by lamellar boundaries (LBs). In both samples, some relatively wide bands with different orientations can be observed, which may be related directly to the initial grains. The widest band observed in Fig. 4.4 and 4.5 is around 10 µm and 4 µm for BI1 and BII5, respectively. Considering that the sample thickness has been reduced to 1/10, this is in general consistent with the initial grain sizes. Some bands have widths less than 1 µm, and it is thus difficult to distinguish their initial grain boundaries. The microstructures of both samples consist of a high density of LABs and HABs. The structural parameters are listed in Tab. 4.5. After rolling, the spacing of HABs along the normal direction (ND) has been reduced below 1 µm in both samples, while that along the rolling direction (RD) is more than twice that of the one along the ND. The spacing of HABs is smaller in BII5, which is due to the initial grain sizes. The variation within the microstructures can be analyzed by defining high misorientation regions

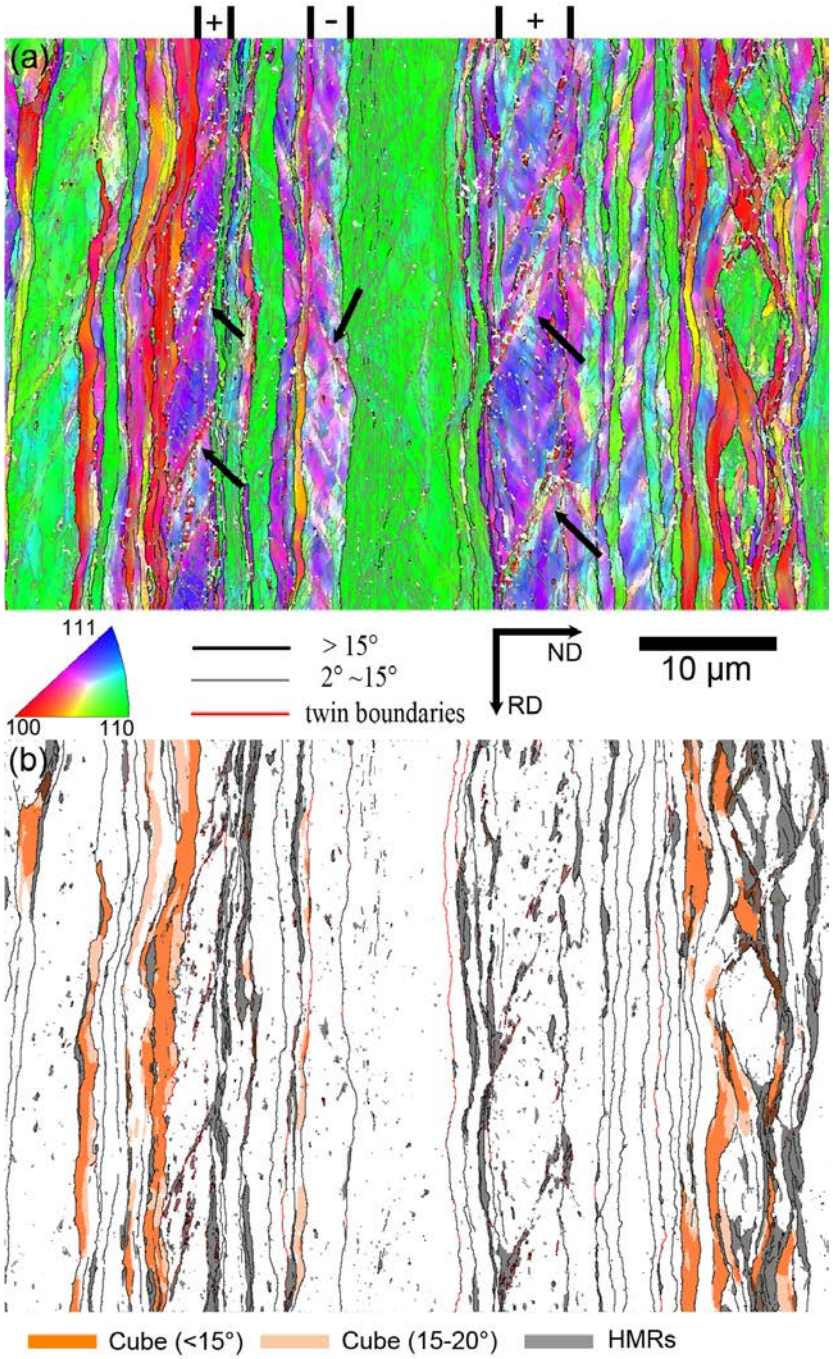

Fig. 4.4: a) Deformation structure of BI1, colored according to the crystallographic direction of the ND; both microstructures are composed of bands with different orientations; some bands with localized shear bands (LSBs) are marked, the +/− represents the directions of the LSBs. Further introduction of the +/− pattern can be found in the next paragraph in the main text. Some of the LSBs are indicated by the black arrows. b) The same map as a) with HMRs highlighted in gray, and cube oriented regions in orange; regions of a near cube texture (15°-20° deviation to the ideal cube orientation) are shown in light orange. The LABs are not shown in b).

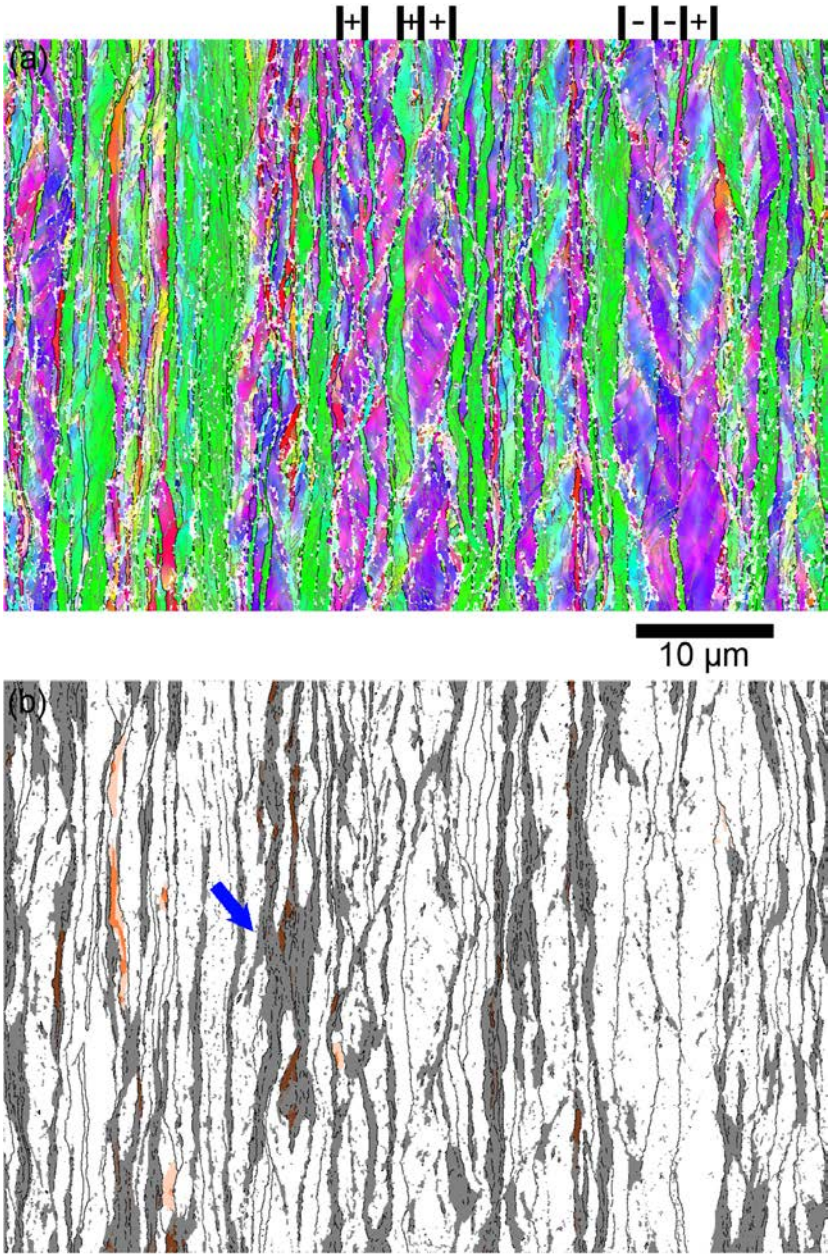

Fig. 4.5: a) Deformation structure of BII5. The color coding and the sample coordinates are the same as those in Fig. 4.4a. Some bands with LSBs are marked by +/− according to the directions of the LSBs. b) The same map as a) with HMRs, cube texture regions and near cube texture regions highlighted in the same manner as Fig. 4.4b. A typical large HMR with cube segments inside is marked by the blue arrow in b).

(HMRs) as suggested by Mishin and Godfrey (2008). The HMRs are defined as regions containing subgrains surrounded by boundaries with a minimum misorientation of 5° and with a maximum size of 2.5 µm^2. The fraction of HMRs in BII5 is more than twice that in BI1 (see Tab. 4.5, Fig. 4.4b and Fig.

4.5b). The HMRs represent high stored energy regions to some extent, since stored energy can be calculated from the density of dislocation boundaries (Godfrey et al. 2007) and high misorientation boundaries have a higher energy-per-unit area than the low misorientation boundaries according to the Read-Shockley equation (Read and Shockley 1950). The stored energy measured by DSC is also higher in BII5.

Tab. 4.5: Microstructural parameters in BI1 and BII5 rolled to 90% thickness reduction. The stored energies were measured by DSC.

	Spacing of HABs along the ND (nm)	Spacing of HABs along the RD (nm)	Fraction of HABs	Fraction of HMRs	Stored energy (J/g)
BI1	896	2106	23%	13%	0.59
BII5	647	1438	34%	32%	0.72

In some bands, shear bands are observed to cut through the bands at around +/− 35° to the RD. These shear bands may form high misorientation boundaries with the other parts of the band. Unlike the macroscopic shear bands that usually extend through several grains or sometimes the entire sample, most of the shear bands in these two samples are limited inside one band, although they may introduce some disturbances at the boundaries of the band and/or neighboring bands. In this study, these shear bands are termed localized shear bands (LSBs) to distinguish from the macroscopic shear bands (such as those developed in low SFE metals or alloys). It needs to be noted that the bands with LSBs tend to have structures containing cell blocks bounded by MBs rather than lamellar structures.

The LSBs are most often observed in bands with copper or S orientations (purple bands in Fig. 4.4 and 4.5), and are rarely observed in brass orientated bands (some of the green bands). The preference of LSBs in copper oriented grains has been reported by many authors through single crystals or bi-crystal investigations (Driver et al. 1994, Liu et al. 1995, Godfrey et al. 2001), although they are termed shear bands or localized glide bands. This preference has also been reported in polycrystals (Duggan and Lee 1992, Hughes 2000, Chang and Duggan 2010). In one band, the LSBs always lie

roughly parallel to each other. The directions of the LSBs observed in this work change systematically with the symmetric variants of the orientation of the bands. Taking the ideal copper orientation as an example, there are two orientation variants (see Tab. 2.1), which can be referred to as copper-I ((112)[11-1] and (-1-1-2)[-1-11]) and copper-II((112)[-1-11] and (-1-1-2)[11-1]). If a clockwise rotation to the RD is defined as a + pattern, and an anticlockwise one as a − pattern, the LSBs observed in copper-I oriented bands are always with a + pattern, and those in copper-II oriented bands are always with a − pattern. The S oriented grains have a similar relationship of a +/− pattern, except that there are four variants of S, which can be grouped into two types.

The links of the LSBs with the S/copper oriented bands and with the orientation variants imply that they may be related to the specific slip activities in these bands. In FCC metals under plane strain compression, four slip systems, including a co-directional (CD) slip system and a co-planar (CP) slip system are activated in both copper and S orientated grains. At lower strains (e.g. around 50% cold-rolling reduction), two sets of asymmetric boundaries form within copper/S grains (Godfrey et al. 1998b). One set of closely spaced boundaries are from the co-directional (CD) slip system, while another set of coarse spaced boundaries are from the co-planar (CP) slip system. Wagner et al. (1995) suggested that localized shear might occur at previously formed CP boundaries, and develop into shear bands. Morii et al. (1985) proposed a similar mechanism that a layered dislocation structure, such as the coarsely spaced boundaries from the CP system, facilitated the formation of shear bands. In this study, the LSBs form always at the same +/− direction as the boundaries from the CP slip system, and the mechanisms above could well explain this dependence. The absence of LSBs in brass oriented bands could also be explained, since brass grains deform relatively homogenously, and do not form asymmetric CP boundaries at low strains (Godfrey et al. 1998a). It however needs to be noted that the mechanisms mentioned above are based on single crystal investigations. There are very few systematic investigations on the microstructural evolution in

polycrystalline copper cold-rolled to high strains, especially the orientation dependence.

It was suggested that the tendency for shear banding increased with increasing grain size (Ridha and Hutchinson 1984, Korbel et al. 1986). However, this tendency is not obvious when comparing Fig. 4.4 and 4.5.

Regions with a cube texture are observed in both samples (Fig. 4.4b and 4.5b). The cube regions can form long cube orientated bands with lamellar structures or be short segments inside or between other bands. In BI1, the cube regions tend to be relatively long and wide bands. For such cube bands, usually only parts of the bands are within 15° to the ideal cube orientation, i.e. belong to a cube texture, while other parts are oriented further away from the ideal cube orientation. These long cube bands are very likely to originate from initial cube grains as suggested by Doherty et al. (1995). In BII5, more short and narrow cube segments can be observed. It is interesting to note that a lot of the short cube segments fall inside the HMRs in BII5. In BI1, there have been much less HMRs, and only a few cube regions in the right part of Fig. 4.4b are located inside HMRs, while most cube bands are not.

4.3.2 Microstructural evolution and recrystallization textures

The onset of recrystallization is observed in BI1 only after 1 h annealing at 150 °C. As shown in Fig. 4.6a, most nucleation occurs in the purple bands, i.e. copper/S oriented bands, while it is hard to find recrystallizing grains in the green bands, i.e. brass/other oriented bands. In some bands, the recrystallizing grains can be unambiguously identified as nucleating in the LSBs, since a chain of grains lie along the LSBs aligned around 35° to the RD. These grains tend to grow faster inside the LSBs and therefore become elongated shaped along the direction of the LSBs. The map shown in Fig. 4.6a was scanned with a step size of 1 µm, which is too large to show the LSBs. However, the direction of the chains of the recrystallizing grains reproduces well the +/− pattern of the LSBs. A preferred nucleation in the LSBs has been reported previously (Ridha and Hutchinson 1982, Duggan and

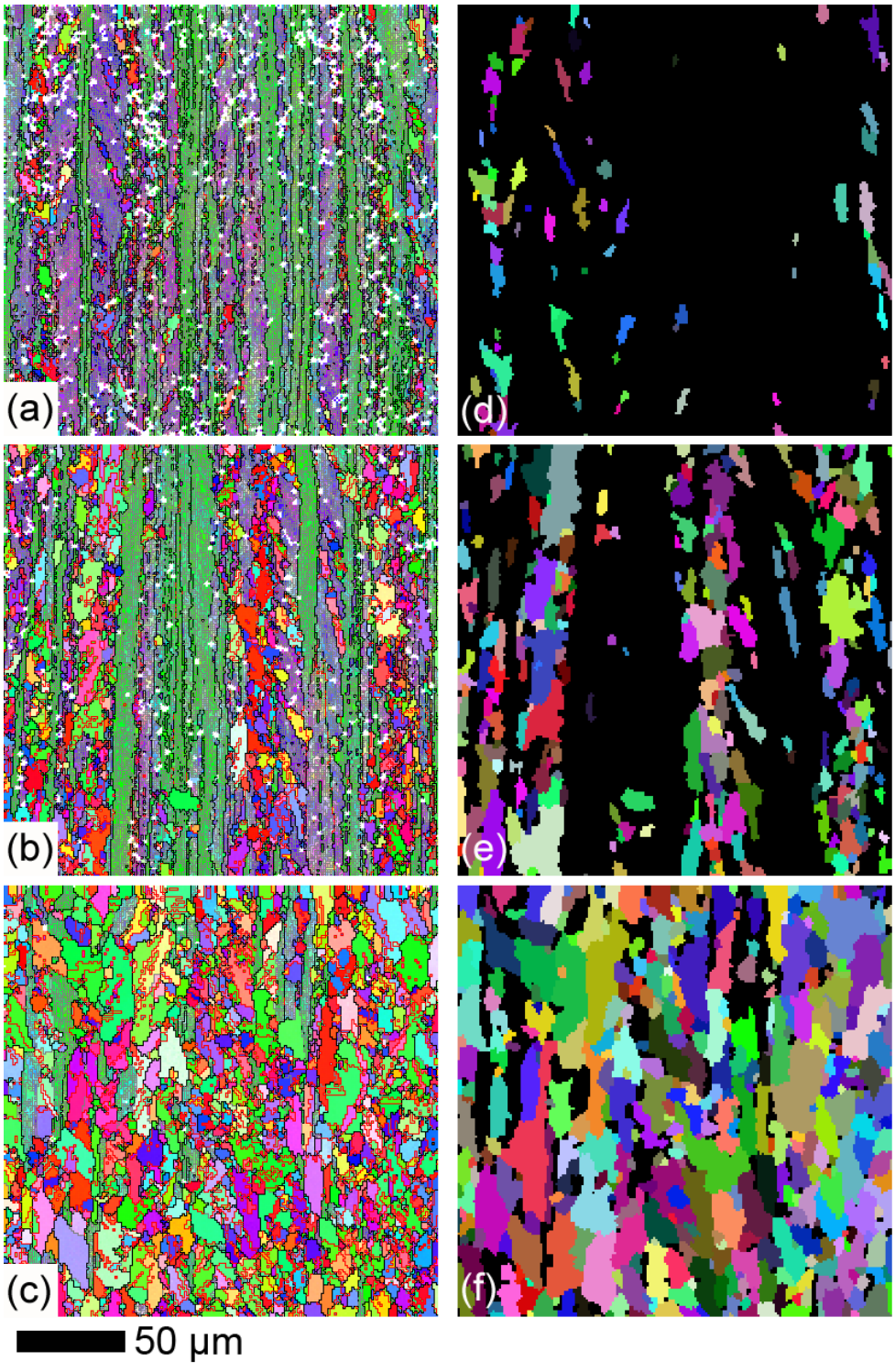

Fig. 4.6: Microstructures of BI1 after 1 h (a), 12 h (b) and 192 h (c) annealing at 150 °C. The color coding and the sample coordinates are the same as those in Fig. 4.4a. Most recrystallizing grains shown in red in a-c belong to the cube texture. Maps d-f highlight the recrystallizing grains in a-c, respectively. The ITB method was used for grain definition, i.e. a grain and its twins are shown in the same color.

Lee 1992). This preferential nucleation and growth of recrystallizing grains in the LSBs should be related to the higher stored energy. As shown in Fig. 4.4, the LSBs are often within HMRs. Godfrey et al. (2007) reported that the stored energy in LSBs was higher than in other parts of the deformed matrix.

After longer time annealing (12 hours in Fig. 4.6 b and e), recrystallizing grains appear in more bands. At this stage, some bands have almost been completely replaced by recrystallizing grains, which impinge on each other inside the bands. However, there are still some bands without nucleation, and most of them are brass/other oriented bands. Recrystallizing grains observed in BI1 have very scattered orientations. The 192 h annealed sample is almost completely recrystallized. The remaining deformed matrix exists as isolated islands, and most of it is of a brass texture. The stability of the brass oriented bands (i.e. less favorable for recrystallization) should be related to the difficulty of both nucleation and growth in these bands. Unfavorable nucleation has been observed by Godfrey et al. (2001) for brass textured single crystals, but they reported very fast growth rates if additional nucleation sites were provided by surface damage. Unfavorable growth of recrystallizing grains in brass bands has, however, been observed in many polycrystals (e.g. Alvi et al. 2008).

The recrystallization in BII5 is much faster. After only 5 minutes annealing at 150 °C, some recrystallizing grains are observed; a few with a grain size bigger than 10 μm (see Fig. 4.7a). The recrystallizing grains can be roughly divided into two groups according to the sizes. The large grains have an elongated shape along the RD, with their size along the RD larger than 20 μm. Most of them are of a cube texture. The number of large grains is limited, but they make a large contribution to the V_V due to their sizes. The small grains can be considered as the other group. The grain orientations within this group are more scattered. These small recrystallizing grains have a certain tendency of clustering into bands. At least part of these grains can be identified as nucleating in the LSBs.

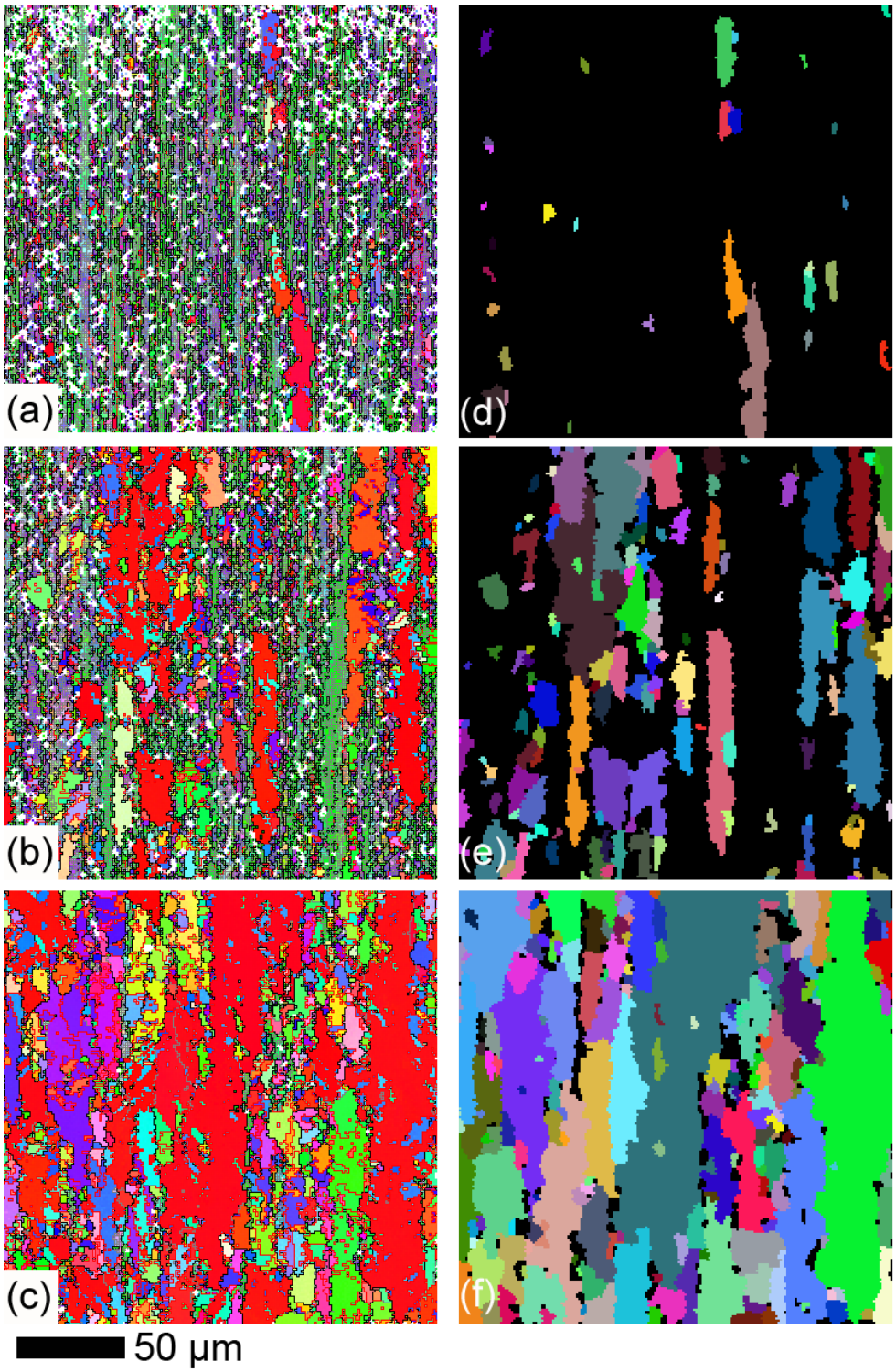

Fig. 4.7: Microstructures of BII5 after 5 minutes (a), 30 minutes (b) and 4 h (c) annealing at 150 °C. The color coding and the sample coordinates are the same as those in Fig. 4.4a. Most recrystallizing grains shown in red in a-c belong to the cube texture. Maps d-f highlight the recrystallizing grains in a-c, respectively. The ITB method was used for grain definition.

After longer time annealing (30 minutes in Fig. 4.7b and e), more and larger cube grains are observed. In this map, those large cube grains also show some tendency of clustering along both RD and ND. However, considering the large sizes of these grains and their elongated shape, this clustering tendency might be a misleading impression. A more objective descriptor of the clustering is needed for an unbiased conclusion. The microstructure of the almost fully recrystallized samples consists of large grains of an elongated shape (some of which are huge) and small grains, which are more equiaxed. Most of the large grains belong to a cube texture, but a few grains with other/rolling textures can also have relatively large sizes. Similar to BI1, most of the remaining deformed matrix are isolated brass oriented bands.

The clustering of recrystallizing grains can be quantified by the contiguity ratio:

$$C_{\alpha\alpha} = 2S_{V,\alpha\alpha} / (2S_{V,\alpha\alpha} + S_{V,\alpha\beta}) \tag{4.3}$$

where $S_{V,\alpha\alpha}$ is the volume density of boundaries between two recrystallizing grains, and $S_{V,\alpha\beta}$ is that of boundaries between recrystallizing grains and the deformed matrix. This parameter was proposed by Gurland (1958) and applied later for describing clustering of recrystallizing grains by Vandermeer (2005). If the recrystallizing grains are randomly distributed, $C_{\alpha\alpha}$ increases with the V_V along the theoretical random curve shown in Fig. 4.8 (Rios et al. 2006). A positive deviation from this "random curve" is an indication of a clustering of recrystallizing grains. As shown in Fig. 4.8, the $C_{\alpha\alpha}$ of BII5 follows roughly the theoretical curve, while that of BI1 has an obvious positive deviation at low Vv. The positive deviation at low V_V has been found in many samples rolled to large strains (Vandermeer 2005, Alvi et al. 2008), and can be related to a tendency of clustered nucleation into bands in these samples. The $C_{\alpha\alpha}$ of BI1 approaches the random curve for large V_V, which should be related to the fairly random distribution of recrystallizing grains along the ND. The $C_{\alpha\alpha}$ of BII5 falls even below the random curve for large V_V. A negative deviation from the random curve is related to an ordered

system (Vandermeer 2005). The negative deviation in BII5 may be from the remaining brass islands, which may be distributed in a close to ordered manner. It has to be noted that the hot-rolled aluminum alloy reported by Alvi et al. (2008) had clustered nucleation ($C_{\alpha\alpha}$ similar to BI1) and developed a strong cube recrystallization texture. However, in the present BII5 sample, which also develops a strong cube texture, the spatial distribution of recrystallizing grains is rather random. The different spatial distributions of recrystallizing grains in the hot-rolled aluminum and in BII5 imply that the mechanisms of the cube texture formation may be very different.

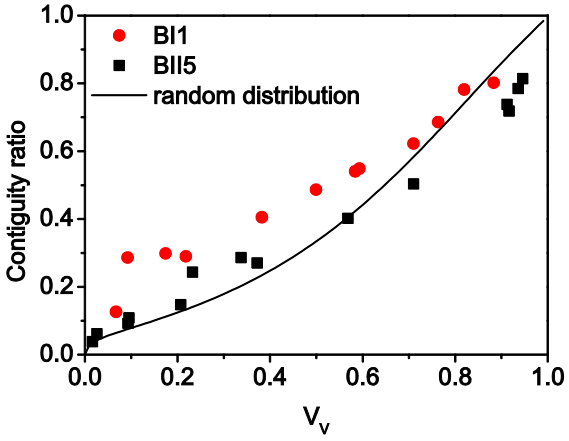

Fig. 4.8: Contiguity ratio $C_{\alpha\alpha}$ as a function of the recrystallized volume fraction V_V for BI1 and BII5. The ITB method was used for this analysis, i.e. annealing twin boundaries are not included as $S_{V,\alpha\alpha}$. The bold curve shows the theoretical contiguity ratio for randomly distributed recrystallizing grains (Rios et al. 2006).

As listed in Tab. 4.4, the recrystallization texture in BII5 is characterized by a strong cube texture. The cube texture in BI1 is however very weak, and the strongest recrystallization texture component is the S.

The microstructures in Fig. 4.6c and 4.7c indicate that the size advantage of some cube grains in BII5 is important for the strong cube recrystallization texture. Fig. 4.9 shows the size distributions of cube grains in the 192 h and 4 h annealed BI1 and BII5 samples, respectively, in which the area fraction instead of number frequency is reported to emphasize large grains. Grains of the rolling and other textures are grouped as noncube grains, and their size

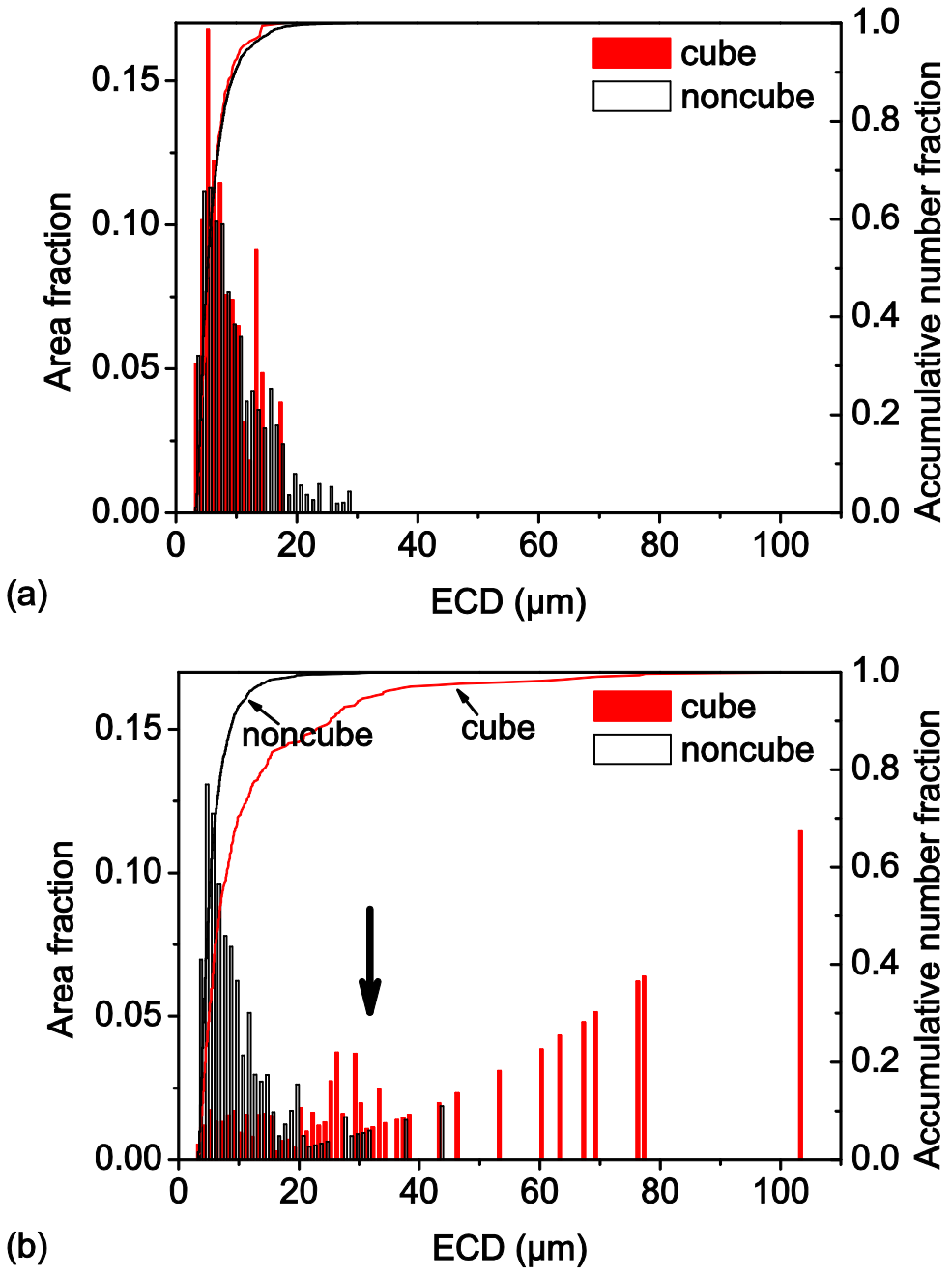

Fig. 4.9: The size distributions of cube and noncube recrystallizing grains in a) BI1 after 192 h annealing at 150 °C and b) BII5 after 4 h annealing at 150 °C. The histograms represent area-weighted size distributions, while the curves represent accumulative number frequencies. The critical size of supercube grains is marked by the arrow in b). The CTB method was applied here.

distributions are plotted in the same figures as references. The size distribution of cube grains in BI1 is limited to sizes below 20 μm, and this distribution is even narrower than that of noncube grains. The size distributions of both cube and noncube grains in BII5 are apparently

composed of two parts: the left and the right part. Each bin in the left part of the histogram contains contributions from several grains, while that in the right part contains only one or two grains. The right part in the size distribution of cube grains is much broader than that of noncube grains, i.e. large grains have a higher area fraction in cube grains. It should be noted that most of the huge grains extend outside the scanned area because of the elongated shape, and their sizes are even underestimated in the present size distribution. The curves of accumulative number fraction shows that 90% of the cube grains have sizes less than 23 μm, and huge grains are a minority in the cube population. If 5 times of the medium cube size is used to separate huge cube grains from the other cube grains in BII5, the critical size is 33 μm. This critical size lies also approximately at the border between the left and the right part of the histogram. We here name these huge cube grains supercube grains to emphasize their contributions to the strong cube recrystallization texture in BII5. In the early literature, large cube grains of an elongated shape were reported in copper samples that developed a strong cube recrystallization texture after cold-rolling (Wassermann and Grewen 1962).

4.3.3 Statistical analysis of recrystallization kinetics

The decrease of the hardness as a function of annealing time at different temperatures is shown in Fig. 4.10. For both samples, there is no significant softening prior to recrystallization. This observation is consistent with that by Cook and Richards (1946) in cold worked copper. It implies that there is limited recovery before recrystallization in these samples. The evolution of V_V is calculated from the hardness values using Eq. 3.7, and plotted in an Avrami plot in Fig. 4.11. The V_V measured from EBSD data for 150 °C annealed samples are plotted in the same figures. The V_V obtained from EBSD and hardness are very close for BI1. For BII5, these two sets of data are also close, except for the first two points, where V_V from the hardness data are lower than those from EBSD. Considering that the plot is on a log-log scale, the difference is actually not so big. In general, V_V estimated

indirectly from the hardness is consistent with the direct measurements by EBSD for the two samples, as has been suggested by Woldt and Juul Jensen (1995) for cold-rolled copper. For BI1, the Avrami plots in Fig. 4.11a are roughly linear. The exponents n are around 1 for 190 °C, 200 °C and 210 °C, while the exponent is lower for 150 °C annealing. For BII5, the Avrami plots are also roughly linear, except that an obvious downwards deviation from a straight line is observed in the 160 °C annealed sample for long time annealing. Considering that the data points at an intermediate stage are most reliable, a straight line is fitted only to the four points in the middle. The exponents for the three temperatures are then all around 1. Woldt and Juul Jensen (1995) found an exponent n around 3 for cold-rolled copper at the initial stage of recrystallization, but their data had a large downwards deviation from the linear line afterwards. A low exponent n around 1, which is similar to the observation in this study, was reported by Hansen et al. (1981) for copper cold-rolled to 95% reduction.

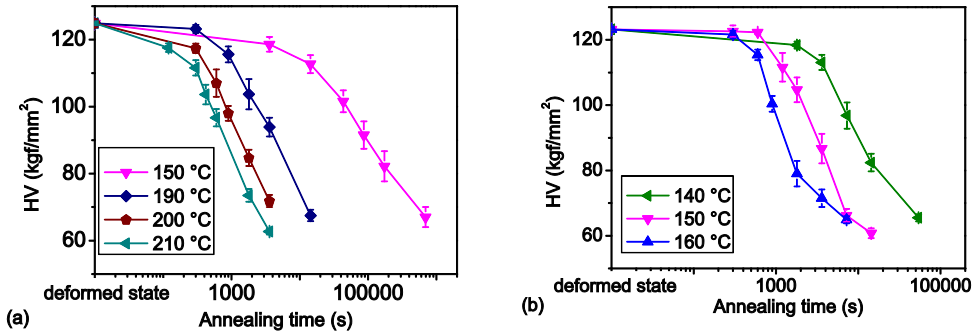

Fig. 4.10: Vickers hardness vs. annealing time for a) BI1 and b) BII5. The error bars show standard errors.

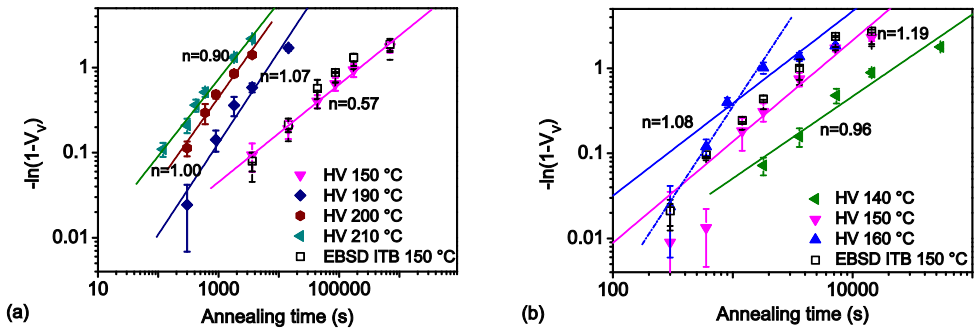

Fig. 4.11: Avrami plots of the recrystallization kinetics, i.e. $-\ln(1-V_V)$ vs. time on a log-log scale for a) BI1 and b) BII5. The error bars show standard errors.

The temperature dependence of the recrystallization time (Fig. 4.12) follows an Arrhenius-type relation:

$$t_R = t_0 \exp(Q_{Rex} / RT) \tag{4.4}$$

where Q_{Rex} is the activation energy of recrystallization, t_R is the characteristic time for recrystallization, R is the gas constant. The Q_{Rex} determined from the slope of Fig. 4.12 is around 150 kJ/mol for BII5. For BI1, the Q_{Rex} is 133 kJ/mol. However, if the point from 150 °C annealed sample, in which the exponent n is significantly different from the others, is excluded, the Q_{Rex} is very close to that for BII5. The values for Q_{Rex} reported previously have a large variation, which is partly due to the different impurity contents. For 3N copper (99.9% purity), the Q_{Rex} varies from 85 kJ/mol to 170 kJ/mol (Jägle and Mittemeijer 2012). The activation energy values observed in this study are between the activation energy for core diffusion (117 kJ/mol) and that for self diffusion (197 kJ/mol) for pure copper.

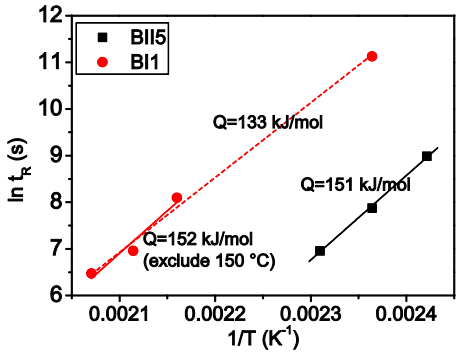

Fig. 4.12: Temperature dependence of the characteristic time t_R for recrystallization, and here t_R is determined as the time for V_V=0.5.

The density of recrystallizing grains per unit volume N_V is derived from the average grain size D (by line intercepts) as (Lü et al. 2011):

$$N_V = 16V_V / 9\pi D^3 \tag{4.5}$$

Fig. 4.13 plots the change of N_V as a function of the annealing time. The density of recrystallizing grains, when the ITB method was applied, increases with annealing time until the saturation of N_V occurring at round V_V=0.5 in both samples. At the initial stage, the nucleation in both samples is close to

the situation of a constant nucleation rate. The saturated N_V is about 3 times in BI1 compared with BII5. The CTB method measures a higher grain density in both samples. The increase of N_V measured from the two methods follows a similar route, but the saturation of N_V is postponed when twins are considered as separated grains. This indicates that twinning continues when no new grains nucleate, which is reasonable, since annealing twins continue to form during the growth. The saturated N_V determined by the CTB method is 3 and 5 times that by the ITB method in BI1 and BII5, respectively. A possible reason for the higher ratio in BII5 may be the large number of tiny twins within the very large grains, such as supercube grains. The evolution of N_V with time in BII5 agrees in general with that reported by Vandermeer and Juul Jensen (1995) in copper cold-rolled to 92% thickness reduction, which also developed a strong cube recrystallization texture.

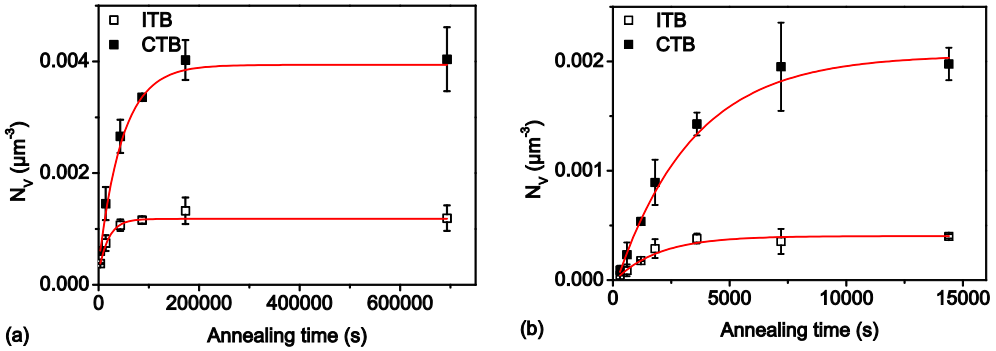

Fig. 4.13: Evolution of volume density of recrystallizing grains N_V in a) BI1 and b) BII5 both annealed at 150 °C. The error bars show standard errors.

The N_V of cube grains (CTB) is 1.8×10^{-4} µm^{-3} and 2.1×10^{-4} µm^{-3} in the BI1 and BII5 at the end of recrystallization. The N_V of cube grains is similar in the two samples. The number fraction of cube grains over all the grains is about 4% and 10%, respectively in BI1 and BII5. Doherty (1997) suggested that a fraction of cube grains (15° deviation) much larger than 2.5% is an indication of oriented nucleation. The fraction of cube grains in BII5 fulfills to a certain extent this criterion. However, as argued in the previous section, the exact nucleation density is found not to be so important, since the strong cube recrystallization texture in BII5 comes from a few supercube grains. The volume density of supercube grains can be calculated similarly. In BII5, the

N_V of supercube grains is 3.8×10^{-5} μm^{-3}, which corresponds to only 18% of the total cube population.

The average growth rates of the recrystallizing grains are calculated using a methodology firstly suggested by Cahn and Hagel (Cahn and Hagel 1962), which eliminates the effects of impingement between recrystallizing grains. The Cahn-Hagel (C-H) method was later extended to include determination of average growth rates of grains of different texture components by Juul Jensen (1992). The extended C-H growth rates are determined as follows:

$$\langle G \rangle_i = (dV_{V,i}/dt)/S_{V,i} \tag{4.6}$$

where $S_{V,i}$ is the volume density of boundaries between recrystallizing grains of each texture component and the deformed matrix, determined from the EBSD data by line intercepts. The $dV_{V,i}/dt$ is the increase of recrystallized volume fraction of each texture component over a short time *dt*. It is determined by fitting the evolution of $V_{V,i}$ as follows:

$$V_{V,i} = V_{V,\infty}(1 - \exp(-\exp(A + B \cdot \ln(t) + C \cdot (\ln(t))^2))) \tag{4.7}$$

where *A*, *B*, *C* and $V_{V,\infty}$ are fitting constants. $dV_{V,i}/dt$ is determined from these fitting constants. The average growth rates for each texture component in BI1 and BII5 samples are plotted in Fig. 4.14 a and b. In both samples the average growth rates decrease with time as $G = G_0 t^{-r}$ except the points for the longest annealing time. It should be noted that the points at the end of recrystallization have large experimental uncertainties because S_V is very low in these high V_V samples. The exponent *r* is around 1 for all the texture components in both samples. Cube grains show an obvious growth advantage in BII5, by a factor around 2. In the BI1 sample, the average growth rates of cube/rolling/other grains are very similar to each other, and no obvious growth advantage is found for cube grains.

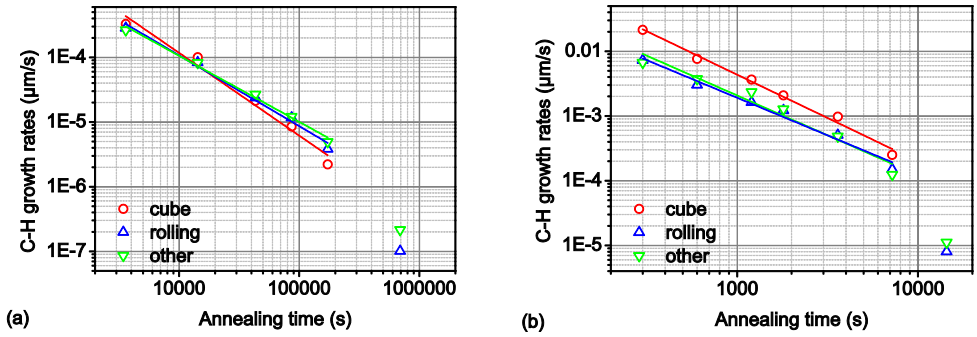

Fig. 4.14: Average Cahn-Hagel (C-H) growth rates for grains of cube/rolling/other texture components in a) BI1 and b) BII5, determined for samples annealed at 150 °C. The CTB method was applied.

If the decrease of the average growth rates G with annealing time is taken into consideration, the traditional JMAK model can be expressed as:

$$V_V = 1 - exp\left[f \int_0^t \dot{N} (Gt)^3 dt \right] \tag{4.8}$$

where $\dot{N}$ is the nucleation rate, and f is a shape factor. A rough estimation of the present two samples can be carried out by assuming a constant nucleation rate and $G = G_0 t^{-1}$. This simplified assumption gives an exponent of 1, which agrees well with the measurement for BII5. For BI1, the measured exponent n is less than 1. This may firstly be caused because the nucleation rates are not constant over time, i.e. the nucleation situation is between the two limiting cases of site saturation and a constant nucleation rate. Secondly, the recrystallizing grains are not randomly distributed as shown in Fig. 4.8.

The estimation above demonstrates that the decrease of growth rates with annealing time is important for the low exponent n in the JMAK equation. The decrease of C-H growth rates with annealing time has been reported in many metals, e.g. silicon iron (English and Backofen 1964, Speich and Fisher 1966), aluminium and copper (Juul Jensen 1995b). Moreover, the measurement of growth rates in silicon iron and in copper by these authors also shows time dependence as t^{-1}, similar to those in the present samples. Dehoff (1986) demonstrated that one dimensional growth lead to that the average boundary migration rate decreased as t^{-1} at long times. However, one dimensional growth produces needle shaped grains, which is not true for the

present samples, as can be seen in the microstructures in Fig. 4.6 and 4.7. Recovery could also lead to a decrease of growth rates (Vandermeer and Gordon 1963, Price 1989). However recovery is not significant in copper (Cook and Richard 1946, see also Fig. 4.10). The variation within the microstructure of a deformed sample is the most likely explanation for the decrease of growth rates. Regions with high stored energy recrystallize first, while regions with low stored energy are hard to recrystallize. Hutchinson et al. (1989) measured the release of stored energy in a copper sample deformed to 93% thickness reduction, and found that the release of stored energy was faster at an early stage of recrystallization. However, Necker et al. (1991) found that the stored energy decreased linearly with increasing V_V in their copper deformed to 90% reduction. In this work, the deformation structures of both samples show a non-uniform distribution of stored energy, as demonstrated by the HMRs in Fig. 4.4b and 4.5b. In BI1, recrystallization occurs first in high stored energy regions (e.g. the LSBs in copper and S oriented bands), and the deformed matrix recrystallizing last belongs to a brass texture, which has been reported to have a low stored energy (e.g. Godfrey et al. 2007). In BII5, the remaining bands after the longest annealing time are also brass oriented. The release of stored energy is thus slower towards the end of recrystallization, i.e. there is no linear relationship between the stored energy and V_V in the present samples. It is therefore reasonable to consider the non-uniform distribution of stored energy as an important factor for the decreasing growth rates. However, the distributions of stored energy in BI1 and BII5 seem to be different, but the growth rates of both samples show the t^{-1} dependence. The coincidence of the time dependence in these two samples, as well as in some other metals mentioned above, is still an open question. It is interesting to mention an extreme growth condition proposed by Hansen et al. (1981) and Juul Jensen (1983) for explaining a low kinetics exponent n around 1: recrystallizing grains grow to a certain limiting size instantaneously. If this growth condition is combined with a constant nucleation rate, the average C-H growth rates decrease then as t^{-1}. Nevertheless, this needs further investigations to determine whether such

an extreme growth condition is valid. For example, growth curves of individual grains determined by 3DXRD can be used for testing this assumption, although they cannot get rid of the effects of impingement. In general, all these possible explanations for the decreasing growth rates have an identical basic idea behind them: with the development of recrystallization, the fraction of rapid moving boundaries decreases, while that of slowly moving or even immobile boundaries increases.

4.3.4 Recrystallization kinetics of individual grains

The BI1 and BII5 samples were in-situ annealed at 165 °C and 130 °C respectively for approximately 250 minutes during the 3XRD experiments. At the end of the experiments, both samples were around 25% recrystallized, estimated from the hardness curves in Fig. 4.10. There are 980 and 825 valid growth curves identified respectively in BI1 and BII5, out of which 149 and 101 growth curves were considered as coming from cube peaks (see Section 3.2 for the definition of cube and noncube peaks). Fig. 4.15 plots a few typical growth curves of BI1 and BII5. The growth curves vary from grain to grain. Large variations of individual growth curves have also been seen in aluminum samples cold-rolled to different strains (Lauridsen et al. 2003, Poulsen et al. 2011, Wu and Juul Jensen 2012). Compared with aluminum, in which almost all recrystallizing grains appear at the beginning of recrystallization, the nucleation time of recrystallizing grains in these two copper samples shows larger variations. Some recrystallizing grains appear at the beginning of recrystallization, while some grains have a significant incubation time before nucleation. Most grains tend to have a large growth rate right after nucleation, followed by a period during which the growth rate decreases. A few grains, such as the one marked in Fig. 4.15b exhibit a stagnation period, after which they continue to grow. It should be noted that many grains have already reached a stable size, although V_V is only around 25% at the end the measurement. Some grains may stop growth due to impingement. However, the impingement should not be too severe at this

stage, considering the microstructures shown in Fig. 4.6 and 4.7. The decrease of growth rates is more likely related to the variation within the microstructure, as argued previously. The stable sizes observed after a short time annealing for many grains suggest that the assumption that grains may grow quickly to a limiting size (see Section 4.3.3) may be valid to some extent in these samples.

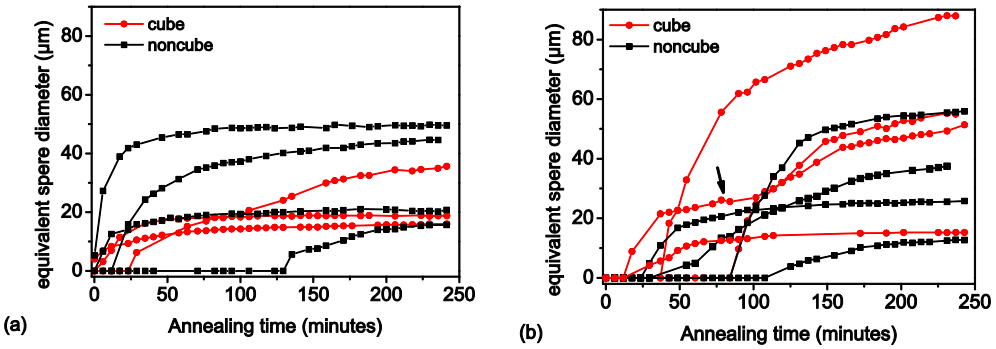

Fig. 4.15: A selection of the measured growth curves showing the variation of growth kinetics of individual grains for a) BI1 and b) BII5. The stagnation period in a cube grain of the BII5 sample is marked by an arrow in b).

Distributions of the nucleation times determined from the growth curves are plotted in Fig. 4.16. In both samples, nucleation takes place during the whole measuring time for both cube and noncube grains. In BI1, the nucleation rates decrease obviously with the annealing time. In BII5, before 100 minutes, the nucleation rates seem to be constant, while afterwards, the nucleation rates decrease. For both samples, the curves of accumulative frequency of cube and noncube grains are very close, which indicates that the nucleation time is similar for cube and noncube grains. This result is in contrast to some oriented nucleation theories, which suggested that cube grains nucleated earlier (Ridha and Hutchinson 1982, Zaefferer et al. 2001). The nucleation time revealed by the 3DXRD data is qualitatively consistent with the statistical measurement of N_V from EBSD data (Fig. 4.13). However, it is hard to compare these two types of data quantitatively. First, a large number of small grains, especially tiny twins are not included in the valid growth curves due to the background noise and the detection limit of the 3DXRD technique. Moreover, the annealing temperatures are different, and

the influence temperature on nucleation has not been studied in the present work.

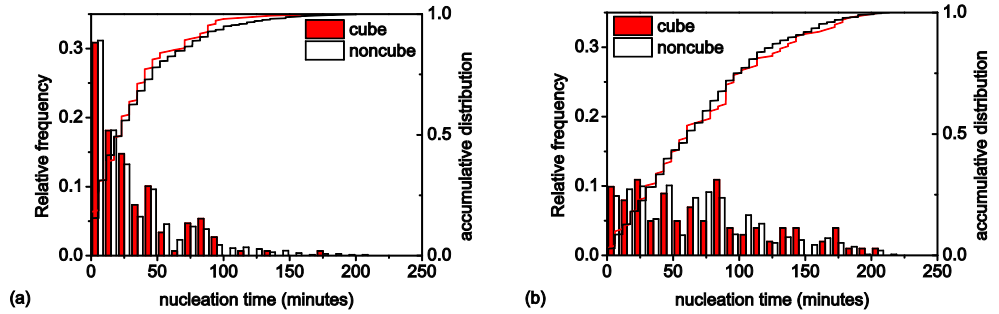

Fig. 4.16: Distributions of the nucleation times of the cube and noncube grains in a) BI1 and b) BII5. The histograms show the relative frequencies, while the curves show the accumulative frequencies.

The size distributions at the end of the experiment are plotted in Fig. 4.17. The size distribution of the cube grains in BI1 is limited to sizes below 40 µm, while most cube grains are below 30 µm. This size limits agrees generally with that from EBSD measurement (20 µm) as shown in Fig. 4.9a, if the stereological coefficient of $4/\pi$ is multiplied to convert the 2D diameters to 3D diameters. It has to be noted that samples are only around 25% recrystallized for the distribution shown in Fig. 4.17a, and the consistency of the maximum size with that in a close to fully recrystallized sample is due to the fact that the grain sizes of a lot of grains increase very slowly after a rapid growing stage, as shown by the growth curves in Fig. 4.15a. The size distribution of the noncube grains is slightly broader than that of cube grains. There seem to be more small cube grains in the distributions. This can be related to the biased minimum size as discussed in section 3.2. The size distribution of the cube grains in BII5 contains more large grains. In the previous section, supercube grains are defined as having an ECD larger than 33 µm. Considering the stereological coefficient of $4/\pi$, cube grains measured by 3DXRD with a size larger than 42 µm are thus classified as supercube grains. 16 out of 101 cube peaks are from supercube grains in BII5, but they represent 72% of the cube volumes of all the 101 cube grains. For the EBSD data, one may argue that some small cube grains may be parts of a big grain, since a lot of twins are developed during the growth of a big grain, which

may break up the big grain in 2D as characterized by EBSD. The 3DXRD data confirm in 3D that there are a large number of small cube grains and the supercube grains are just a minority of the cube population.

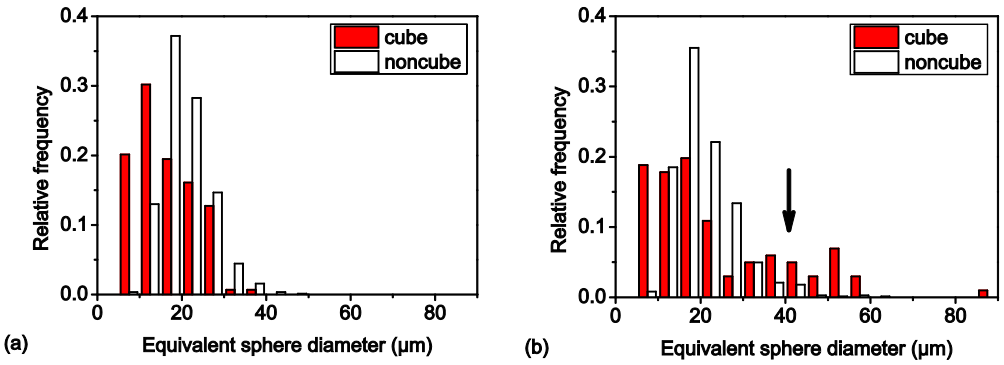

Fig. 4.17: Size distributions of the cube and noncube grains in a) BI1 and b) BII5. The critical size for supercube grains is marked in b).

4.4 Supercube grains

By comparing BI1 (initially coarse grained) and BII5 (initially fine grained), it is found that supercube grains are the key to a strong cube texture after recrystallization in the present samples. It is therefore interesting to analyze how and why these cube grains could grow to a large size. In this section, the supercube grains are compared with the other cube grains in the BII5 sample.

4.4.1 Recrystallization kinetics of supercube and the other cube grains

3DXRD measurements make it possible to investigate the recrystallization kinetics of the supercube and the other cube grains separately. In this study, the supercube grains are defined according to the size at the end of the measurement. As argued above, the selected critical size for supercube grains is 42 μm based on the previous investigation by EBSD. The EBSD and 3DXRD experiments were conducted at slightly different temperatures.

However, the annealing temperature does not have strong effects on the grain sizes according to Section 4.2, and it is thus acceptable to use the same critical size. It has to be noted that the 3DXRD measurement was stopped at a low V_V. A cube grain is considered as a supercube grain only if it has reached the size limit within the measurement. In other words, some cube grains that are not considered as supercube grains here may also be supercube grains, if they keep growing and reach the critical size afterwards.

Fig. 4.18 shows 5 typical growth curves of the supercube and the other cube grains each. The supercube grains do not show any obvious advantage in nucleation time. Recrystallizing grains with an incubation time longer than 150 minutes can be observed in both groups of cube grains. The growth rates of most grains decreases rapidly with time, no matter whether they are supercube grains or the other cube grains. The idea that some grains may achieve a size advantage by keeping a growth rate for a longer time (e.g. due to less impingement), is not applicable here. Actually, the two groups of curves look similar to each other when the scale of the y axis is ignored, which indicates that supercube grains behave similarly to the other cube grains except for their large growth rates, especially at the initial stages. It has to be noted here that although some cube grains have the possibility to become supercube grains if they continue to grow, it is unlikely for most grains in Fig. 4.18b to reach the critical size afterwards. Except for the grain that nucleates after 180 minutes, the growth rates of the other grains in Fig.

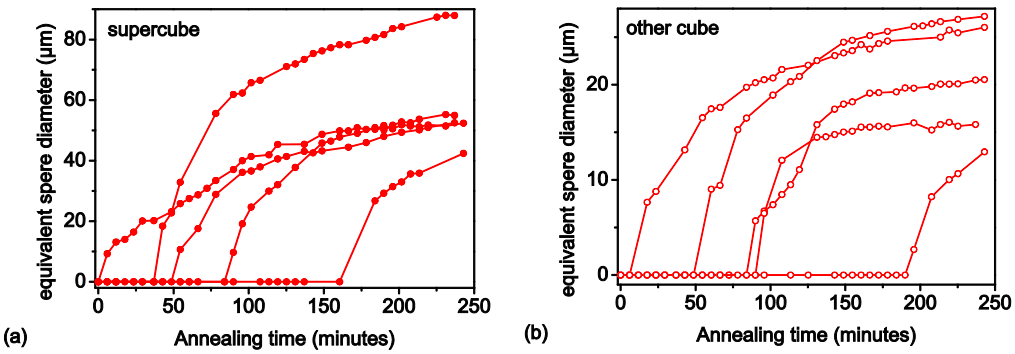

Fig. 4.18: A selection of the measured growth curves of a) supercube grains and b) the other cube grains in BII5.

4.18b have decreased to very low values. A division of supercube and the other cube grains by their sizes at the end of the 3DXRD measurement is therefore appropriate, i.e. there are only a few supercube grains that may be mislabeled due to the early stop of the recrystallization process in the in-situ experiment.

The distributions of the nucleation times of the supercube and the other cube grains are plotted in Fig. 4.19 to give a quantitative description of the nucleation situations. The accumulative frequency of the nucleation times of the noncube grains is also plotted as a reference. Most supercube grains nucleate before 100 minutes annealing, but two supercube grains were found to nucleate after 170 minutes annealing. Similarly for the other cube grains, some grains nucleate right after annealing, while a few grains were observed to have a very long incubation time. The accumulative frequency of the nucleation times of the other cube grains is close to that of the noncube grains. There seems to be a slightly larger fraction of supercube grains that nucleated before 100 minutes annealing. However, considering the poor statistics of the supercube grains and the existence of late nucleating supercube grains, the supercube grains do not nucleate obviously earlier than the other cube grains or the noncube grains.

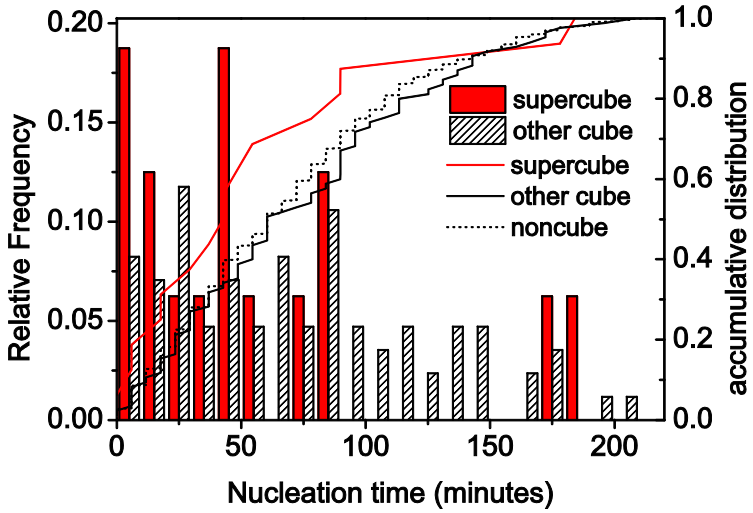

Fig. 4.19: Distributions of the nucleation times for the supercube grains (16 grains) and the other cube grains (85 grains) in BII5. The accumulative frequency of the nucleation times of the noncube grains is plotted, also.

The growth rate of an individual grain changes with time. Here the highest growth rate in each growth curve is used as the characteristic growth rate for each grain. Except for a few grains with a stagnation period, most grains have the highest growth rates right after nucleation. Fig. 4.20 plots the highest growth rate of individual cube grains as a function of the grain sizes at the end of the experiment. There is a general tendency that big grains have higher growth rates, although the growth rates can have a large spread for a similar final grain size. The average value of the characteristic growth rates of the supercube grain is 2.4 times that of the noncube grains (0.25 μm/minute), while the other cube grains have a similar average growth rate compared with the noncube grains.

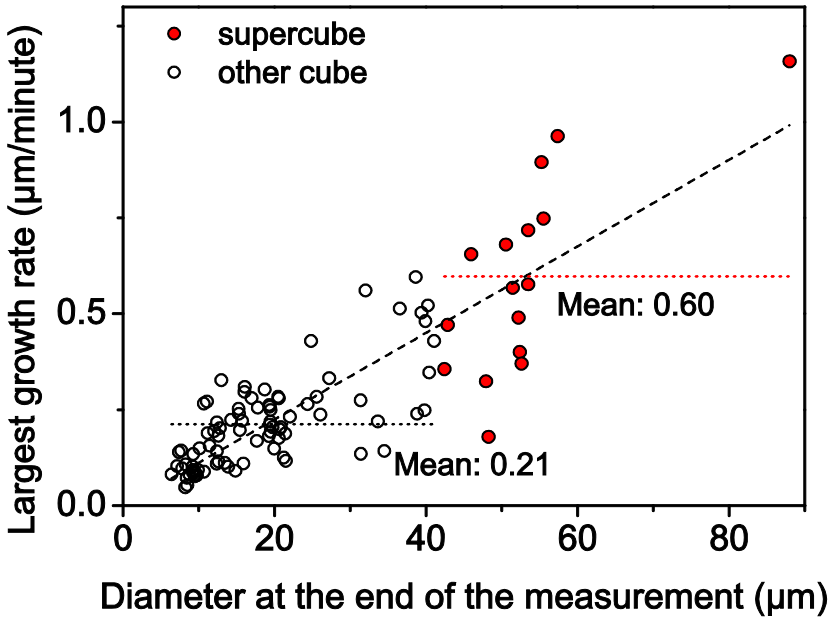

Fig. 4.20: The highest growth rate in each growth curve as a function of the equivalent sphere diameters at the end of the experiment for the cube grains in BII5. The big grains tend to have larger growth rates, and this tendency is illustrated by the dashed line.

As a summary, the strong cube recrystallization texture developed in the initially fine grained sample BII5 is from a few supercube grains which have very large sizes. In other words, the strong cube texture is not because there are more cube recrystallizing grains in the microstructure. The supercube grains do not nucleate obviously earlier than the other cube grains or the

noncube grains. They do not have longer growth periods either. Their size advantage should be primarily related to their high growth rates.

4.4.2 Mechanisms for the rapid growing of supercube grains

As argued in the previous section, supercube grains have high growth rates. It is however interesting to investigate why these grains could have higher growth rates, especially compared with the other cube grains. The following analysis will be based on the EBSD data, since it provides more information on grain orientations, misorientations, as well as the deformed matrix.

The orientations of the supercube and the other cube grains are considered firstly. Although both are grouped to cube grains, the deviation to the ideal cube orientation could be as large as 15°. Engler (1998) suggested that cube grains with the ideal cube orientation have the best growth condition. The orientation deviation of both supercube and other cube grains from the ideal cube orientation are calculated for the sample after 4 h annealing at 150 °C (see Fig. 4.21). Since EBSD is a 2D characterization technique, to avoid the possibility that one small cube grain may be part of a supercube grain in 3D, all the small cube grains at the edge of the scanned area or with an orientation within 1° of an observed supercube grain are excluded in the analysis. 94% of the supercube grains are within 10° to the ideal cube orientation, while 38% of the supercube grains are within 5° to the ideal cube orientation. The orientation of other cube grains spread over the whole 15° range, with 70% and 16% within 10° and 5° deviation, respectively. It seems that a slightly higher fraction of supercube grains have orientations close to the ideal cube orientation. However, one supercube grains is observed to have a larger than 10° deviation. Moreover, the two grains with an orientation closest to the ideal cube orientation are in fact not supercube grains. In general, the higher growth rates of the supercube grains compared with the other cube grains should not be related to an orientation closer to the ideal cube orientation.

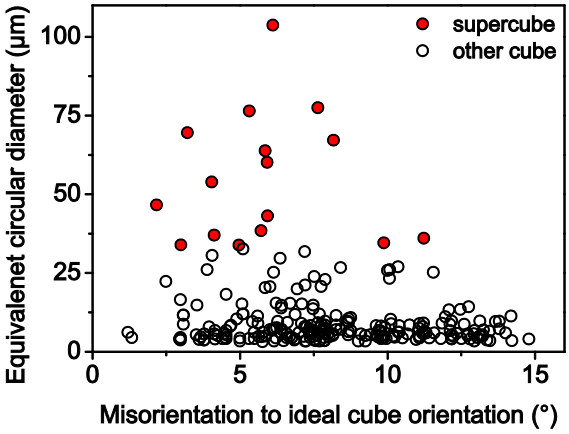

Fig. 4.21: Sizes of the cube recrystallizing grains as a function of the deviations to the ideal cube orientation in the BII5 sample annealed at 150 °C for 4 h.

The local misorientation may be the reason for the higher growth rates of the supercube grains. This analysis is based on the EBSD data of the BII5 sample annealed for 20 minutes at 150 °C, when 20% of the total volume is recrystallized. The histograms in Fig. 4.22 show the distributions of the misorientations of the supercube and the other cube grains to their neighboring deformed matrix, respectively. The two misorientation distributions are very similar. Both misorientation distributions peak at around 52°. The rotation axes of supercube grains are more concentrated around a pole near (111), but shifted a little towards (110), while the other cube grains have a wider distribution of rotation axes. The fractions of Σ7 (40° <111>) boundaries are only 3% for both supercube and the other cube grains. Although not identical to each other, the misorientation distributions of the supercube and the other cube grains are not considered to be significantly different. This analysis of misorientation from the EBSD data has a disadvantage due to the so-called “destroyed evidence” problem (Duggan et al. 1993). The growth curves of the supercube grains (Fig. 4.18a) show that the highest growth rates usually appear right after nucleation. It is however only possible to distinguish supercube grains from the EBSD data when they have reached a certain size and when the deformed microstructures that are most favorable for the growth have been replaced. Zhang et al. (2009) tried to overcome this problem by annealing the sample in several steps, and

characterizing the microstructures after each annealing step. They obtained similar conclusions for pure nickel rolled to 96% reduction that misorientation distributions of the cube grains growing rapidly were similar to those growing slowly.

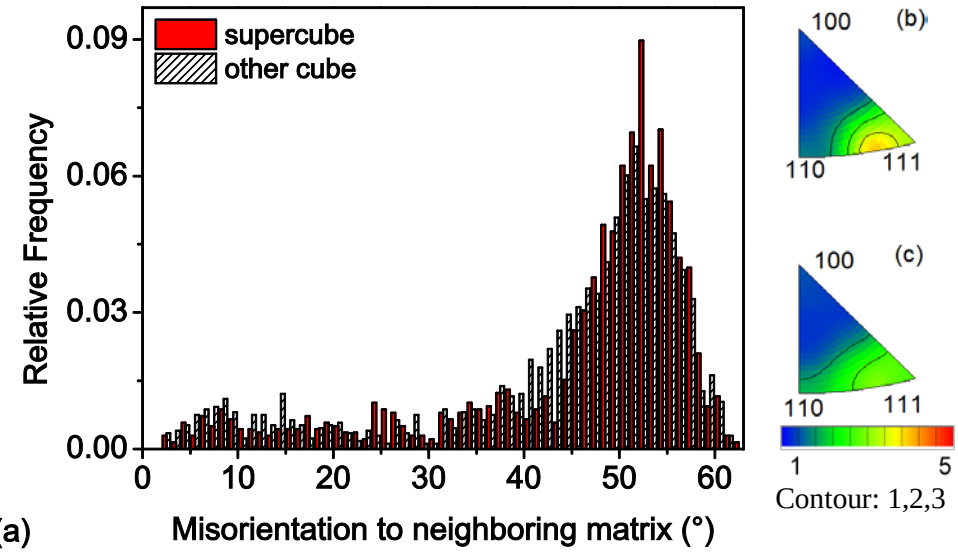

Fig. 4.22: a) Misorientation distributions of the supercube and the other cube grains to their neighboring deformed matrix in BII5 after annealing at 150 °C for 20 minutes. The inverse pole figures (IPFs) show the distributions of the rotation axes for b) the supercube and c) the other cube grains.

Another possible explanation for the large growth rates of the supercube grains relates to the variation within the deformation structure as shown in Fig. 4.5. The boundary migration rates are generally considered proportional to the stored energy, into which the recrystallizing grains are growing. If a cube grain happens to nucleate and grow in a region with high stored energy, it will have a high driving force and may have the possibility to become a supercube grain.

The local environment of a supercube grain is shown in Fig. 4.23. This supercube grain has an elongated shape. Below this supercube grain, there is a smaller grain, which has an identical orientation. It is very likely that these two cube grains are one supercube grain in 3D. In the same map, another small cube grain can be observed. This grain has a very different orientation from the previous supercube grain, so it should be an independent grain. Although this map is from a lightly recrystallized sample, this small cube

grain is more likely not to be a supercube grain, since usually a supercube grain has a very large growth rate right after nucleation, and reaches a relatively large size in a short time. Another recrystallizing grain indicated in this map nucleates in the LSB, but the size of the grain is very small. In general, the map in Fig. 4.23 includes some typical recrystallizing grains in the initially fine grained BII5 sample.

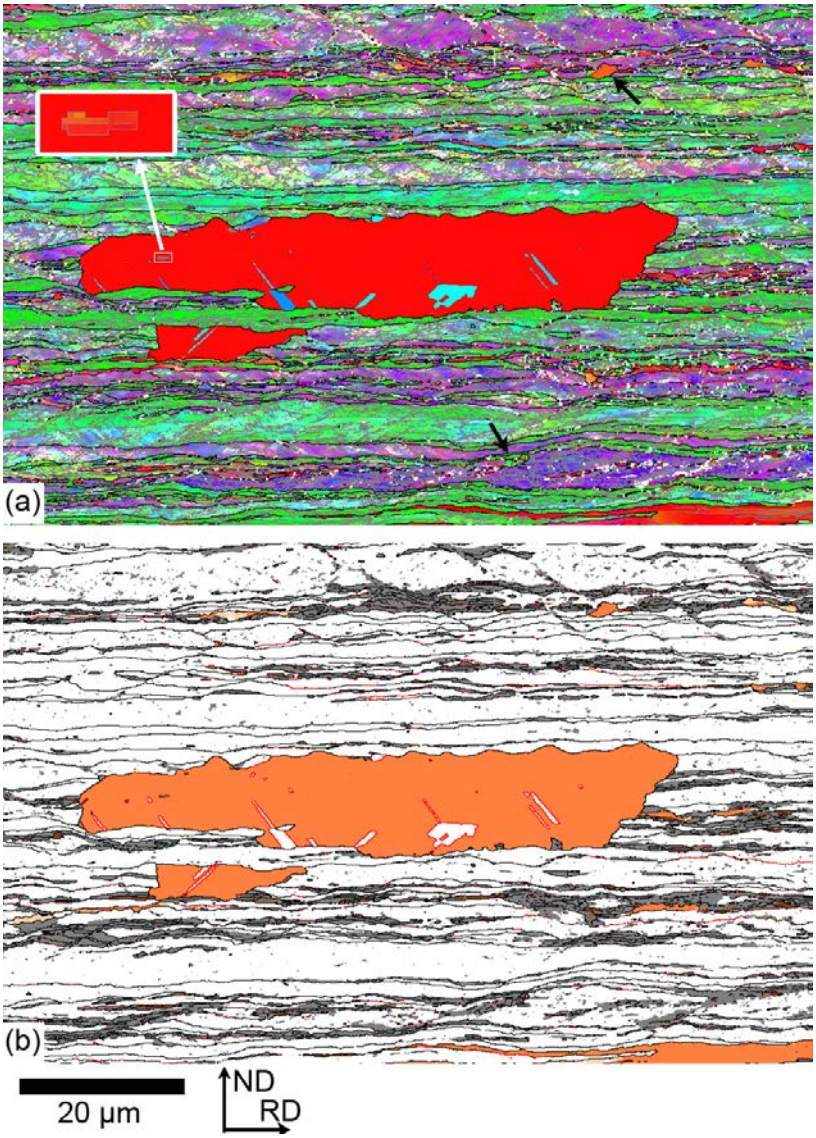

Fig. 4.23: a) Microstructure of BII5 after annealing at 150 °C for 5 minutes. A supercube grain appears in the center of the map. A small segment of the deformed matrix inside the supercube grain is enlarged. Two small recrystallizing grains are marked by the black arrows, one of which is cube grain. b) The same map as a) with HMRs, cube texture regions and near cube texture regions highlighted. The color coding is the same as that in Fig. 4.4.

The correlation of supercube grains with the variation within the deformation structure can be analyzed by the evolution of HMRs. The fraction of HMRs decrease from 32% (Fig. 4.5b) to 22% (calculated from a map covering 100 × 100 μm^2, and Fig. 4.23 is part of the map), which implies that this large supercube grain may have replaced a region with high stored energy. It is very difficult to know the exact microstructure that the supercube grain has grown into. Nevertheless, the remaining parts of the bands in the neighborhood of the supercube grain are a cluster of thin bands with various orientations. Some cube segments are also observed in the neighborhood. It seems very likely that a HMR like the one indicated by the blue arrow in Fig 4.5b has been replaced. The large size of the HMR may provide a very good growth environment at the beginning of recrystallization, and the growth rates will decrease later when this grain grows out of the HMR. The elongated shape of the supercube grains may be inherited from the shape of the HMRs. In contrast to the supercube grain, the small cube grain is not inside any large HMR. After nucleation, this cube grain is growing towards regions with relatively low stored energy, which are unfavorable for its growth. This mechanism can be illustrated by sketches below (Fig. 4.24).

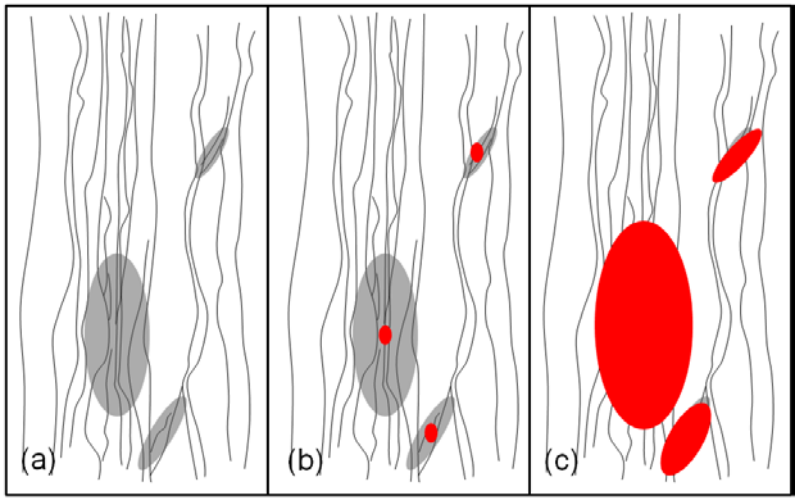

Fig. 4.24: Schematic diagrams illustrating the formation of recrystallizing grains in a non-uniform deformation structure. The gray parts illustrate the high stored energy regions, and the red shapes represent the recrystallizing grains. One grain grows to a large size, since it is located in a large region with high stored energy.

It is interesting to note that inside this supercube grains (Fig. 4.23), there is a small cube segment with misorientations of around 8° to the recrystallizing grain and with some internal misorientations of maximum 5°. In an earlier paper, this type of tiny deformed matrix is considered as a “nuclear spot” (Burgers and Tiedema 1953), although this is not always observed (Beck and Hu 1963). However, it is hard to confirm in this study that this remaining cube segment is the origin of the supercube grain, since some other cube segments can be observed next to this supercube grain, also. A complete investigation of the nucleation requires a non-destructive 3D technique that can resolve the deformed microstructure, which is still not easily available.

Another interesting feature of the supercube grain in Fig. 4.23 is that it is most likely separated into two parts, so that it may have a U-shape in 3D. A brass band lies in between. Zhang et al. (2011) found that boundaries of recrystallizing grains may form protrusions and retrusions. The U-shape boundary in 3D can be considered as boundaries of large protrusions and retrusions. It is not clear how this shape of a little strange is formed, and whether it is common for supercube grains. It may also be very interesting to investigate if this shape may be helpful for further growth.

The effects of the variation within the microstructure (i.e. the large HMRs) have been emphasized in the previous paragraphs for the growth of the supercube grains. However, it should be noted that the cube orientation is also a favorable factor, if supercube grains are compared with noncube grains. In the almost fully recrystallized BII5 sample (Fig. 4.7c), some noncube grains have an elongated shape and a relatively large size, also. The appearance of some large noncube grains is also confirmed by the size distributions (Fig. 4.9b and 4.17b). These large noncube grains may also have a favorable local environment, but their growth may not be as rapid as that of the supercube grains. As has been suggested by the oriented growth theories, the main texture components among the typical rolling textures, especially the S component, are more favorable for the growth of cube grains (e.g. Engler and Lücke 1992). On the other hand, noncube grains, especially grains belonging

to the rolling textures, may be inhibited by local orientation pinning (Juul Jensen 1995b), even if they nucleate in a large HMR.

The mechanism illustrated in Fig. 4.24 can be used to suggest an explanation for the absence of supercube grains in BI1. As shown in Fig 4.4, the fraction of HMRs is much lower in BI1, and the size of each HMR is small. An important condition for the supercube grains is to locate in a large HMR, which is not available in the BI1 sample. On the other hand, the small HMRs lead to the formation of many small recrystallizing grains, such as those nucleating in the LSBs. Many small HMRs in the BI1 sample are LSBs. The shapes and sizes of many recrystallizing grains in the BI1 sample are closely related to the shapes and sizes of the LSBs.

It is also interesting to check the evolution of the cube bands in the BI1 sample. Fig. 4.25 shows two maps containing cube bands after 1 h annealing at 150 °C (overall V_V=0.08). In Fig. 4.25a, there is a cube band in the center. The cube band has begun to bulge out along its upper part. The bulging out from a cube band has been suggested as the origin of cube recrystallizing grains (Ray et al. 1975, Ridha and Hutchinson 1982). The cube band has also developed a cube recrystallizing grain with an equiaxed shape. However, none of these cube grains or potential cube grains from this cube band develops into supercube grains, as shown by the microstructural evolution investigated in Section 4.3.2. The limited sizes of these cube grains may be related to the low stored energy regions they are growing into. In Fig. 4.25b, a cluster of cube bands has been replaced by recrystallizing grains of noncube orientations. In general, in the present work, it is observed that the presence of cube bands in the deformation structure is not enough for the development of a strong cube texture after recrystallization. Whether a cube band can stimulate cube recrystallizing grains, and whether the cube recrystallizing grains can grow to a large size depend significantly on the local environment.

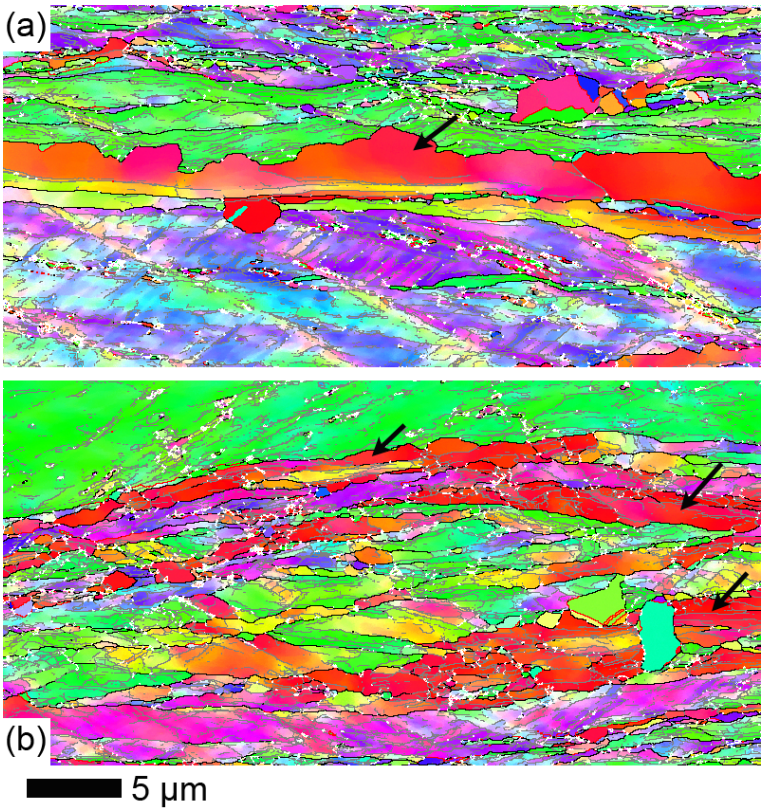

Fig. 4.25: Cube bands (in red, also indicated by arrows) observed in BI1 after annealing at 150 °C for 1 h. The color coding and the sample coordinates are the same as those in Fig. 4.23a. The cube band in a) begins to bulge out along its upper part, while an equiaxed cube grain has also been developed from this band. Parts of the cube bands in b) have been replaced by recrystallizing grains of noncube orientations.

4.5 Recrystallization in other samples

The sample widening and the strain are other factors that affect the recrystallization kinetics and textures, as identified in the previous sections. In the following, the samples BII1 and BI1_95cr are reported. Except for the significant widening, BII1 is identical to BII5, i.e. it has a fine initial grain size. This sample will be discussed in comparison with BII5. BI1_95cr is the initially coarse grained BI1 sample rolled to 95% reduction, and it will be compared primarily with its low strain counterpart BI1. The initially fine grained BII5 sample will also be compared to emphasize the importance of

the initial grain sizes. The development of the cube texture in these two samples will be discussed using the mechanisms of the formation of supercube grains suggested in the previous section.

4.5.1 Recrystallization in the widened sample

The deformation microstructure of BII1 is shown in Fig. 4.26. Compared with that of BII5, this microstructure contains more green bands and less purple and blue bands. The green bands represent bands with a {110} fiber texture. A few of these green bands have the brass orientation, but most of them are not. The volume fraction of the rolling texture components is 63%, while that in the BII5 sample is 77%. The S texture component decreases the most: from 40% in BII5 to 31% in BII1. The weakening of the rolling textures may be related to the change in the strain state of the widening sample, i.e. it deviates from plane strain compression towards uniaxial compression. The fraction of HMRs, as well as the size of individual HMRs, also decreases compared with BII5 (Fig. 4.5b). A few cube segments inside HMRs can be observed. More structural parameters are listed in Tab. 4.6. The spacing along the ND is similar to BII5, and that along the RD is a little larger in BII1. The fraction of HABs is also less in BII1. It has to be noted that the overall stored energy measured by DSC is similar to BII5, but the fraction of HMRs is lower in BII1. This indicates that although the HMRs represent regions with high local stored energy, the fraction of HMRs should not be used as a quantitative descriptor of the overall stored energy.

Tab. 4.6: Microstructural parameters in BII1 (fine initial size and widening). Those in the BII5 (fine initial size) reported in Tab. 4.5 are repeated here to facilitate comparison.

	Spacing of HABs along the ND (nm)	Spacing of HABs along the RD (nm)	Fraction of HABs	Fraction of HMRs	Stored energy (J/g)
BII1	624	1734	26%	24%	0.74
BII5	647	1438	34%	32%	0.72

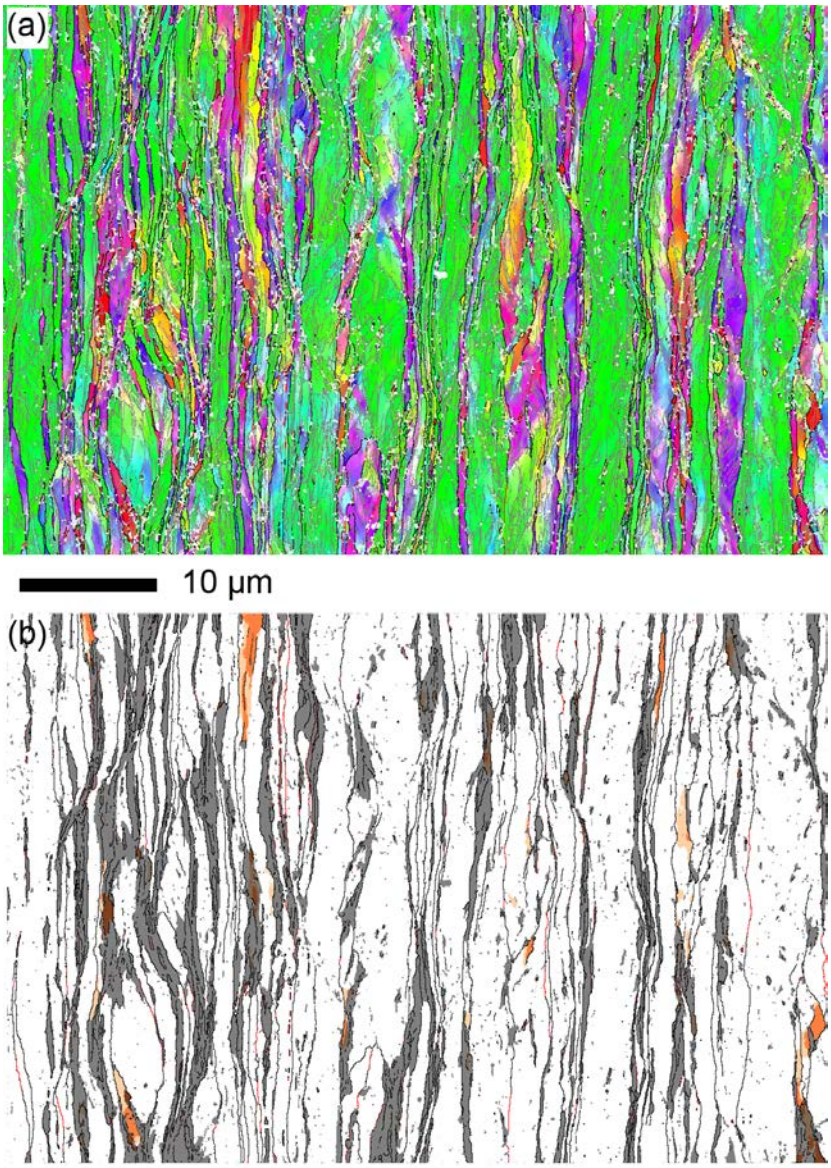

Fig. 4.26: a) Deformation structure of BII1. b) The same map as a) with HMRs, cube texture regions and near cube texture regions highlighted. The color coding and the sample coordinates are the same as those in Fig. 4.4.

The recrystallization in BII1 is investigated through isothermal annealing at 150 °C by EBSD. The evolution of V_V is plotted in Fig. 4.27. The recrystallization process is slightly retarded compared with BII5.

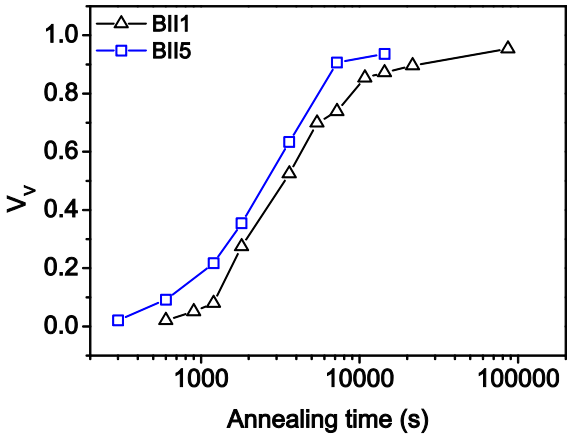

Fig. 4.27: Evolution of the recrystallized volume fraction V_V as a function of annealing time for BII1 and BII5, both annealed at 150 °C. The ITB method was used.

Fig. 4.28 is a typical microstructure of BII1 after a short time annealing. The map contains one elongated large grain (to the right) and some small grains. The volume density of recrystallizing grains is not very high at this stage. The large elongated grain in the map has a cube orientation, but large noncube grains are also observed in the same sample. Moreover, the size advantage of these large elongated grains is not as significant as in the BII5 sample.

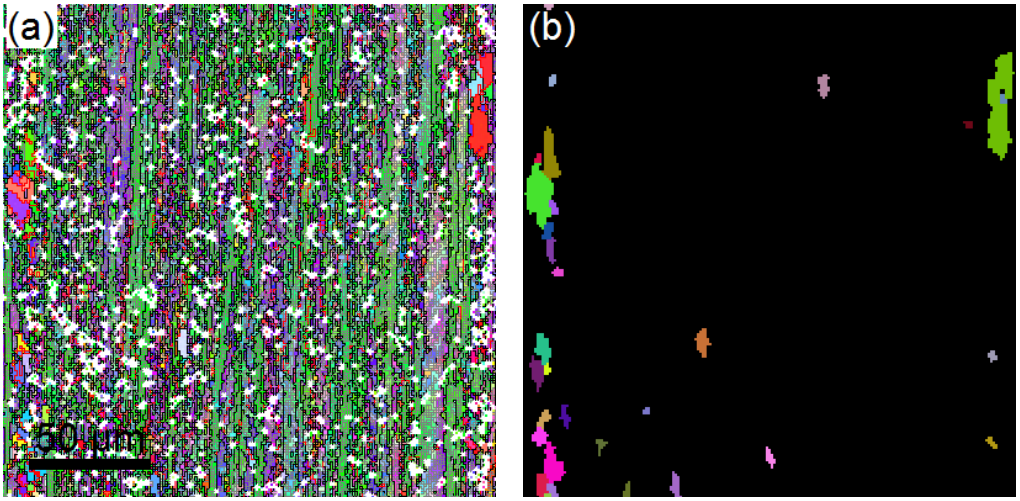

Fig. 4.28 a) Microstructure of BII1 after 10 minutes annealing at 150 °C. The color coding and the sample coordinates are the same as those in Fig. 4.4a. The same map is shown in b) highlighting the recrystallizing grains with random colors. The ITB method was used for grain identification.

After annealing for 24 h, the sample is almost fully recrystallized. The microstructure (Fig. 4.29a) contains some relatively big cube grains, as well as some noncube grains of a similar size. The volume fraction of the cube recrystallization texture is 13.1%. The size distributions of the cube and the noncube grains of the 24 h annealed sample are plotted in Fig. 4.29b. This size distribution of cube grains is similar to that of BII5: The area-weighted fraction contains two parts. If the size definition of supercube grains in BII5 (33 µm) is applied, a few cube grains have a size above this critical size. However, these few supercube grains only contribute 14% of the total cube area, while the contribution of the supercube grains in the BII5 sample is 58%. It is also interesting to note that in BII1 the largest grain in the size distributions is a noncube grain.

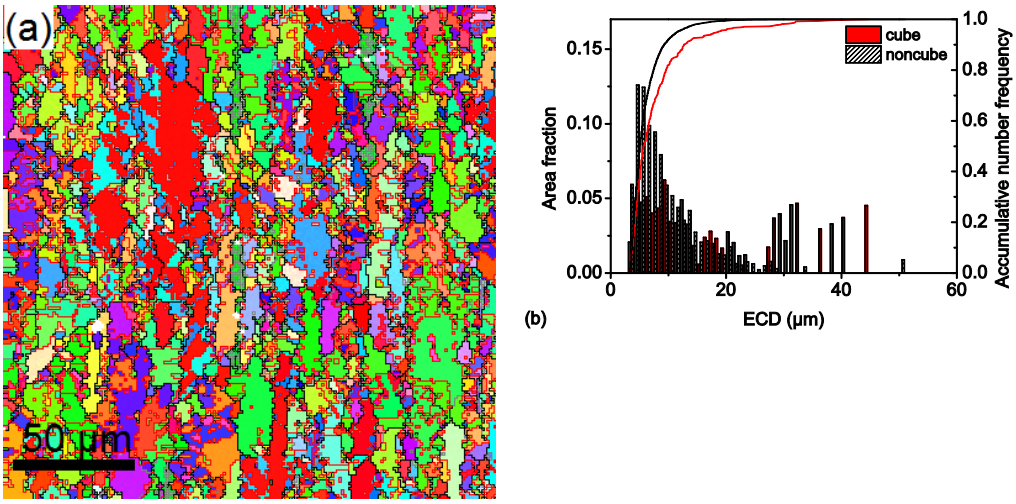

Fig. 4.29: a) Microstructure of BII1 after 24 h annealing at 150 °C. The color coding and the sample coordinates are the same as those in Fig. 4.4a. b) The size distributions of cube and noncube grains in this sample. The histograms show the area-weighted distributions, while the curves show the accumulative number frequencies. The CTB method was used to define cube and noncube grains.

The weakening of the cube texture is due to the less development of the supercube grains in BII1, which can be related to two factors. The first is the lower fraction of HMRs and the smaller size of individual HMRs, which are proposed to be important for the growth of supercube grains at the initial stage. The other is the weaker rolling textures, especially the large decrease in the volume fraction of the S component.

4.5.2 Recrystallization in the sample rolled to 95% reduction

The deformation structure (Fig. 4.30) is slightly finer in the BI1_95cr sample compared with BI1. The refinement of the microstructure in this sample is more obvious when the microstructural parameters are compared with those of BI1 (see Tab. 4.7). The spacing of HABs along the ND is reduced from 896 nm to 774 nm when the rolling reduction increases from 90% to 95%. The sample thickness after 95% reduction is only half that after 90% reduction, but the decrease of HAB spacing is not that much. This observation agrees with the finding by Hughes and Hansen (2000) that the decrease of boundary spacing is slow at strains higher than 1 (63% thickness reduction).

It should be noted that, in spite of the higher strain, the spacing in the BI1_95cr sample is still larger than BII5, which has a smaller initial grain size. The stored energy, as well as the fraction of HMRs, is also lower than BII5. It is a little surprising that a sample rolled to 95% reduction could have a lower stored energy than a sample rolled to 90% reduction, which has a smaller initial grain size. This emphasizes further the importance of the initial grain sizes.

Some relatively large HMRs can be observed in Fig. 4.30b in a purple (copper oriented) band, but HMRs are few and small in other regions. LSBs in copper and S oriented bands still exist. The deformation texture in the BI1 sample is a little stronger after being rolled to 95%, as the volume fraction of rolling texture components increases from 76% to 81%.

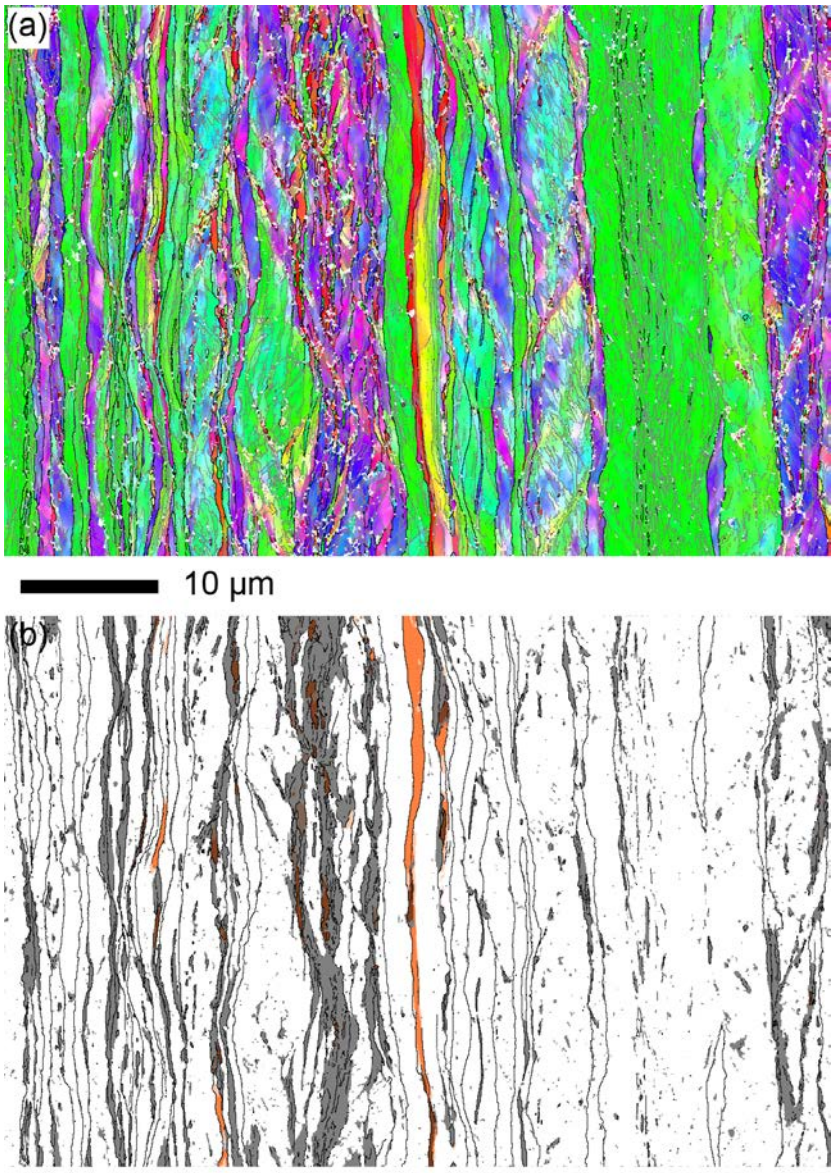

Fig. 4.30 a) Deformation structure of BI1_95cr. b) The same map as a) with HMRs, cube texture regions and near cube texture regions highlighted. The color coding and the sample coordinates are the same as those in Fig. 4.4.

Tab. 4.7: Microstructural parameters in BI1_95cr (coarse initial size). Those in BI1 (coarse initial size) and BII5 (fine initial size) reported in Tab. 4.5 are repeated here to facilitate comparison.

	Spacing of HABs along the ND (nm)	Spacing of HABs along the RD (nm)	Fraction of HABs	Fraction of HMRs	Stored energy (J/g)
BI1_95cr	774	1957	26%	18%	0.68
BI1	896	2106	23%	13%	0.59
BII5	647	1438	34%	32%	0.72

The microstructure of the initial stage of recrystallization in BI1_95cr is shown in Fig. 4.31. The size and the spatial distributions of recrystallizing grains are similar to the BI1 sample at the initial stage (Fig. 4.6a). The size variation of the recrystallizing grains is not large. The density of recrystallizing grains is high, and the grains tend to cluster in bands. Some grains show characteristic as nucleating in the LSBs. Cube grains do not behave obviously differently compared with other grains at this stage.

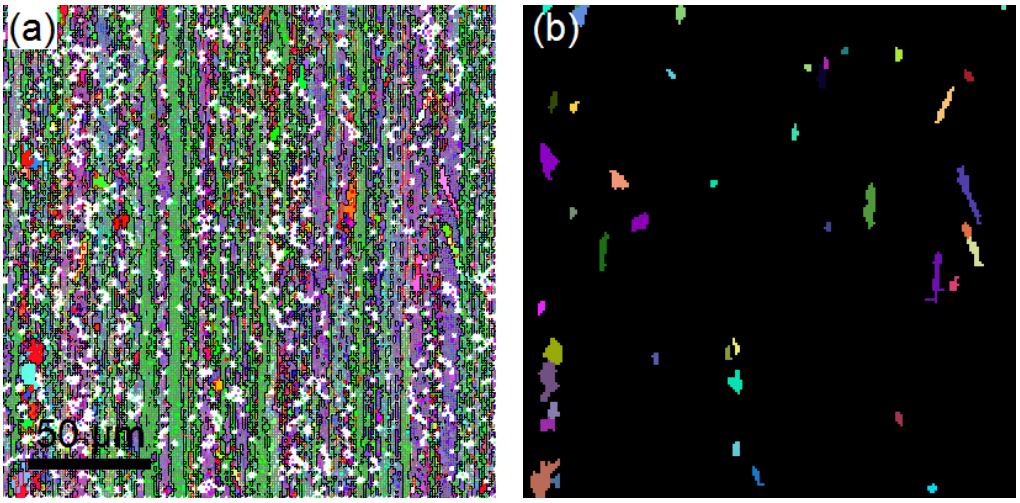

Fig. 4.31: a) Microstructure of BI1_95cr after 30 minutes annealing at 150 °C. The color coding and the sample coordinates are the same those as in Fig. 4.4a. The same map is shown in b) highlighting the recrystallizing grains with random colors. The ITB method was used for grain identification.

After annealing for a longer time at a slightly higher temperature (167 °C for 6 h), the microstructure is almost fully recrystallized (Fig. 4.32a). The volume fraction of the cube texture is 14.1%, which is higher than that in BI1 (3.6%). The size distributions are plotted in Fig. 4.32b. Compared with noncube grains, a higher fraction of cube grains is found between 10-20 µm. The size distribution of the noncube grains is very similar to that of BI1 (Fig. 4.9a). The size distribution of cube grains is instead broader than that of cube grains of BI1. The broadening of the size distribution of the cube grains is responsible for the higher fraction of the cube texture in this sample. This broadening may be related to the stronger rolling textures in the deformed sample.

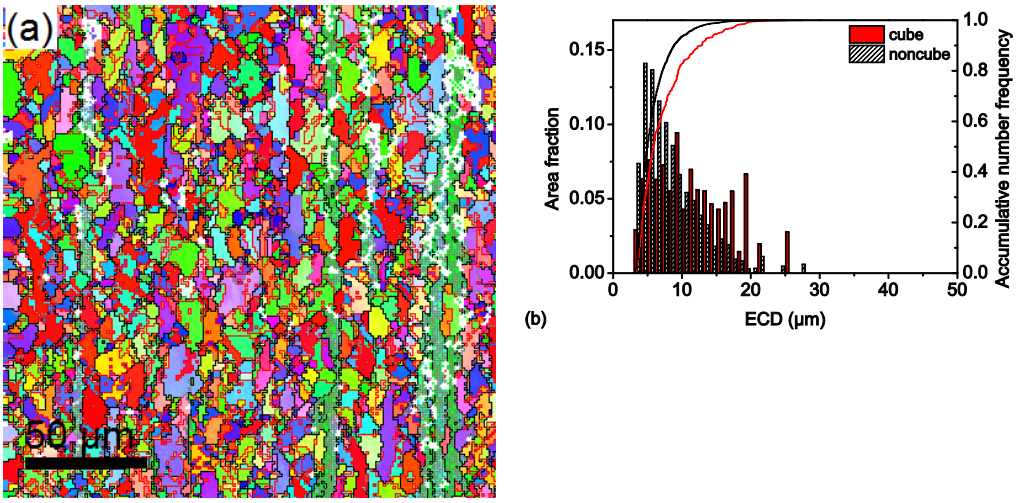

Fig. 4.32 a) Microstructure of BI1_95cr after 6 h annealing at 167 °C. The color coding and the sample coordinates are the same as those in Fig. 4.4a. b) The size distributions of the cube and the noncube grains in this sample. The histograms show the area-weighted distributions, while the curves show the accumulative number frequencies. The CTB method was used to define cube and noncube grains.

4.6 Summary

Samples with different initial grain sizes were cold-rolled to 90% thickness reduction. It is found that the initial grain sizes have strong effects on the subsequent recrystallization kinetics and the textures after recrystallization. The sample with a fine initial grain size recrystallizes much faster, and develops a strong cube texture after recrystallization. The cube texture after recrystallization is very weak in the sample with a coarse initial grain size.

The microstructures of both initially coarse and fine grained samples have been refined through the deformation. The weak initial textures have been replaced by the typical rolling textures after deformation in both samples. Both microstructures are composed of bands with different orientations. The initially fine grained sample has a smaller spacing of high angle boundaries (HABs) and a higher fraction of HABs. The volume fraction of high misorientation regions (HMRs) and the stored energy are also higher in the initially fine grained sample.

Localized shear bands (LSBs) develop in both samples, which tend to locate in bands with copper/S orientation at +/− 35° to the rolling direction. The +/− pattern of the LSBs changes systematically with the symmetric variants of the orientation of the band. It is suggested that the formation of LSBs is related to the active slip systems. The nucleation in LSBs is observed for both initially coarse and fine grained samples.

The evolutions of the recrystallized volume fraction (V_V), when plotted in Avrami plots, have lower exponents than predictions from the idealized JMAK model. Nucleation takes place throughout the recrystallization process before saturation, which occurs when 50% of the material has recrystallized. The volume density of recrystallizing grains is much higher in the sample with coarse initial grain sizes. The growth rates of recrystallizing grains are not constant but decrease with annealing time as $G = G_0 t^{-r}$, where r is around 1 for both samples. The decreasing growth rates are an important reason for the low Avrami exponents observed. Cube grains have a growth advantage by a factor of about 2 in the initially fine grained sample, and this growth advantage is not observed in the initially coarse grained sample.

Recrystallization kinetics of individual grains were measured in-situ by 3DXRD at 165 °C for the initially coarse grained sample and at 130 °C for the initially fine grained sample. Each recrystallizing grain has its own kinetics, and even grains with similar orientations grow differently. The nucleation times show large variations. The growth rates vary with time. Most grains have large growth rates after nucleation, which decrease over time, and some grains reach a stable size during a short annealing time. The decreasing growth rates for the individual grains, as well as the decreasing average growth rates determined from EBSD, are related to the variation within the deformed structure.

The strong cube texture after recrystallization in the initially fine grained sample is mainly attributed to a few very large cube grains, named supercube grains in this work. The nucleation time of supercube grains is not obviously earlier than the other cube grains or noncube grains, but the supercube grains

have large growth rates, especially at the initial stage of growth. Other cube grains, however, do not have larger growth rates compared with noncube grains. Compared with the other cube grains, supercube grains do not have orientations closer to the ideal cube orientation, and they do not have special misorientations with the neighboring deformed matrix either. It is suggested that the high growth rates of supercube grains compared with the other cube grains are related to their local environment.

The cube recrystallization texture in the initially coarse grained sample is slightly enhanced when the sample was rolled to 95% thickness reduction. On the other hand, the cube recrystallization texture in the initially fine grained sample becomes weaker when the sample had a significant relative widening during rolling. The relative widening of the sample is related to the width of the sample, as well as the diameter of the rolls.

The different impurity contents of the three OFHC coppers used in this study do not have strong effects on the recrystallization texture, but the recrystallization temperature is sensitive to impurity content. The recrystallization texture is not very sensitive to annealing temperature either. However, if the samples are annealed at a high temperature, and grain growth occurs after recrystallization, the cube texture can be enhanced. Long term storage at room temperature does not significantly affect the recrystallization texture, but recrystallization may occur during the storage. Formation of a shear texture in the sample surfaces is found to result in different recrystallization textures through the sample thickness: a strong cube texture in the center and a very weak texture in the surfaces.

Chapter 5
Recrystallization in nanostructured samples

The concept of ultrafine grained metals and nanostructured metals has been a popular topic over many years. Numerous synthesis techniques have been proposed, among which severe plastic deformation (SPD) processes (e.g. accumulative roll bonding (ARB), equal channel angular extrusion (ECAE), high-pressure torsion (HPT)) (Saito et al. 1999, Valiev et al. 2000) are the most discussed methods. Dynamic plastic deformation (DPD) is a technique developed by the group at IMR, China, which can effectively reduce the grain sizes to the nano-regime (Zhao et al. 2005). Pure copper deformed by DPD has been reported to have a high strength and a high electrical conductivity (Zhang et al. 2007). In the present work, nanostructured samples were produced by DPD with and without additional rolling. The recrystallization kinetics and microstructural evolutions in these nanostructured samples were investigated. The effects of annealing on the mechanical properties are also discussed shortly in this chapter.

5.1 Dynamic plastic deformation

The experimental set-up is illustrated in Fig. 5.1. A cylinder sample is placed on the lower anvil, and is compressed when the upper impact anvil

falls down from a certain height. The strain rates are very high, depending on the height from which the anvil is released. The deformation temperature can be reduced by immersing the sample in liquid nitrogen during deformation.

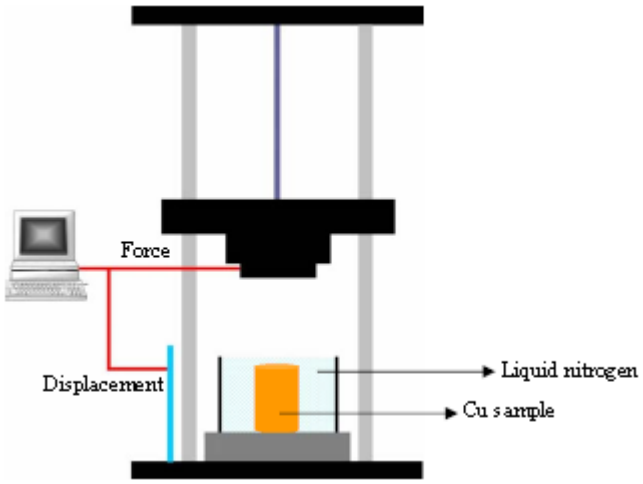

Fig. 5.1: A schematic illustration of the DPD set-up, reproduced from Zhang (2010).

In this work, 99.995% purity copper of an initial grain size of 200 μm was used. A cylinder 9 mm in diameter and 26 mm in height was processed by DPD at liquid nitrogen temperature. The cylinder was deformed by 17 impacts. The height reduction at each step varied from 2 mm at the beginning to 0.1 mm at the end. The final height of the sample was 3.3 mm, corresponding to an equivalent strain of 2.0. The strain rate applied to the sample was estimated to be about 10^2-10^3 s^{-1}. The material is from the same batch as that used in Li et al. (2008a) and Zhang et al. (2008), and the deformation parameters are also similar. It is therefore possible to relate the present investigation to the previous characterizations by transmission electron microscopy (TEM) and the previous measurements of mechanical properties, i.e. the results on similar samples obtained by the IMR group.

5.2 Recrystallization kinetics and microstructural evolution of DPD samples

5.2.1 Deformation microstructure

An orientation map of a DPD sample is shown in Fig. 5.2a, and is colored according to the crystallographic direction of the compression axis. As expected, EBSD resolves the microstructure only poorly. The white points represent non-indexed points. In the following, the EBSD information is supplemented with information from previous TEM observations (Li et al. 2008a). The orientation map reconstructed from EBSD, however, gives an excellent overview over the heterogeneity of the DPD sample.

The microstructure can be classified into three different structures. The green regions (Type A microstructure) in the map belong to a {110} fiber texture (i.e. have the compression axis parallel to a <110> crystallographic direction). Inside the Type A regions, there are a large number of low angle boundaries (LABs) with a misorientation lower than 15°, while high angle boundaries (HABs) are rarely observed. The Type A microstructure should originate from dislocation slip. The blue regions (Type B microstructure) belong to a {111} fiber texture (i.e. have the compression axis parallel to a <111> crystallographic direction), and some twin boundaries are observed almost perpendicular to the compression axis. Twin bundles were observed in the DPD samples by TEM with most of the twin boundaries aligned perpendicular to the compression axis (Li et al. 2008a). Although not stated directly in the TEM characterization, the twin bundles are most likely to have a {111} fiber texture since coherent twin boundary planes are {111} planes, so the Type B microstructure observed by EBSD corresponds to the twin bundle regions observed by TEM. It should be noted that the twin boundary spacing in Fig. 5.2a (around 500 nm) is much larger than that from TEM analysis (44 nm), which is due to the limited spatial resolution of EBSD

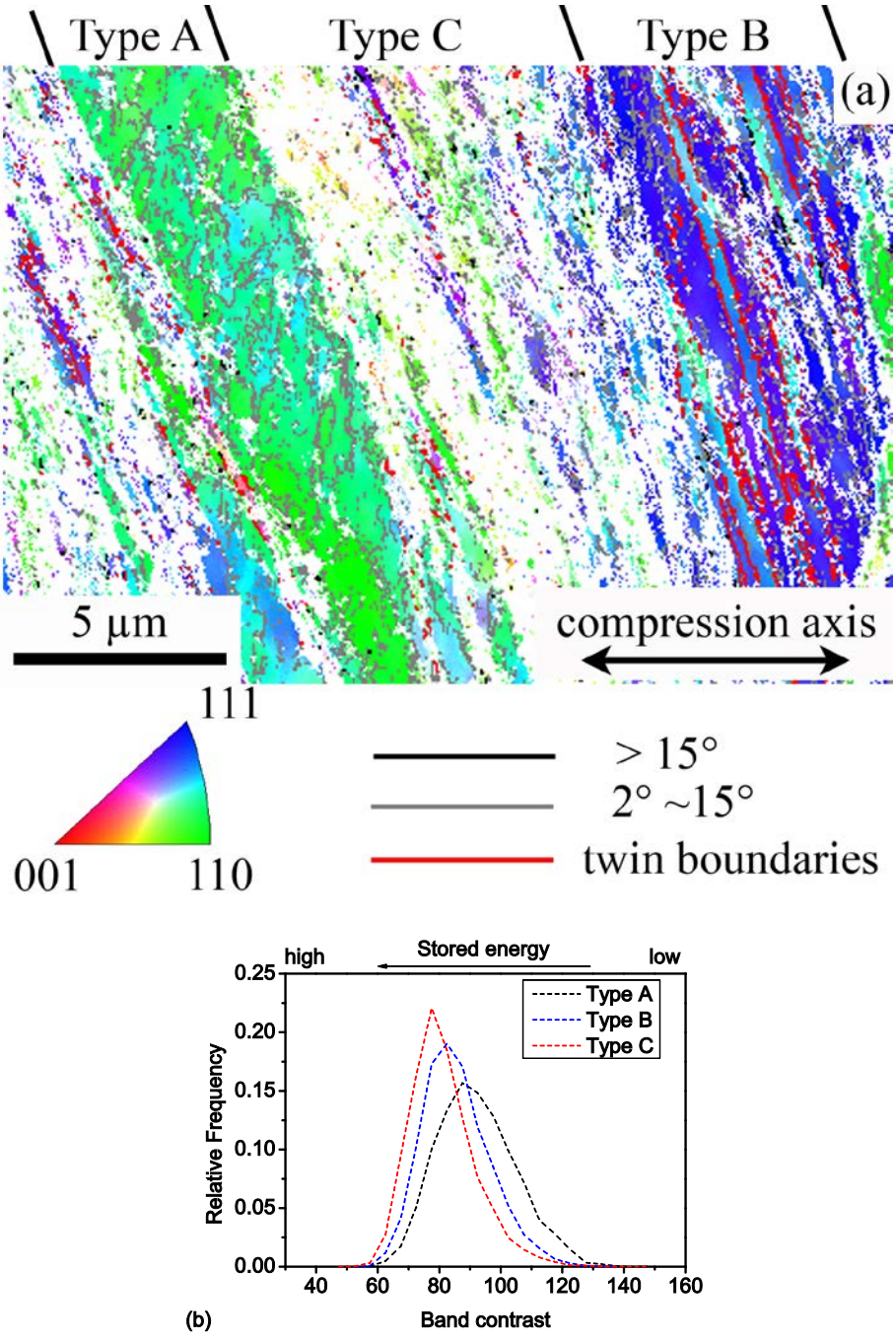

Fig. 5.2: a) Orientation map of the deformation structure of a DPD sample viewed from the cross section. The colors represent the crystallographic direction of the compression axis. b) Distributions of band contrasts in Type A/B/C microstructures.

(Alimadadi et al. 2012). The white regions (non-indexed points) in Fig. 5.2a are mostly grouped into a Type C microstructure. Based on the previous TEM investigation (Li et al. 2008a), the Type C microstructure is considered to include nano-sized grains originating from shear bands and fragmented twin

bundles and maybe some twin bundles. All of these structures have boundary spacings less than 100 nm (Li et al. 2008a), and hence, are difficult to be characterized by EBSD.

The band contrasts (BCs) from the EBSD data can be used as an indication of the stored energy (Gerber et al. 2004). The band contrast is a parameter evaluated by the EBSD acquisition program Channel 5, and it is based on the image contrast of the electron backscatter pattern. Low BCs are indications of high stored energy, and vice versa. The distributions of BCs of the three types of microstructures are plotted in Fig. 5.2b. The BCs in all three types of microstructures have a bell shaped distribution, but the peaks of the three distributions can be clearly distinguished. The stored energy is highest in the Type C microstructure and lowest in the Type A microstructure. Yan et al. (2012) calculated the stored energy based on microstructures from a TEM characterization in a similar DPD deformed copper sample. In their study, the microstructure was divided into three types: dislocation slip (DS) regions, shear band (SB) regions and nanotwin (NT) regions, and the stored energy in the three regions was determined to be 0.83, 1.60 and 2.17 J/g, respectively. The DS regions are identical to the Type A microstructure, and the SB regions are part of the Type C microstructure. The NT regions include both nanotwin bundles (Type B) and fragmented twin bundles (Type C). The stored energies in different types of microstructures estimated from the distributions of BCs are in general consistent with their quantitative determination.

Altogether, it is found that the three types of microstructures (A, B, C) in the DPD sample are very heterogeneously distributed. It needs to be noted that Fig. 5.2a is specially selected to include all three types of microstructures, and it is more often observed that one type of microstructure dominates large areas. The deformation microstructure of a DPD sample is thus very heterogeneous, which strongly affects the recrystallization behavior and the spatial distribution of the recrystallizing grains. The effects of the heterogeneity on the recrystallization behavior will be discussed later.

The heterogeneity of the deformation microstructure may be related to the initial grain sizes and grain orientations. Fig. 5.3 shows the microstructure of the same sample at a lower strain. The initial grain boundaries can be easily recognized in this map. The microstructure shows large variations on the grain scale. Some grains deform by dislocation slip, while others deform by twinning. The deformation mechanisms in different grains depend on the orientations of the grains. The orientations of grains deformed by dislocation slip and by twinning are illustrated by the inverse pole figures in Fig. 5.3 b and c, respectively. Orientations close to a {100} fiber texture are observed only for grains containing twins. This observation agrees well with that reported by Hong et al. (2009) in pure copper deformed by DPD to a strain of 0.33. Moreover, grains closest to a {110} fiber texture (the green grains in the map) deform very homogeneously without formation of deformation bands. It

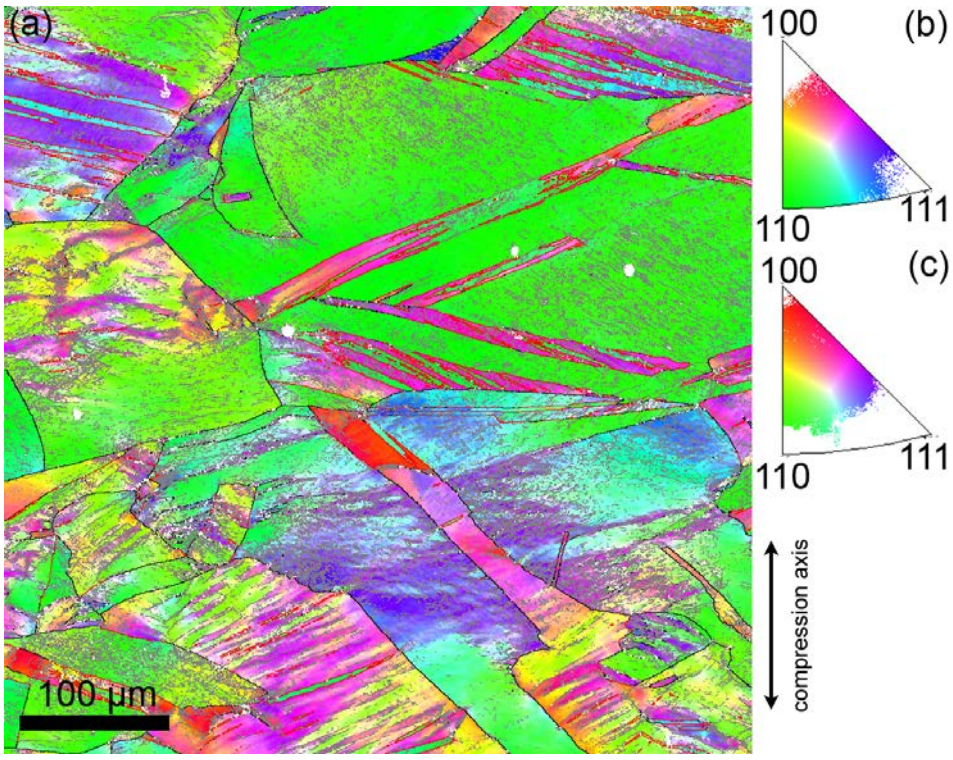

Fig. 5.3: a) Microstructure of the sample deformed by DPD to a strain of 0.4. The color coding is the same as that in Fig. 5.2. The crystallographic directions of compression axes are shown in inverse pole figures for grains b) without deformation twins and c) with deformation twins.

has been reported that grains with a {110} fiber texture have the lowest banding tendency during compressive deformation (Lee et al. 1996). The DPD process is a high strain rate compression deformation, and Luo et al. (2012) found in nickel that DPD is even more favorable for the formation of large regions with only LABs compared with low strain rate compression. It is therefore very possible that each large Type A region is from one grain initially with a {110} fiber texture, which deforms rather homogeneously through dislocation slip. The size of an individual Type A region depends to a certain extent on the initial grain size, while the fraction of Type A regions is related to the initial texture. Therefore, the control of the initial grain sizes and the initial texture can modify the heterogeneity of the DPD sample.

5.2.2 Microstructural evolution during annealing

Two maps after 150 °C 2 minutes annealing are shown in Fig. 5.4 a and b. The spatial distribution of the recrystallizing grains is very heterogeneous, which may be related to different annealing behaviors in the three types of deformation structures presented previously. The recrystallization occurs first in regions with a Type C microstructure. This agrees with expectations because these regions are assumed to have a high stored energy as well as a reasonable fraction of HABs. In particular, the shear bands, which are part of the Type C microstructure, have been reported as strong nucleation sites by many authors (e.g. Hughes 2000, Paul et al. 2002). Regions with a Type C microstructure thus provide many potential nucleation sites, which quickly develop into recrystallizing grains. These recrystallizing grains impinge upon each other quickly afterwards. On the other hand, very few recrystallizing grains are found in regions with Type A or Type B microstructures at an early stage of recrystallization. Inside a Type A microstructure, almost all of the dislocation boundaries are LABs with low mobility, and the mean misorientation angle measured by TEM is only 3.8° (Yan et al. 2011). Therefore, such areas are not expected to nucleate many recrystallizing grains. The Type B microstructure is composed of twin bundles. Twin

boundaries are considered to be immobile and nucleation is thus also difficult there.

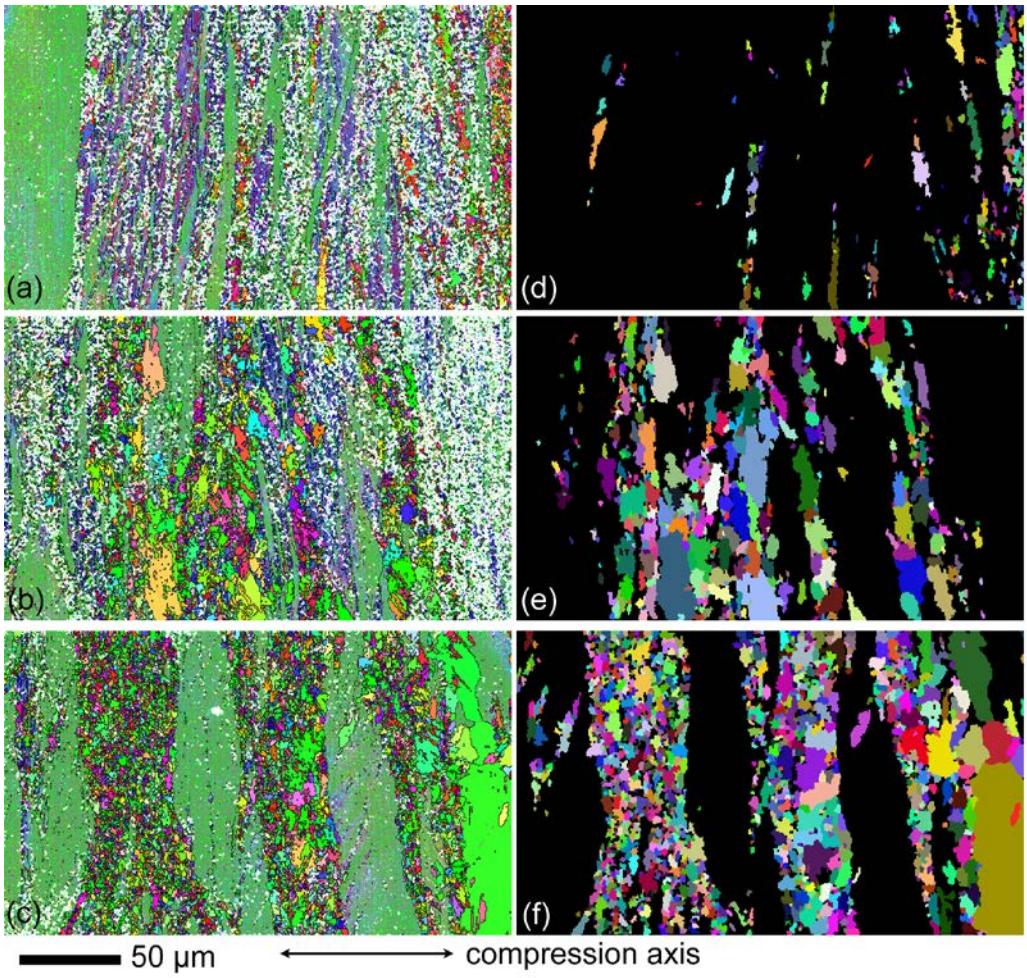

Fig. 5.4: Partly recrystallized microstructures of the DPD samples annealed at 120 °C for 2 minutes (a and b) and 1 h (c). The color coding is the same as that in Fig. 5.2. Maps d-f highlight the recrystallizing grains in maps a-c, respectively, in random colors. The ITB method was used for grain definition (i.e. a grain and its twins are shown in the same color).

After annealing for 1 h, the type C microstructure has almost disappeared (Fig. 5.4c). Most of the remaining deformed matrix belongs to the Type A microstructure, and a few Type B twin bundles can be observed in the up-left corner of Fig. 5.4c. A few large recrystallizing grains can be observed in the right part of Fig. 5.4c. These large recrystallizing grains seem to grow at the expense of the Type A microstructure according to the remaining parts of the regions they are growing into. Twins of these large recrystallizing grains are very small, which indicates that these grains may be more favorable to grow

in the local environment than their twins. Most of the large recrystallizing grains belong to a {110} fiber texture. This agrees with the observations that in nickel deformed by uniaxial compression some large grains of a {110} fiber texture appeared at a later stage of recrystallization by consuming microstructures from a relatively homogeneous deformation (Hasegawa and Fukutomi 2002). Moreover, a rapid growth of certain grains into regions with low stored energy has been reported by Godfrey et al. (2001) in brass oriented aluminum single crystals deformed by channel-die compression, although the mechanisms of the high growth rates are still not clear. In general, for the DPD samples the recrystallization process is very heterogeneous, and the heterogeneity in the deformation structure has been transferred into the annealed samples.

5.2.3 Statistical analysis of recrystallization kinetics

The DPD samples were isothermally annealed at 120 °C for time periods from 2 minutes to 4 h. The recrystallized volume fraction V_V is plotted as a function of annealing time in Fig. 5.5a. The standard deviations of V_V are large, especially at the beginning of annealing, which is related to the recrystallization behavior. Among the 7 maps characterized for the 2 minutes annealed sample, the minimum V_V is 0.016, while the maximum is 0.69. The

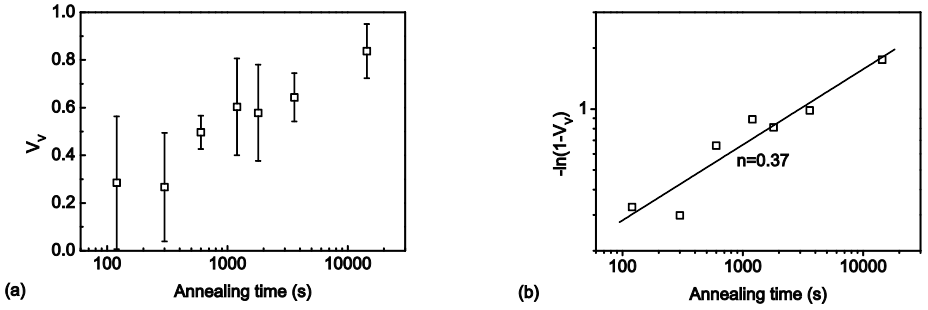

Fig. 5.5: a) Evolution of the recrystallized volume fraction V_V as a function of annealing time for the DPD samples. The error bars show the standard deviations of V_V. b) Avrami plot of the same data as in a). The ITB method was used.

standard deviation of V_V decreases slightly after longer time annealing. Nevertheless, it is still as high as 0.11 after 4 h annealing. The same data plotted in an Avrami plot fit nicely to a straight line, but the slope of the line is very low, even compared with many experimental data (e.g. the cold-rolled copper in Chapter 4 and other examples listed in Doherty et al. 1986).

The nucleation density is plotted in Fig. 5.6a. The volume density of recrystallizing grains N_V (ITB method) increases with time before saturation occurs at around 30 minutes (V_V around 0.6). N_V increases similarly if the CTB method was applied. The saturated N_V by the CTB method is 3.5 times of that by the ITB method. The growth rates decrease with time as $G = G_0 t^{-1}$. The time dependence of the growth rates is similar to that in the cold-rolled copper in Chapter 4, as well as that in many other metals reported in earlier literature (some examples are listed in Doherty et al. 1986). If in the JMAK model, a constant nucleation rate and decrease of growth rates as $G = G_0 t^{-1}$ is assumed, the exponent n will be 1 according to Eq. 4.8. This calculated exponent is still much larger than the measured value. The lower measured exponent is partly from the nucleation rate which may decrease with time. However, at least at the beginning of recrystallization, the nucleation rate is close to constant, and more discussion on the low exponent is therefore needed.

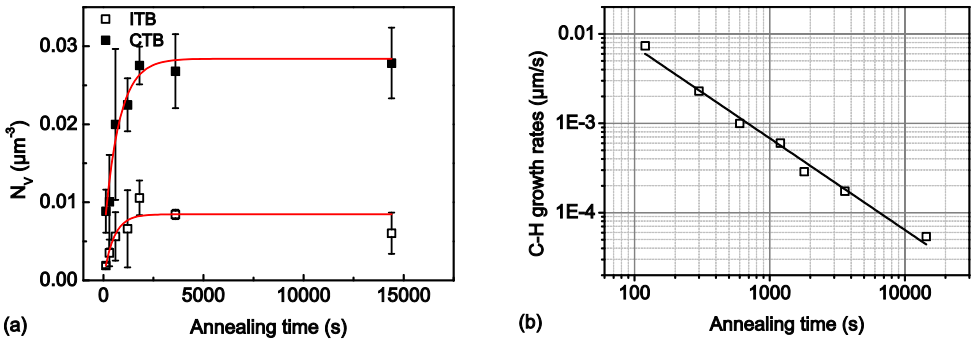

Fig. 5.6: a) Evolution of volume density of recrystallizing grains as a function of annealing time, which is calculated using Eq. 4.5. Both ITB and CTB methods were used. The error bars show standard errors. b) Cahn-Hagel growth rates as a function of annealing time, which were calculated using Eq. 4.6-4.7. The ITB method was applied.

One may speculate that a possible reason for such a low exponent could be recrystallization during the storage. The DPD samples were kept at -18°C for around 6 months plus some days at room temperature during transportation from China to Denmark and sample preparation. It is possible that part of the 30% volume fraction of recrystallizing grains after 2 minutes annealing existed before furnace annealing, and were formed during the storage and/or sample preparation. The recrystallization time t should then be $t+t_s$, where t_s is the storage time converted into an equivalent time for annealing at 120 °C. If t_s is set to 20 minutes and 1 h, the fitted exponent n increases from 0.37 to 0.65 and 0.96 respectively (Fig. 5.7a). However even 20 minutes may be an overestimation. The reported recrystallization activation energy varies from 58 to 170 kJ/mol (Jägle and Mittemeijer 2012), and even if the lowest activation energy is taken, 6 months storage at -18°C corresponds to only 18 minutes annealing at 120 °C. The DPD samples were rechecked after 18 months storage, and the recrystallized volume faction was found to be 17.5% ± 16.7%. By assuming that the pre-existing grains do not growth further, the recrystallization during storage may be incorporated in the analysis as:

$$V_V^{'} = (V_V - V_{V,0})/(1 - V_{V,0}) \tag{5.1}$$

where $V_{V,0}$ is the recrystallized volume fraction after storage. The Avrami plot of $V_V^{'}$ is shown in Fig. 5.7b, and the exponent n equals 0.56, i.e. the exponent n is still very low.

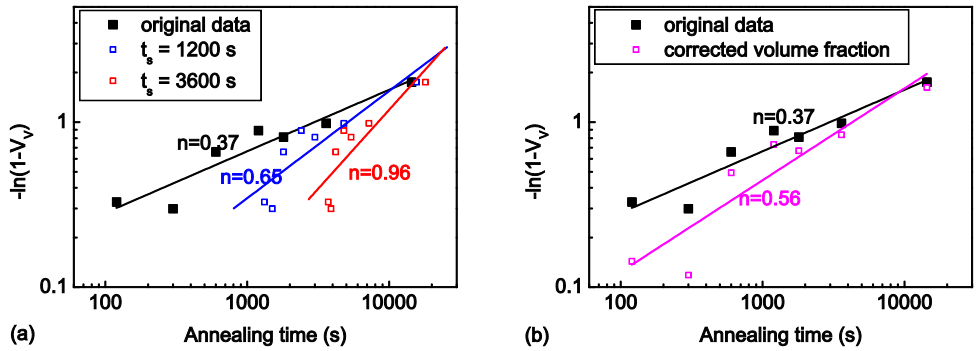

Fig. 5.7: Avrami plots of the recrystallized volume fraction a) by assuming the low temperature storage time corresponds to 20 minutes and 1 h annealing time t_s at 120 °C, b) corrected by Eq. 5.1.

Another explanation for the low exponent n could be the heterogeneous distribution of stored energies, and thus different recrystallization kinetics in different regions of the sample. Both the large standard deviation of V_V (Fig. 5.5a) and the heterogeneous distributed recrystallizing grains in Fig. 5.4 confirm the existence of different recrystallization kinetics in different regions. The heterogeneous recrystallization leads to severe clustering of recrystallizing grains. Because of this, the requirement of a random spatial distribution of recrystallizing grains in the JMAK model is not satisfied. A simple model can be established assuming different recrystallization kinetics in different regions of the sample. Based on the microstructures in Fig. 5.4, it is reasonable to assume that at least two different types of regions exist in the sample, namely fast recrystallizing regions (FRRs) and slowly recrystallizing regions (SRRs). The FRRs may be the Type C regions, while the SRRs could be the Type A and B regions. To get an idea of how such heterogeneous recrystallization may affect the overall recrystallization kinetics, it is for simplicity assumed that both FRRs and SRRs follows the theoretical JMAK equation for a constant nucleation rate with n=4 in both regions. By further assuming that recrystallizing grains grow only within their own regions, the overall kinetics can then be expressed as:

$$\begin{aligned} V_V &= x \cdot V_{V,FRRs} + (1-x) \cdot V_{V,SRRs} \\ &= x \cdot (1 - exp(-k_{FRRs} t^4)) + (1-x) \cdot (1 - exp(-k_{SRRs} t^4)) \end{aligned} \tag{5.2}$$

where x is the volume fraction of FRRs. This type of model was suggested previously by Doherty et al. (1986) and Rollett et al. (1989). The overall Avrami plots applying Eq. 5.2 are shown in Fig. 5.8a for various x and in Fig. 5.8b for various k_{FRRs}/k_{SRRs}. The overall V_V curve follows the kinetics line of the FRRs at the beginning and the SRRs at the end, each with a slope close to 4. In between, the line bends over, and the slope at an intermediate stage may decrease to less than 1. It should be noted that this model is very simplified. First, the k_{FRRs}/k_{SRRs} may have been exaggerated in Fig. 5.8. The difference of stored energy is about 2 to 3 times according to the calculation of Yan et al. (2012). If only considering the effects of stored energy on the growth rates of recrystallizing grains, the k_{FRRs}/k_{SRRs} should be about 8-27. Furthermore, even

inside the FRRs and SRRs, the grains are less likely to grow with constant growth rates due to changes of local environment, i.e. the slopes of the individual lines of FRRs and SRRs should be less than 4. However, this simple model shows the possibility that the exponent n, when obtained from relatively few experimental points at intermediate stages of recrystallization, can show very low values because of the heterogeneity within the deformation matrix.

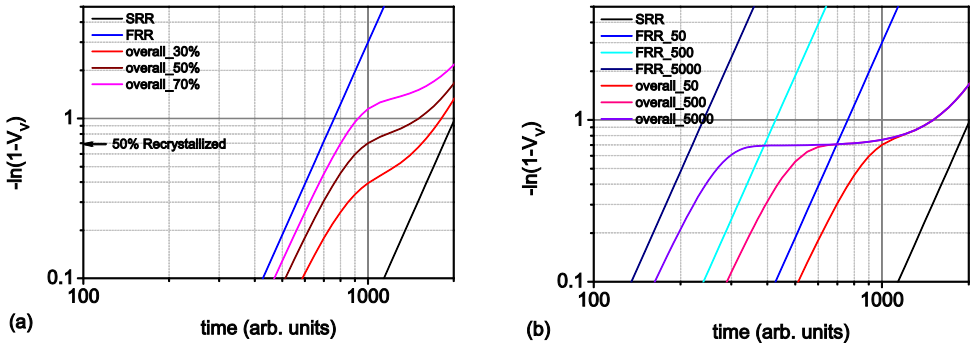

Fig. 5.8: Theoretical kinetics curves by assuming that there are two distinct regions in the sample, namely fast recrystallizing regions (FRRs) and slowly recrystallizing regions (SRRs). Each region follows JMAK recrystallization kinetics independently of each other with different k values. a) k_{FRRs}/k_{SRRs}=50, with different volume fraction of FRRs, b) 50% volume fraction of FRRs, with different values of k_{FRRs}/k_{SRRs}.

5.2.4 Recrystallization kinetics of individual grains

The DPD sample was in-situ annealed at 105 °C for around 140 minutes in the 3DXRD experiment. A selection of typical growth curves is plotted in Fig. 5.9. Recrystallization has already begun during low temperature storage, and bright diffraction peaks originating from recrystallizing grains can be observed before heating the sample in the 3DXRD experiment. Among the selected growth curves, two belong to pre-existing recrystallizing grains. These two curves represent the typical behaviors of the pre-existing grains. Some of the pre-existing grains are observed to continue their growth during the in-situ annealing, while some keep constant sizes. These non-growing grains may be impinged by other grains or have grown into a deformation microstructure unfavorable for growth.

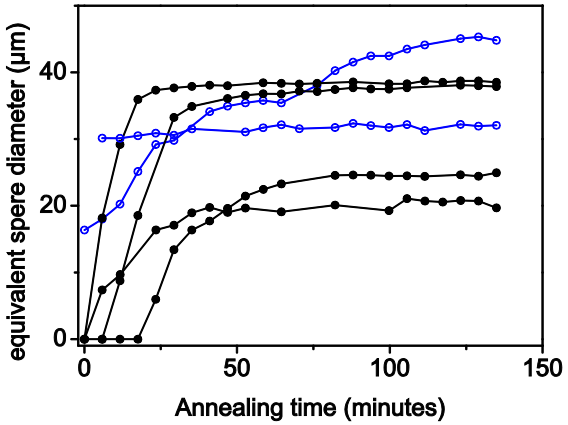

Fig. 5.9: A selection of measured growth curves of recrystallizing grains in the DPD sample. The blue curves represent grains that already exist before in-situ annealing, while the black curves represent grains appearing during the annealing.

Many recrystallizing grains nucleate right after the start of the annealing, and only a few grains nucleate later. The distribution of nucleation times is plotted in Fig. 5.10, and the pre-existing grains have been excluded. The nucleation situation is closer to the site saturation, as 78% of the grains nucleate within the first 20 minutes. This is in contrast to the evolution of volume density of recrystallizing grains N_V measured by EBSD (Fig. 5.6a). A possible reason is the different detection limits of the two techniques. As shown in Fig. 5.4 d-f, the majority of recrystallizing grains recognized by EBSD are small grains. Moreover, each grain in Fig. 5.4 d-f already includes all its twins. If twins are considered as separated grains, the grain sizes would be even smaller. However, most of these small grains are ignored in the 3DXRD data analysis, as discussed in Chapter 3. If a larger critical size of 7 µm is applied for defining recrystallizing grains for the EBSD data, the N_V remains constant at around 4×10^{-4} μm^{-3}, which is then closer to site saturation, similar to the observations by 3DXRD.

Among the curves in Fig. 5.9, two exhibit very high growth rates at the beginning, which decrease quickly to zero. This rapid size saturation is also very common in DPD samples. Compared with the growth curves in cold-rolled copper samples in the previous chapter, grains in the DPD sample reach stable sizes much faster. This is certainly related to the annealing

temperature applied, but the more severe impingement observed in this DPD sample also affects the growth curves.

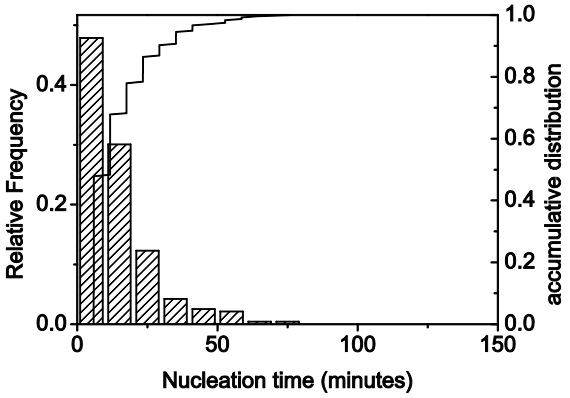

Fig. 5.10: Distribution of nucleation times in the DPD sample. Pre-existing grains are not included.

5.3 Recrystallization kinetics and microstructural evolution of DPD+CR samples

The nanostructured DPD sample was further cold-rolled at room temperature to 75% thickness reduction using a manual rolling mill with a roll diameter of 30 mm. The rolling plane coincided with the compression plane. This sample is termed the DPD+CR sample. The purpose of the additional rolling is to improve the ductility of the nanostructured DPD sample, which is inspired by the work on aluminum by Huang et al. (2006). It has been observed that in aluminum processed by ARB, which has a high strength but a low ductility, the sample ductility can be improved by applying additional rolling. For the DPD sample, the tensile uniform elongation increases from 1% to 4.5% with an increase of the rolling reduction up to 75%, and the uniform elongation remains constant for even higher rolling reductions (Zhang et al. 2008).

5.3.1 Deformation microstructure

An orientation map of the DPD+CR sample is shown in Fig. 5.11a. Here fewer non-indexed points (<20%) are observed in the EBSD data due to dynamic recovery during the additional rolling (Zhang et al. 2008). The microstructure is a mixture of lamellae and slightly elongated cells. The lamellar boundaries are almost aligned with the RD, but are frequently very wavy. The slightly elongated cells tend to form bands parallel to the RD, also. These cells are at least partly surrounded by HABs. There is no evidence of Type A and C structures any longer. These structures have obviously been replaced by the typical rolling lamellar structure, although it is quite possible that the slightly elongated cells may be recovered Type C regions. Some Type B structure of twin bundles (e.g. in the left part of the map) “survived” the rolling, but their volume fraction is quite limited. In the vicinity of twin bundles, lamellar bands or bands formed by cells are wavier than elsewhere.

The microstructure of the DPD+CR sample is more homogeneous compared with that of the DPD sample, and Fig. 5.11a does represent the general microstructure of larger areas. The distribution of stored energy was analyzed by plotting the distributions of BCs in different regions. Fig. 5.11b shows the distributions in three selected regions (marked by frames in Fig. 5.11a), which represent twin bundles (1), lamellar bands (2) and elongated cell (3) regions. The distributions of BCs in regions 2 and 3 are very similar, while the peak of the distribution of region 1 has a slight shift towards lower BCs. However, in general the heterogeneous distribution of stored energy in the DPD sample has been suppressed through the additional rolling. It needs to be noted that this homogeneity is on a large length scale, while local variation still exists, which is illustrated in Fig. 5.11c by defining high misorientation regions (HMRs), using the method introduced in Chapter 4.

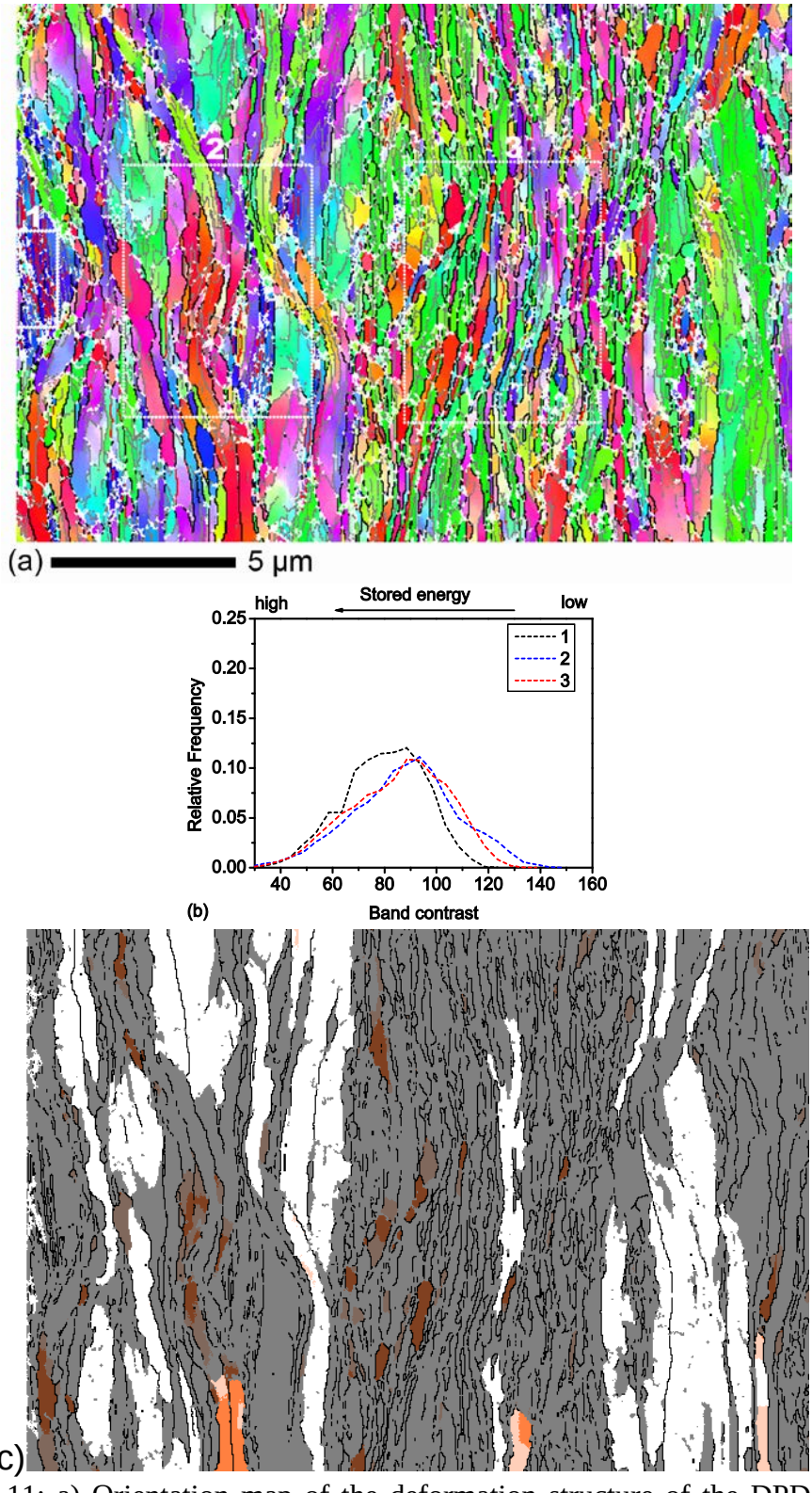

Fig. 5.11: a) Orientation map of the deformation structure of the DPD+CR sample. b) Distributions of band contrasts in framed regions 1/2/3. c) The same map as a) with HMRs, cube and near cube textured regions highlighted. The color coding and the sample coordinates are the same as those in Fig. 4.4.

With the additional rolling, the initial DPD microstructure composed of different types of regions has been transferred to the lamellar structure, which is typical for high strain cold-rolled samples. It is therefore interesting to compare the microstructure of the DPD+CR sample with that of a cold-rolled sample, investigated in Chapter 4. The DPD+CR sample was first compressed to a strain of 2.0 at high strain rates and a low temperature, and was then rolled to a strain of 1.4. Considering the change of strain paths, deformation temperatures, strain rates, as well as the recovery during the rolling, it is hard to decide which cold-rolled sample should be compared here. Since the microstructure of the DPD+CR sample is very fine, it may be suitable to choose the sample rolled to the highest strain from Tab. 4.3, i.e. the BI1_95cr sample, corresponding to a strain of 3.0. Moreover, the initial grain size of the DPD+CR sample is 200 µm, and it is thus more reasonable to use this initially coarse grained sample, although the initial grain size of BI1_95cr is only 77 µm. The deformation microstructure of the BI1_95cr sample (Fig. 4.30) is composed mainly of lamellar structures surrounded by LABs. There are very few cells surrounded by HABs in BI1_95cr. The two microstructures show an obvious difference. The structural parameters of the DPD+CR sample are listed in Tab. 5.1, which can be compared with the parameters of BI1_95cr. In order to facilitate reading, the microstructural parameters of BI1_95cr sample in Tab. 4.7 are repeated in Tab. 5.1. The spacing of HABs in the DPD+CR sample is about half of that in BI1_95cr, and the fraction of HABs is also much higher. Moreover, the volume fraction of HMRs has reached 59% (calculated from a map covering 100 × 100 μm^2, and Fig. 5.11 is part of the map), i.e. HMRs become the major component in the DPD+CR microstructure. For the BI1_95cr sample, even if it is rolled further to higher strains, it is hard to decrease the HAB spacing substantially, since the decreasing of the HAB spacing is very slow at high strains. It is also difficult to increase the fraction of HABs and HMRs of BI1_95cr through further rolling to the same level as that in the DPD+CR sample. In general, compared with rolling, the DPD+CR process is a more effective way to refine the microstructure.

Tab. 5.1: Microstructural parameters in the DPD samples with additional manual and automatic rolling to 75% thickness reductions. The microstructural parameters in the BI1_95cr sample reported in Tab. 4.7 are repeated here for comparison.

Sample	Spacing of HABs along the ND (nm)	Spacing of HABs along the RD (nm)	Fraction of HABs	Fraction of HMRs
DPD+CR (manual)	354	820	45%	59%
DPD+CR (automatic)	225	448	56%	92%
BI1_95cr	774	1957	26%	18%

The rolling texture in the DPD+CR sample is much weaker than in the BI1_95cr. The volume fraction of rolling texture components (copper, S and brass) in the DPD+CR sample is only 36%. Considering that the DPD deformation is closer to uniaxial compression, which is more favorable for a {110} fiber texture, and only the additional rolling to 75% thickness reduction may be favorable for the formation of rolling texture, it is reasonable that the rolling texture in the DPD+CR sample is much weaker than in the BI1_95cr sample. However, the volume fraction of rolling texture components in the DPD+CR sample is even much lower than that in copper samples cold-rolled to 75% thickness reduction (Necker et al. 1991, Gerber et al. 2003). The difference in texture may be related to the strong {110} fiber texture in the DPD sample and the twin bundles and the de-twinning process that occurs during the additional rolling, as well as the recovery.

It should be noted that a manual rolling mill was utilized here. The sample was only slightly deformed during each rolling pass, since the DPD sample has a very high strength. This rolling process does not satisfy the requirement of a homogeneous rolling (Truszkowski et al. 1980). However, there is no obvious texture difference in the center and in the surfaces of the sample. Another DPD sample was rolled in an automatic rolling mill following the conventional homogeneous rolling rule. In this sample, the volume fraction of rolling texture components is 31%, which is even lower than the manually

rolled one. The microstructural parameters of the automatically rolled DPD sample are also listed in Tab. 5.1. The HABs spacing is even smaller, and the fraction of HABs is higher. The difference in the microstructure may be related to the different strain rates during the manual and automatic rolling, as it has been suggested that the deformation of nanostructured materials is very sensitive to the strain rates (Göken et al. 2012). This automatically rolled DPD sample is only for comparison with the manually rolled one, and the recrystallization in this sample is not investigated in this work.

5.3.2 Microstructural evolution during annealing

Two maps after 150 °C 20 minutes annealing are shown in Fig. 5.12 a and b. Compared with the DPD samples, the spatial distribution of the recrystallizing grains in the DPD+CR samples is more random, although many recrystallizing grains tend to locate along bands. The latter is typical for many cold-rolled pure metals (e.g. Sükösd et al. 2007 and samples in Chapter 4). The recrystallizing grains are considered to develop from the slightly elongated cells in the deformation structure, which are partly surrounded by HABs. They could grow easily into the neighboring deformed matrix by the migration of HABs. The two maps obtained in different regions of the same sample have similar V_V, i.e. the partial recrystallization microstructure is relatively homogeneous over a large length scale.

With a longer annealing time (Fig. 5.12c), the recrystallizing grains impinge upon each other firstly along the RD, while the distribution of the recrystallizing grains along the ND is still rather random. Some large recrystallizing grains can be observed, and they are located along a band parallel to the RD. One of these large grains belongs to the cube texture, but the orientations of the large grains are in general rather diversified. These large grains here have a more or less equiaxed shape. The mechanism of the formation of supercube grains, suggested in Chapter 4, is not relevant here for the large grains, since a significant size advantage of a few grains is only observed after a long time annealing. The band with large grains seems to be

related to a deformed matrix, which is suitable for the growth of these grains. The formation of these large grains may be similar to that in the DPD sample at a longer annealing time (see Fig. 5.4c).

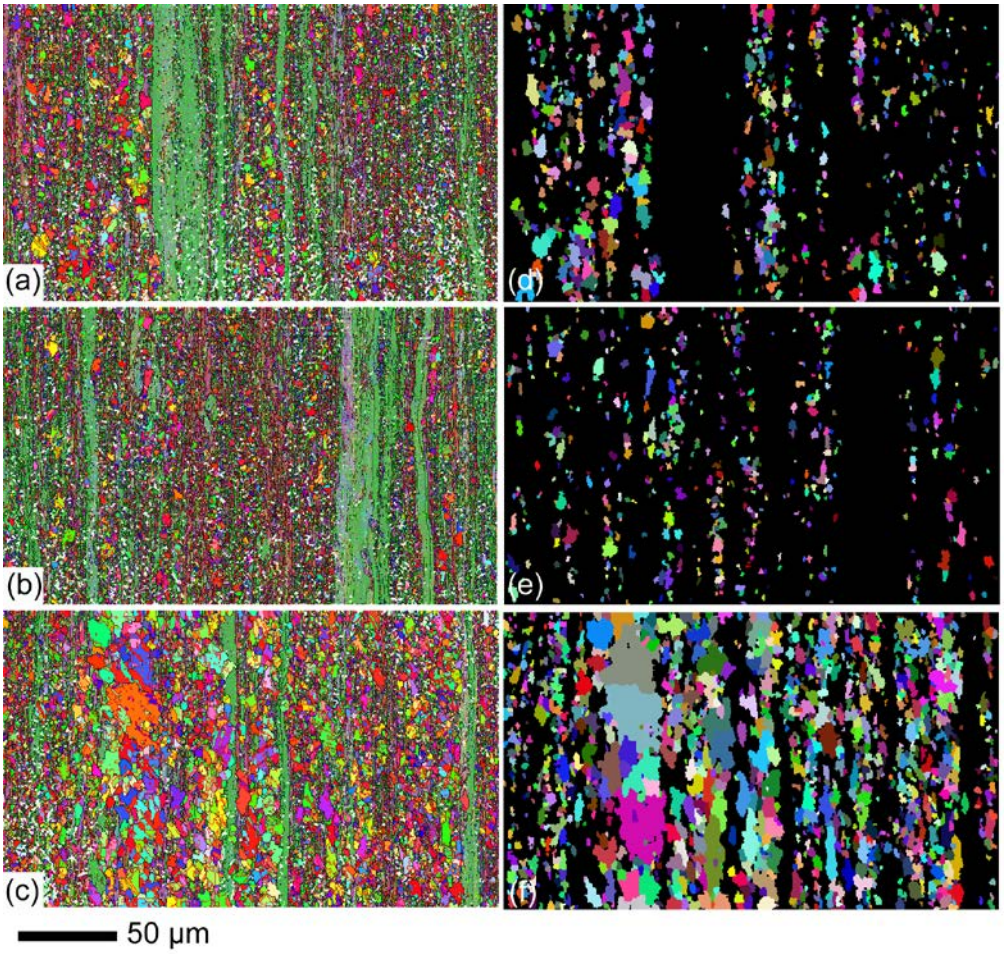

Fig. 5.12: Partly recrystallized microstructures of DPD+CR samples annealed at 140 °C for 20 minutes (a and b) and 1 h (c). The color coding and the sample coordinates are the same as those in Fig. 4.4a. Maps d-f highlight the recrystallizing grains of map a-c in random colors. The ITB method was used for grain definition.

The cube texture after recrystallization is rather weak, although in the deformed sample, the volume fraction of the cube component is 4%, higher than in the cold-rolled samples investigated in Chapter 4. The average size of cube grains is not obviously larger than the noncube grains. Considering the weak rolling texture in the as-deformed DPD+CR sample, it should be expected that a cube texture component is not strong after recrystallization.

5.3.3 Statistical analysis of recrystallization kinetics

The DPD+CR samples were isothermally annealed at 140 °C for time periods from 10 minutes to 4 h. The recrystallization temperature is higher than the DPD sample due to the dynamic recovery during rolling. The evolution of V_V determined from the EBSD data as a function of time and the Avrami plot are shown in Fig. 5.13. The standard deviations of V_V in different regions of the same sample are very small compared with those in Fig. 5.5. The exponent n equals 1.06 if a linear line is fitted for all the data points in the Avrami plot (Fig. 5.13b). However, the last point has an obvious deviation from this line, and if only the first four points are fitted, the exponent equals 1.57. An exponent around 1 has been observed in many cold-rolled samples, such as BI1 and BII5 in Chapter 4. The deviation downwards at the end of recrystallization is also common for cold-rolled copper samples (e.g. Doherty et al. 1986, Vandermeer and Juul Jensen 1995b).

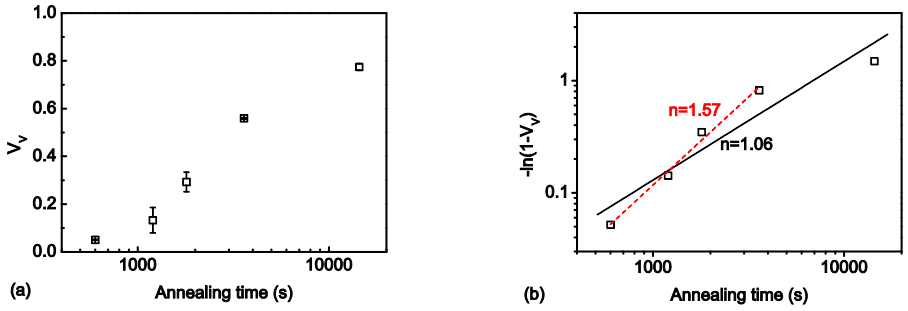

Fig. 5.13: a) Evolution of the recrystallized volume fraction V_V determined from the EBSD data as a function of annealing time for the DPD+CR sample. The error bars show the standard deviations of V_V. b) Avrami plot of the same data as in a). The ITB method was used.

The evolution of volume density of recrystallizing grains is plotted in Fig. 5.14a. The N_V determined with the ITB method increases at the beginning of recrystallization, and saturation occurs at around 30 minutes (V_V around 0.3). The saturated N_V determined with the CTB method is around 4 times that with the CTB method. The evolution of N_V is similar to that of BI1, BII5 and DPD, except the saturation occurs at a lower V_V. The saturated N_V is similar to that of the DPD sample. It should be noted that the step size of EBSD

scanning and the critical size for recrystallizing grain definition are different for the DPD, DPD+CR samples (1.5 μm) and the cold-rolled samples in Chapter 4 (3 μm), and the N_V should not be compared directly. If the critical size for recrystallizing grains is set as 3 μm, the same as that for the cold-rolled samples, the N_V of the DPD+CR is then about twice that in the BI1. The higher density N_V may be related to the high fraction of elongated cells (see Fig. 5.11), which provide a large number of potential nucleation sites. The growth rates of cube, rolling and other textured grains decrease all with time as $G = G_0 t^{-1}$, but the last data points fall far below (Fig. 5.14b). This time dependence has been observed for all the samples (BI1, BII5, DPD and DPD+CR) in this study. The arguments for the decreasing growth rates in Chapter 4 should also be applicable here. However, the distributions of stored energy in these samples are different from each other, and it is still an open question why one expression can apply for all. The growth rates of grains belonging to different texture groups are very similar. Cube grains do not have an obvious growth advantage for this sample, which is consistent with the observation of the partly recrystallized microstructures, that cube grains do not show a size advantage.

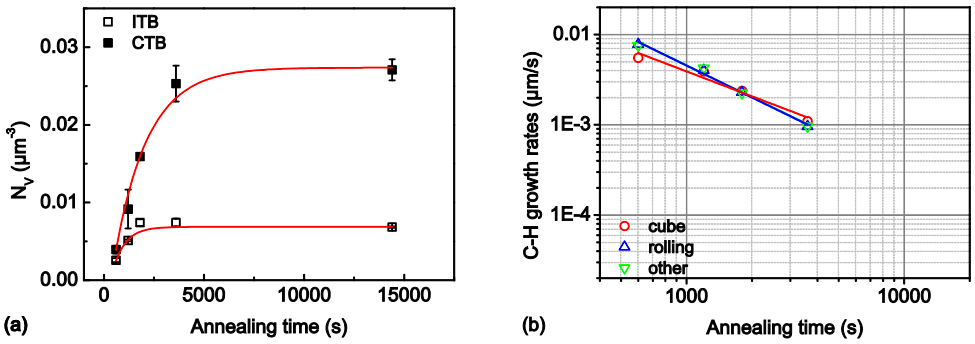

Fig. 5.14: a) Evolution of volume density of recrystallizing grains N_V as a function of annealing time. The N_V was calculated using Eq. 4.5. b) Cahn-Hagel growth rates of differently textured recrystallizing grains, calculated using Eq. 4.6-4.7. The CTB method was used for the determination of growth rates of different textured grains.

5.3.4 Recrystallization kinetics of individual grains

The sample was annealed in-situ at 110 °C for 100 minutes during 3DXRD experiments. The annealing temperature was then increased to 130 °C for another 100 minutes. This sample is more thermally stable compared with the DPD sample, but still a few recrystallizing grains exist before annealing, such as the grain Nr. 1 in Fig. 5.15. There are more grains that appear at the beginning of annealing, and the nucleation rate seems to decrease with time. But in this sample, the annealing temperature was increased during the measurement, and there are 46% and 26% cube and noncube grains, which nucleate after the temperature increase, respectively. The higher temperature not only promotes nucleation, but also favors the growth. Some grains have reached stable sizes, but reassume growth after the temperature increase (e.g. Nr. 3). The increase of growth rates is expected, since the boundary migration of recrystallizing grains is a thermally activated process. However, some grains (e.g. Nr. 4) are less sensitive to the temperature, and the growth rates do not increase at the higher temperature. An unchanged growth rate after a temperature change has been reported for a few grains by Vandermeer et al. (2004) in copper and by Poulsen et al. (2011) in aluminum. There is no unique, single apparent activation energy that could be associated with the

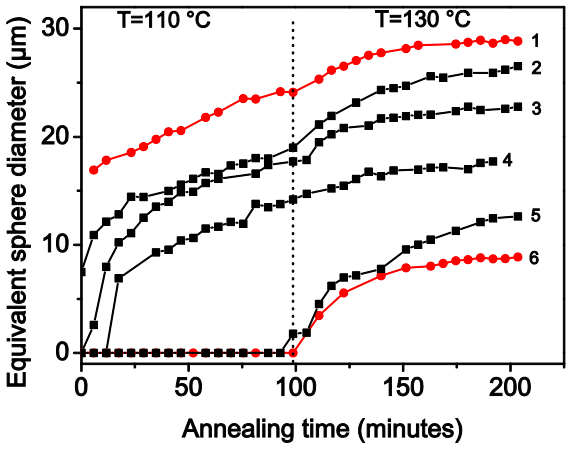

Fig. 5.15: A selection of the measured growth curves of recrystallizing grains in the DPD+CR sample. The red curves represent cube grains, while the black curves represent noncube grains.

growth of individual grains. The growth curves of cube grains are not obviously different from those of noncube grains. The largest cube grain has a very similar size compared to the largest noncube grains.

5.4 Effects of annealing on mechanical properties

Nanostructured metals produced by severe plastic deformations often have a high strength, but the poor ductility of such materials limits their practical usage (Koch 2003). Thermal annealing is in some cases an effective way to increase ductility with a limited loss in strength (e.g. Wang et al. 2002). The nanocrystalline matrix, which stores a large density of dislocations, provides a high strength, while the recrystallized grains of a micrometre scale can work-harden, and may increase the ductility of the whole sample. However, the efficiency of the recrystallized grains for improving ductility may be very different, such as in the DPD and DPD+CR samples investigated in this study. Li et al. (2008b) found that the partly recrystallized DPD samples have

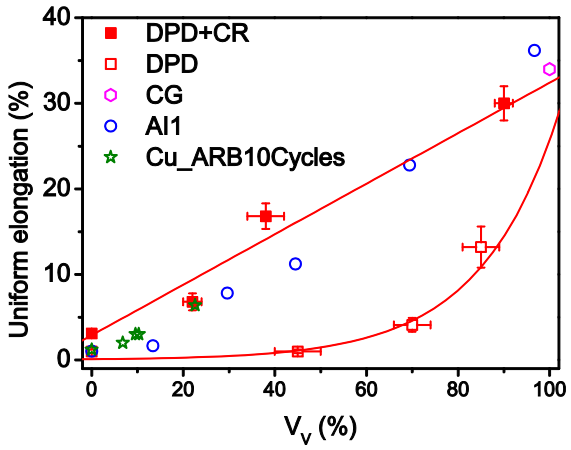

Fig. 5.16: The tensile uniform elongation as a function of the recrystallized volume fraction V_V for various copper samples. The DPD, DPD+CR and the CG (coarse grained) data are reproduced from Zhang (2010). The curve and the line are fitted to the DPD and DPD+CR data, respectively. AI1 is the cold-rolled copper studied in Chapter 4 (see Tab. 4.3). The ARB data are from Tsuji et al. (2012).

very limited uniform elongation in tensile tests even up to very high V_V (see Fig. 5.16). This is in strong contrast to the results of DPD+CR samples, in which the uniform elongation increases linearly with V_V (Zhang 2010). This suggests that there are more parameters than V_V which may affect the ductility of the partly recrystallized samples.

Important structural parameters are investigated in the following by comparing DPD and DPD+CR samples at around V_V=60%, where the uniform elongation is very different (1% for the DPD sample and 15% for the DPD+CR sample). For the DPD sample, the V_V in samples annealed from 10 minutes to 1 h are all around 60%, and they are thus all included in the following analysis.

For the samples approximately 60% recrystallized, the average ECDs of recrystallized grains (ITB method) is around 4 μm for both samples. The grain size distribution is plotted in Fig 5.17. In both DPD and DPD+CR samples, the grain size distributions peak at around 5 μm, and a few grains have an ECD larger than 5 times the average. Compared with the DPD+CR sample, the size distribution of the DPD sample has a longer tail. However, grains larger than 30 μm only count for 4.8% of the total area in the DPD samples. It is thus difficult to imagine that the significant difference in the

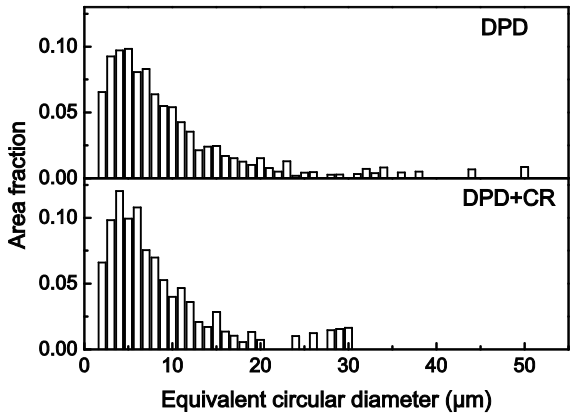

Fig. 5.17: Area-weighted size distributions of recrystallized grains in DPD (120 °C 10 minutes to 1 h) and DPD+CR sample (140 °C 1 h). The recrystallized grains were defined by the ITB method.

uniform elongation can be related to the less than 5% large grains in DPD samples.

The most significant difference between the DPD and DPD+CR samples according to the previous characterizations is the heterogeneity within the samples: both in the deformed and partly recrystallized state. In the DPD sample the deformation microstructure is heterogeneous with broad banded regions of different morphologies and stored energies, and the recrystallizing grains are severely clustered in broad bands, whereas the DPD+CR samples have a more homogeneous deformation microstructure and more dispersed recrystallizing grains. It must be expected that the plastic deformation during subsequent tensile testing may lead to a more pronounced build-up of local stress concentrations in heterogeneous structures. This may explain the difference in mechanical properties of the present partly recrystallized DPD and DPD+CR samples. There have been several models or simulation work on composite structures with a soft and ductile dispersed phase in a hard "brittle" matrix (e.g. Xia and Wang 2010, Abdeljawad et al. 2011), and it is suggested that a dispersed soft phase is favorable for an improvement of the ductility. The simulation and modeling work supports the importance of homogeneity of the sample on the ductility.

The work hardening ability of the remaining (i.e. not recrystallized) deformed matrix may be another important parameter. The uniform elongation of the as-deformed DPD sample is only 1%, while that of the as-deformed DPD+CR sample is 4.5%. The increased ductility in the as-deformed DPD+CR sample may be from the recovered microstructure as shown in Fig 5.11. Compared with the DPD sample, the work hardening ability is slightly better in the DPD+CR sample. It is however hard to estimate the work hardening ability of the remaining deformed matrix as it will be different from that in the deformed state. Firstly, recovery may occur in the deformed matrix during annealing. Secondly, the recrystallization occurs preferably within the regions with high stored energy, and the work hardening ability of the remaining regions with low stored energy is not known. However, it is interesting to consider the behavior of the cold-rolled

copper sample AI1, as plotted also in Fig. 5.15. The uniform elongation of the as-deformed sample is similar to the DPD sample, i.e. a limited work hardening ability in the deformed state. The uniform elongation increases almost linearly, but the uniform elongation is below the line defined by the DPD+CR sample. Tsuji et al. (2012) measured the tensile uniform elongation for OFHC copper ARB processed for 10 cycles and annealed. Their data points are similar to the AI1 data. By comparing the uniform elongation changes in cold-rolled, DPD and DPD+CR samples, the slight difference of the work hardening ability in the deformed state as revealed from the uniform elongation, and hence the difference of work hardening ability in the "hard" phase of the "composite" microstructure may only have weak effects.

As a summary, the heterogeneity of the deformation microstructure in the DPD sample results in a severely clustered distribution of recrystallizing grains. This heterogeneity may have strong effects on the tensile uniform elongation of the sample. It emphasizes further the importance of microstructural heterogeneity in practical applications.

5.5 Summary

Recrystallization in two nanostructured samples, namely the DPD and the DPD+CR samples, was investigated in this chapter.

The DPD sample has a very heterogeneous microstructure, originated from different deformation mechanisms. The microstructure can be divided into three different types: the type A microstructure is formed by dislocation slip, the type B microstructure is twin bundles, and the type C microstructure includes several microstructures, such as shear bands and fragmented twin bundles. The stored energy is highest in the type C microstructure.

The overall stored energy is high, and the sample is thermally unstable. Recrystallization occurs during low temperature storage. During isothermal annealing at 120 °C, recrystallization occurs first in the type C

microstructure, which results in a severely clustered distribution of recrystallizing grains.

The evolution of V_V during 120 °C isothermal annealing has a very low exponent when fitted to the JMAK equation. The volume density of recrystallizing grains increase with annealing time until saturation occurs at V_V=0.6. The growth rates decrease with time as $G = G_0 t^{-1}$. The low JMAK exponent n is related to the decreasing growth rates and the clustered nucleation, which are both related to the heterogeneous deformation structure. A simple recrystallization model is suggested by assuming a fast recrystallizing region and a slowly recrystallizing region, each following its own kinetics. This simplified model shows the possibility of a low exponent at an intermediate stage of recrystallization.

The recrystallization kinetics of individual grains was measured in-situ by 3DXRD at 105 °C. Some recrystallizing grains formed during storage continue to grow during the in-situ annealing, while some do not increase in size. Apart from these grains, most grains form at the beginning of recrystallization, which is in contrast to the continuous nucleation observed from EBSD measurement. This disagreement has been related to the different detection limits of the two techniques. The recrystallizing grains have generally largest growth rates at an initial stage, which decrease very rapidly later. Many grains reach constant sizes in a short time.

The microstructure of the DPD+CR sample is a combination of elongated cells and lamellar bands, together with some residual twin bundles. The distribution of stored energy is more homogenous compared with the DPD sample.

The sample is more thermally stable, and the recrystallization temperature is higher in this sample. During annealing, recrystallizing grains show a certain tendency of clustering in bands along the rolling direction, but the distribution along the normal direction is rather random.

The evolution of V_V during 140 °C isothermal annealing has an exponent n of 1.06 when fitted to the JMAK equation. The sample shows continuous

nucleation before saturation occurs at V_V=0.3, and growth rates of recrystallizing grains decrease with time as $G = G_0 t^{-1}$. Cube grains do not have an obvious growth advantage.

The kinetics of individual grains was measured at 110 °C, and the temperature was increased to 130 °C after 100 minutes annealing. Nucleation takes places through the entire measurement, and some grains nucleate after the increase of the temperature. When the temperature is increased, the growth rates increase for many grains, but a few grains are observed to have a constant growth rate before and after the temperature increase.

The partly recrystallized microstructure of the DPD and DPD+CR samples can be considered as a composite structure with the deformed matrix as a hard phase, and the recrystallizing grains as a soft and ductile phase. The ductility, represented by tensile uniform elongation in this study, has a very different dependence with the V_V in the two nanostructured samples. The DPD+CR sample already has a larger uniform elongation at a low V_V, while the DPD sample has very limited uniform elongation until more than 70% of the material has recrystallized. The better ductility at a low V_V for the DPD+CR sample may be related to the more homogeneous deformation microstructure and the more dispersed recrystallizing grains.

Chapter 6

Conclusions and outlook

The objective of this study was to investigate the recrystallization kinetics and microstructural evolution in copper samples deformed to high strains. Two types of samples are included: commercial oxygen free high conductivity (OFHC) copper deformed by cold-rolling and copper of 99.995% purity deformed by dynamic plastic deformation (DPD). The latter has a nanostructure after deformation. The recrystallization kinetics was investigated statistically by the electron backscatter diffraction (EBSD) and hardness tests, while the recrystallization kinetics of individual grains was investigated in-situ by 3D X-ray diffraction (3DXRD). The main new findings of this study and suggestions for future work are drawn in the following.

In the cold-rolled samples, it is found that the development of the cube recrystallization texture is closely related to a few extremely large cube grains, named supercube grains in the present study. These supercube grains grow faster than noncube grains and many other cube grains, especially at the initial stage. The nucleation time of the supercube grains, however, is not obviously earlier. Compared with the other cube grains, supercube grains do not have orientations closer to the ideal cube orientation. The distributions of misorientations with the neighboring deformed matrix are also similar for the supercube and the other cube grains. The larger growth rates of supercube grains are proposed to be related to the local environment.

The development of a cube recrystallization texture has been investigated in many metals, and the mechanisms of oriented nucleation and oriented

growth have been discussed in particular. However, the observation of supercube grains in the present samples suggests that it may be helpful to consider not only the average behavior of all cube grains. Instead, more attention needs to be paid to the growth of individual grains, which has been made possible with the development of more advanced in-situ and 3D characterization techniques. It is therefore interesting to review recrystallization in many other metals, focusing more on the individual behavior of recrystallizing grains.

The growth of individual supercube grains was followed by the 3DXRD technique in the present work. However, limited by the detection limit of the present experiments, it is still not clear how these supercube grains nucleate. A non-destructive 3D technique that can resolve deformation microstructures is needed to investigate this nucleation process. Moreover, more work on the local deformed microstructure, into which the boundaries of the supercube grains are moving, is needed to understand better how these boundaries can migrate at high velocities.

The deformation structure of the DPD sample is very heterogeneous, which results in different recrystallization behaviors in different regions of the sample. The recrystallizing grains are thus severely clustered. The heterogeneity of the deformation microstructure also affects the recrystallization kinetics, and leads to a very low Avrami exponent in this sample. The effects of a heterogeneous deformation structure on the recrystallization kinetics are demonstrated in this work by a simplified kinetics model. The deformation structure becomes more homogeneous by applying additional rolling to the DPD sample (the DPD+CR sample), and the recrystallizing grains then distribute more randomly. The as-deformed DPD and the DPD+CR samples both have a high strength, but a limited ductility (represented by the tensile uniform elongation). The slightly recrystallized DPD+CR samples have an improved ductility, which is not observed in the slightly recrystallized DPD samples. This difference of the mechanical properties of the partly recrystallized samples may be related to the heterogeneous deformation structure, and the clustering of the recrystallizing

grains, which may lead to localized deformation. However, this suggestion needs to be further demonstrated by detailed measurements of local stress variations or scanning electron microscopy (SEM) characterization of the tensile samples. Furthermore, it could be of interest to compare the mechanical properties of the present samples to some plasticity models. Finally, it is worth noticing the high degree of alignment of the deformation structure as well as recrystallizing grains forming preferentially in wide or narrow bands in the annealed DPD and DPD+CR samples respectively. This may lead to significant flow stress anisotropy in both types of samples, which may be worth more work on the mechanical properties.

Both the formation of supercube grains in the cold-rolled samples, and the clustered distribution of recrystallizing grains in the DPD samples are related to the variation within the deformation structure on different length scales. Moreover, it is found that the average growth rates of recrystallizing grains decrease significantly with time. The individual growth rates of most recrystallizing grains also decrease with time. The decreasing growth rates are related to the local variation within the deformation microstructure, also. In other words, the variation within the deformation microstructure is very important for the subsequent recrystallization. With the development of characterization techniques, deformation structures are described in detail on multiple length scales. In contrast to the complexity of deformation structures, most recrystallization models are still based on very simplified assumptions. These simplified models, such as the classical JMAK model, often show deviations from the behavior of real materials. It is suggested that a good recrystallization model should be able to take the variation on various length scales into account. The in-situ growth curves, measured in this study can serve as good validation data, i.e. a good model should be able to reproduce the growth curves with large variations.

References

Abdeljawad, F., Fontus, M. and Haataja, M. 2011 Ductility of bulk metallic glass composites: microstructural effects. Appl. Phys. Lett. 98, 031909.

Alimadadi, H., Fanta, A.B. and Pantleon K. 2012 High-resolution orientation imaging of nano-twins. In 33rd Risø Int. Symp. On Materials Science (eds S. Fæster et al.), pp. 175-180. Roskilde, Denmark: Department of Wind Energy, Technical University of Denmark.

Alvi, M.H., Cheong, S.W., Suni, J.P., Weiland, H. and Rollett, A.D. 2008 Cube texture in hot-rolled aluminum alloy 1050 (AA1050) – nucleation and growth behavior. 56, 3098-3108.

Asbeck, H.O. and Mecking, H. 1978 Influence of friction and geometry of deformation on texture inhomogeneities during rolling of Cu single crystals as an example. Mater. Sci. Eng. 34, 111-119.

Avrami, M. 1939 Kinetics of phase change I. J. Chem. Phys. 7, 1103-1112.

Avrami, M. 1940 Kinetics of phase change II. J. Chem. Phys., 8, 212-224.

Avrami, M. 1941 Kinetics of phase change III. J. Chem. Phys. 9, 177-184.

Beck, P.A., Sperry, P.R. and Hu, H. 1950 The orientation dependence of the rate of grain boundary migration. J. Appl. Phys. 21, 420-425.

Beck, P.A. and Hu, H. 1963 The origin of recrystallization textures. In Recovery and recrystallization of metals. (eds L.Himmel) pp. 393-420. Interscience Publishers, New York.

Bunge, H.J. 1970 Some applications of the Taylor theory of polycrystals plasticity. Kristall. Und. Technik. 5, 145-175.

Burgers, W.G. and Tiedema, T.J. 1953 Notes on the theory of annealing textures – comments on a paper by Beck, P.A. with the same title. Acta Metal. 1, 234-238.

Cahn, J.W. and Hagel, W.C. 1962 Theory of diffusional growth. In decomposition of Austenite by diffusional processes (eds Zackay and Aaronson), pp 131-196. Jonh Wiley & Sons (Interscience), New York.

Chang, C.S.T. and Duggan, B.J. 2010 Relationships between rolled grain shape, deformation bands, microstructures and recrystallization textures in Al-5%Mg. Acta Mater. 58, 476-489.

Christian, J.W. 2002 The theory of transformations in metals and alloys. 2nd edn. Oxford, UK: Pergamon.

Cook, M. and Richards, T.L.L. 1946 Observations on the rate and mechanism of recrystallization in copper. J. Inst. Met. 73, 1-31.

DeHoff, R.T. 1986 Microstructural evolution during recrystallization. In 7th Risø Int. Symp. On Metallurgy and Materials Science (eds N. Hansen et al.), pp. 35-52. Roskilde, Denmark: Risø National Laboratory.

Dillamore, I.L. and Katoh, H. 1974 The mechanisms of recrystallization in cubic metals with particular reference to their orientation-dependence. Metal Sci. 8, 73-83.

Doherty, R.D., Rollett A.D. and Srolovitz D.J. 1986 Structural evolution during recrystallization. In 7th Risø Int. Symp. On Metallurgy and Materials Science (eds N. Hansen et al.), pp. 53-67. Roskilde, Denmark: Risø National Laboratory.

Doherty, R.D., Samajdar, I., Necker, C.T., Vatne, H.E. and Nes, E. 1995 Nucleation of recrystallization in cold and hot deformed polycrystals. In 16th Risø Int. Symp. On Materials Science (eds N. Hansen et al.), pp. 1-23. Roskilde, Denmark: Risø National Laboratory.

Doherty, R.D. 1997 Recrystallization and texture. Prog. Mater. Sci. 42, 39-58.

Driver, J.H., Juul Jensen, D. and Hansen, N. 1994 Large-strain deformation structures in aluminum crystals with rolling texture orientations. Acta Metal. Mater. 42, 3105-3114.

Duckham, A., Knutsen, R.D. and Engler, O. 2001 Influence of deformation variables on the formation of copper-type shear bands in Al-1Mg. Acta Mater. 49, 2739-2749.

Duggan, B.J. and Lee, C.S. 1992 Deformation banding, original grain size and recrystallization in FCC intermediate-to-high SFE metals. Scr. Metal. Mater. 27, 1503-1507.

Duggan, B.J., Lücke, K., Köhlhoff, G. and Lee, C.S. 1993 On the origin of cube texture in copper. Acta Metall. Mater. 41, 1921-1927.

Engler, O. and Lücke, K. 1992 Mechanisms of recrystallization texture formation in aluminium alloys. Scr. Metal. Mater. 27 1527-1532.

Engler, O. 1998 On the influence of orientation pinning on growth selection of recrystallization. Acta Meter. 46, 1555-1568.

English, A.T. and Backofen, W.A. 1964 Recrystallization in hot-worked silicon-iron. Trans. TMS-AIME 220, 396-407.

Gerber, Ph., Tarasiuk, J., Chauveau, Th. and Bacroix, B. 2003 A quantitative analysis of the evolution of texture and stored energy during annealing of cold rolled copper. Acta Mater. 51, 6359-6371.

Gerber, Ph., Baudin, T., Jakani, S., Mathon, M.H. and Bacroix, B. 2004 Estimation of stored energy distribution from EBSD Measurements. Mater. Sci. Forum 467-470, 51-56.

Godiksen, R.B., Schmidt, S. and Juul Jensen, D. 2007 Effects of distributions of growth rates on recrystallization kinetics and microstructure. Scr. Mater. 57, 345-348.

Godfrey, A., Juul Jensen, D. and Hansen, N. 1998a Slip pattern, microstructure and local crystallography in an aluminum single crystal of brass orientation {110}<112>. Acta Mater. 46, 823-833.

Godfrey, A., Juul Jensen, D. and Hansen, N. 1998b Slip pattern, microstructure and local crystallography in an aluminum single crystal of copper orientation {112}<111>. Acta Mater. 46, 835-848.

Godfrey, A., Juul Jensen, D. and Hansen, N. 2001 Recrystallisation of channel die deformed single crystals of typical rolling orientations. Acta Mater. 49, 2429-2440.

Godfrey, A., Hansen, N. and Juul Jensen, D. 2007 Microstructural based measurement of local sotred energy variations in deformed metals. Metall. Mater. Trans. 38A, 2329-2339.

Gurland, J. 1958 The measurement of grain contiguity in two-phase alloys. Trans. A.I.M.E. 212, 452-455.

Göken, M., Höppel, H.W., Hausöl, T., Bach, J., Maier, V., Schmidt, C.W. and Amberger, D. 2012 Grain refinement and deformation mechanisms in heterogeneous ultrafine-grained materials processed by accumulative roll bonding. In 33rd Risø Int. Symp. On Materials Science (eds S. Fæster et al.), pp. 31-48. Roskilde, Denmark: Department of Wind Energy, Technical University of Denmark

Hammelrath, H., Butler Jr, J.F., Juul Jensen, D., Leffers, T., Hu, H. and Lücke, K. 1991 An ODF study of the deformation and recrystallization textures of rolled and channel-die compressed high purity copper. Texture. Microstruct. 13, 165-187.

Hammersley, A., 2012 http://www.esrf.eu/computing/scientific/FIT2D.

Hansen, N., Leffers, T. and Kjems, J.K. 1981 Recrystallization kinetics in copper investigated by in situ texture measurements by neutron diffraction. Acta Metal. 29, 1523-1533.

Hasegawa, M. and Fukutomi, H. 2002 Microstructure evolution of polycrystalline pure nickel during static recrystallization. Mater. Trans. 43, 2243-2248.

Hong, C.S., Tao, N.R., Lu, K. and Huang, X. 2009 Grain orientation dependence of deformation twinning in pure Cu subjected to dynamic plastic deformation. Scr. Mater. 61, 289-292.

Huang, X. and Hansen, N. 1997 Grain orientation dependence of microstructure in aluminium deformed in tension. Scr. Mater. 37, 1-7.

Huang, X., Hansen, N. and Tsuji, N. 2006 Hardening by annealing and softening by deformation in nanostructured metals. Sci. 312, 249-251.

Huang, X. and Winther, G. 2007 Dislocation structures. Part I. Grain orientation dependence. Phil. Mag. 33, 5189-5214.

Hughes, D.A. and Hansen, N. 1993 Microstructural evolution in nickel during rolling from intermediate to large strains. Metall. Trans. 24A, 2021-2037.

Hughes, D.A. 2000 Deformation microstructures and selected examples of their recrystallization. In 21th Risø Int. Symp. On Materials Science (eds N. Hansen et al.), pp. 49-70. Roskilde, Denmark: Risø National Laboratory.

Hughes, D.A. and Hansen, N. 2000 Microstructure and strength of nickel at large strains. Acta Mater. 48, 2985-3004.

Humphreys, F.J. 2001 Review: Grain and subgrain characterization by electron backscatter diffraction. J. Mater. Sci. 36, 3833-3854.

Hutchinson, W.B., Jonsson, S. and Ryde, L. 1989 On the kinetics of recrystallization in cold-worked metals. Scr. Metal. 23, 671-676.

Jazaeri, H. and Humpherys, F.J. 2004 The effect of initial grain size on the microstructures developed during cold rolling of a single-phase aluminium alloy. Mater. Sci. Forum 467-470, 63-68.

Johnson, W.A. and Mehl, R.F. 1939 Reaction kinetics in processes of nucleation and growth. Trans. AIME 135, 416-458.

Juul Jensen, D. 1983 A fast in-situ texture measuring technique and its use for an investigation of recrystallization kinetics. Ph.D. Dissertation, Roskilde, Denmark: Risø National Laboratory.

Juul Jesnen, D. 1992 Growth of nuclei with different crystallographic orientations during recrystallization. Scr. Metal. Mater. 27, 533-538.

Juul Jensen, D. 1995a Growth rates and misorientation relationships between growing nuclei/grains and the surrounding deformed matrix during recrystallization. Acta Metall. Mater. 43, 4117-4129.

Juul Jensen, D. 1995b Effects of orientation on growth during recrystallization. In 16th Risø Int. Symp. On Materials Science (eds N. Hansen et al.), pp. 119-137. Roskilde, Denmark: Risø National Laboratory.

Jägle, E.A. and Mittemeijer, E.J. 2012 The kinetics of and the microstructure induced by the recrystallization of copper. Metall. Mater. Trans. A. 43A, 1117-1131.

Koch, C.C. 2003 Optimization of strength and ductility in nanocrystalline and ultrafine grained metals. Scr. Mater. 49, 657-662.

Kolmogorov, A. 1937 On the static theory of metal crystallization. Izv. Akad. Nauk. USS- Ser-Matermat. 1(3), 355-360.

Korbel, A., Embury, J.D., Hatherly, M., Martin, P.L. and Erbsloh, H.W. 1986 Microstructural aspects of strain localization in Al-Mg alloys. Acta Metall. 34, 1999-2009.

Köhlhoff, G.D., Malin, A.S., Lücke, K. and Hatherly, M. 1988 Microstructure and texture of rolled {112}<111> Copper single crystals. Acta Metall. 36, 2841-2847.

Lauridsen, E.M., Juul Jensen, D. and Poulsen, H.F. 2000 Kinetics of individual grains during recrystallization. Scr. Mater. 43, 561-566.

Lauridsen, E.M., Schmidt, S., Suter, R.M. and Poulsen, H.F. 2001 Tracking: a method for structural characterization of grains in powders or polycrystals. J. Appl. Crystallogr. 34, 744-750.

Lauridsen, E.M., Poulsen, H.F., Nielsen, S.F. and Juul Jensen, D. 2003 Recrystallization kinetics of individual bulk grains in 90% cold-rolled aluminium. Acta Mater. 51, 4423-4435.

Lee, C.S., Lee, C.F. and Smallman, R.E. 1996 Texture and microstructure of compressed copper. Texture. Microstruct. 26-27, 137-147.

Li, X.L., Liu, W., Godfrey, A., Juul Jensen, D. and Liu, Q. 2007 Development of the cube texture at low annealing temperature in highly rolled pure nickel. Acta Mater. 55, 3531-3540.

Li, Y.S., Tao, N.R. and Lu, K., 2008a Microstructural evolution and nanostructure formation in copper during dynamic plastic deformation at cryogenic temperatures. Acta Mater. 56, 230-241.

Li, Y.S., Zhang, Y., Tao, N.R. and Lu, K. 2008b Effect of thermal annealing on mechanical properties of a nanostructured copper prepared by means of dynamic plastic deformation. Scr. Mater. 59, 475-478.

Lin, F.X., Godfrey, A. and Winther, G. 2009 Grain orientation dependence of extended planar dislocation boundaries in rolled aluminium. Scr. Mater. 61, 237-240.

Liu, Y.L., Hu, H. and Hansen, N. 1995 Deformation and recrystallization of a channel die compressed aluminum bicrystal with (112)[111]/(123)[412] orientation. Acta Metal. Mater. 43, 2395-2405.

Liu, Q., Juul Jensen, D. and Hansen, N. 1998 Effect of grain orientation on deformation structure in cold-rolled polycrystalline aluminium. Acta Mater. 46, 5819-5838.

Luo, Z.P., Mishin, O.V., Zhang, Y.B., Zhang, H.W. and Lu, K. 2012 Microstructural characterization of nickel subjected to dynamic plastic deformation. Scr. Mater. 66, 335-338.

Lü, Y.P., Molodov, D.A. and Gottstein, G. 2011 Recrystallization kinetics and microstructure evolution during annealing of a cold-rolled Fe-Mn-C alloy. Acta Mater. 59, 3229-3243.

Mao, W.M. 1990 Influence of widening on the rolling and recrystallization texture in high purity Al with initial cube texture. Chin. J. Met. Sci. Technol. 6, 325-332.

Mishin, O.V. and Godfrey, A. 2008 Microstructure of ECAE-processed copper after long-term room-temperature storage. Metall. Mater. Trans. 39A, 2923-2930.

Morii, K., Mecking, H. and Nakayama, Y. 1985 Development of shear bands in FCC single-crystals. Acta Metal. 33, 379-386.

Necker, C.T., Doherty, R.D. and Rollett A.D. 1991 Quantitative measurement of the development of recrystallization texture in OFE copper. Texture. Microstruct. 14-18, 635-640.

Paul, H., Driver, J.H. and Jasienski, Z. 2002 Shear banding and recrystallization nucleation in a Cu-2%Al alloy single crystal. Acta Mater. 50, 815-830.

Poulsen, H.F., Juul Jensen, D. and Vaughan G.B.M. 2004 Three-dimensional X-ray diffraction microscopy using high-energy X-rays. MRS Bull. 29, 166-169.

Poulsen, S.O., Lauridsen, E.M., Lyckegaard, A., Oddershede, J., Gundlach, C., Curfs, C. and Juul Jensen, D. 2011 In situ measurements of growth rates and grain-averaged activation energies of individual grains during recrystallization of 50% cold-rolled aluminium. Scr. Mater. 64, 1003-1006.

Price, C.W. 1989 comments on the extent of simultaneous recovery during recrystallization and its effect on recrystallization kinetics. Scr. Metal. 23, 1273-1276.

Ray, R.K., Hutchinson, W.B. and Duggan, B.J. 1975 Study of nucleation of recrystallization using HVEM. Acta Metal. 23, 831-840.

Read, W.T. and Shockley, W. 1950 Dislocation models of crystal grain boundaries. Phys. Rev. 78, 275-289.

Richards, T.LL., Pugh, S.F. and Stokes, H.J. 1956 The kinetics of recovery and recrystallization of copper from hardness and thermoelectric-power measurements. Acta Metall. 4, 75-83.

Ridha, A.A. and Hutchinson, W.B. 1982 Recrystallization mechanisms and the origin of cube texture in copper. Acta Metall. 30, 1929-1939.

Rios, P.R., Godiksen, R.B., Schmidt, S., Juul Jensen, D. and Vandermeer, R.A. 2006 Analytical expression for the evolution of interfacial area density between transformed grains during nucleation and growth transformation. Scr. Mater. 54, 1509-1513.

Rollett, A.D., Srolovitz, D.J., Doherty, R.D. and Anderson, M.P. 1989 Computer simulation of recrystallization in non-uniformly deformed metals. Acta Metall. 37, 627-639.

Ryde, L., Hutchinson, W.B. and Jansson, S. 1990 Recrystallization mechanisms, kinetics and textures in cold rolled copper, Recrystallization 90, TMS (eds T. Chandra), pp. 313-318.

Saito, Y., Utsunomiya, H., Tsuji, N. and Sakai, T. 1999 Novel ultra-high straining process for bulk materials development of the accumulative roll-bonding (ARB) process. Acta Mater. 47, 579-583.

Sindel, M., Köhlhoff, G.D., Lücke, K. and Duggan, B.J. 1990 Development of cube texture in coarse grained copper. Texture. Microstruct. 12, 37-46.

Speich, G.R. and Fisher, R.M. 1966 Recrystallization in rapidly heated 3 ¼% silicon iron. In Recrystallization, grain growth and textures. (eds H. Margolin) pp. 563-598. Amer. Soc. For Metals, Metals Park, OH

Storm, S. and Juul Jensen, D. 2009 Effects of clustered nucleation on recrystallization. Scripta Mater. 60, 477-480.

Sükösd, Z., Hanneson, K., Wu, G.L. and Juul Jensen, D. 2007 3D spatial distribution of nuclei in 90% cold rolled aluminium. Mater. Sci. Forum 558-559, 345-350.

Truszkowski, W., Krol, J. and Major, B. 1980 Inhomogeneity of rolling texture in fcc metals. Metal. Trans. 11A, 749-758.

Tsuji, N. et al. 2012 unpublished work.

Valiev, R.Z., Islamgaliev, R.K. and Alexandrov, I.V. 2000 Bulk nanostructured materials from severe plastic deformation. Prog. Mater. Sci. 45, 103-189.

Vandermeer, R.A. and Gordon, P. 1963 The influence of recovery on recrystallization in aluminum. In Recovery and recrystallization of metals. (eds L.Himmel) pp. 211-239. Interscience Publishers, New York.

Vandermeer, R.A. and Rath, B.B. 1989 Modeling recrystallization kinetics in a deformed iron single crystal. Metal. Trans. 20A, 391-401.

Vandermeer, R.A. and Juul Jensen, D. 1994 On the estimation of Cahn-Hagel interface migration rates. Scr. Metal. Mater. 30, 1575-1580.

Vandermeer, R.A. 1995a Analytical modeling of the kinetics of recrystallization. In 16th Risø Int. Symp. On Materials Science (eds N. Hansen et al.), pp. 193-213. Roskilde, Denmark: Risø National Laboratory.

Vandermeer, R.A. and Juul Jensen, D. 1995b Quantifying recrystallization nucleation and growth - kinetics of cold-worked copper by microstructural analysis. Metall. Mater. Trans. 26A, 2227-2235.

Vandermeer, R.A. and Juul Jensen, D. 2001 Microstructural path and temperature dependence of recrystallization in commercial aluminum. Acta Mater. 49, 2083-2094.

Vandermeer, R.A., Lauridsen, E.M. and Juul Jensen, D. 2004 Growth rate distributions during recrystallization of copper. Mater. Sci. Forum 467-470, 197-202.

Vandermeer, R.A. 2005 Microstructural descriptors and the effects of nuclei clustering on recrystallization path kinetics. Acta Mater. 53, 1449-1457.

Viswanathan, R. and Bauer, C.L. 1973 Kinetics of grain boundary migration in copper bicrystals with [001] rotation axes. Acta Metal. 8, 1099-1109.

Wagner, P., Engler, O. and Lücke, K. 1995 Formation of Cu-type shear bands and their influence on deformation and texture of rolled FCC (112)[111] single-crystals. Acta Metal. Mater. 43, 3799-3812.

Wang, Y.M., Chen, M.W., Zhou, F.H. and Ma, E. 2002 High tensile ductility in a nanostructured metals. Nature 419, 912-915

Warren, B.E. 1990 X-ray Diffraction. Dover Publications, Inc. New York.

Wassermann, G. and Grewen, J. 1962 Texturen metallischer Werkstoffe, Springer-Verlag, Berlin, 307-326.

Winther, G. and Huang, X. 2007 Dislocation structures. Part II. Slip system dependence. Phil. Mag. 33, 5215-5235.

Woldt, E. 1992 The relationship between isothermal and non-isothermal description of Johnson-Mehl-Avrami-Kolmogorov kinetics. J. Phys. Chem. Solids. 53, 521-527.

Woldt, E. and Juul Jensen, D. 1995 Recrystallization kinetics – comparison between techniques. Metall. Mater. Trans. 26A, 1717-1724.

Wu, G.L. and Juul Jensen, D. 2008 Automatic determination of recrystallization parameters based on EBSD mapping. Mater. Charact. 59, 794-800.

Wu, G.L. and Juul Jensen, D. 2012 In-situ measurement of annealing kinetics of individual bulk grains in nanostructured aluminium. Phil. Mag. 92, 3381-3391.

Xia, S.H. and Wang, J.T. 2010 A micromechanical model of toughening behavior in the dual-phase composite. Int. J. Plasticity 26, 1442-1460.

Yan, F., Zhang, H.W., Tao, N.R. and Lu, K. 2011 Quantifying the microstructures of pure copper subjected to dynamic plastic deformation at cryogenic temperature. J. Mater. Sci. Technol. 27, 673-679.

Yan, F. and Zhang, H.W. 2012 Evaluation of stored energy from microstructure of multi-component nanostructured Cu. J. Mater. Sci. Technol. 28, 289-293.

Zaefferer, S., Baudin, T. and Penelle, R. 2001 A study on the formation mechanisms of the cube recrystallization texture in cold rolled Fe-36%Ni alloys. Acta Meter. 49, 1105-1122.

Zhang, Y., Li, Y.S., Tao, N.R. and Lu, K. 2007 High strength and high electrical conductivity in bulk nanograined Cu embedded with nanoscale twins. Appl. Phys. Lett. 91, 211901.

Zhang, Y., Tao, N.R. and Lu, K. 2008 Mechanical properties and rolling behaviors of nano-grained copper with embedded nano-twin bundles. Acta Mater. 56, 2429-2440.

Zhang, Y.B., Godfery, A., Liu, Q., Liu, W. and Juul Jensen, D. 2009 Analysis of the growth of individual grains during recrystallization in pure nickel. Acta Mater. 57, 2631-2639.

Zhang, Y. 2010 Investigations on the strengthening and toughening of bulk nanostructured Cu and Cu-Al alloy. Ph.D. Dissertation, Institute of Metal Research, Shenyang, China.

Zhang, Y.B., Godfrey, A. and Juul Jensen, D. 2011 Local boundary migration during recrystallization in pure aluminium. Scr. Mater. 64, 331-334.

Zhao, W.S., Tao, N.R., Guo, J.Y., Lu, Q.H. and Lu, K. 2005 High density nano-scale twins in Cu induced by dynamic plastic deformation. Scr. Mater. 53, 745-749.

Danmarks Tekniske Universitet
DTU Vindenergi
Nils Koppels Allé
Bygning 403
2800 Kgs. Lyngby
Telefon 45 25 25 25
info@vindenergi.dtu.dk
www.vindenergi.dtu.dk